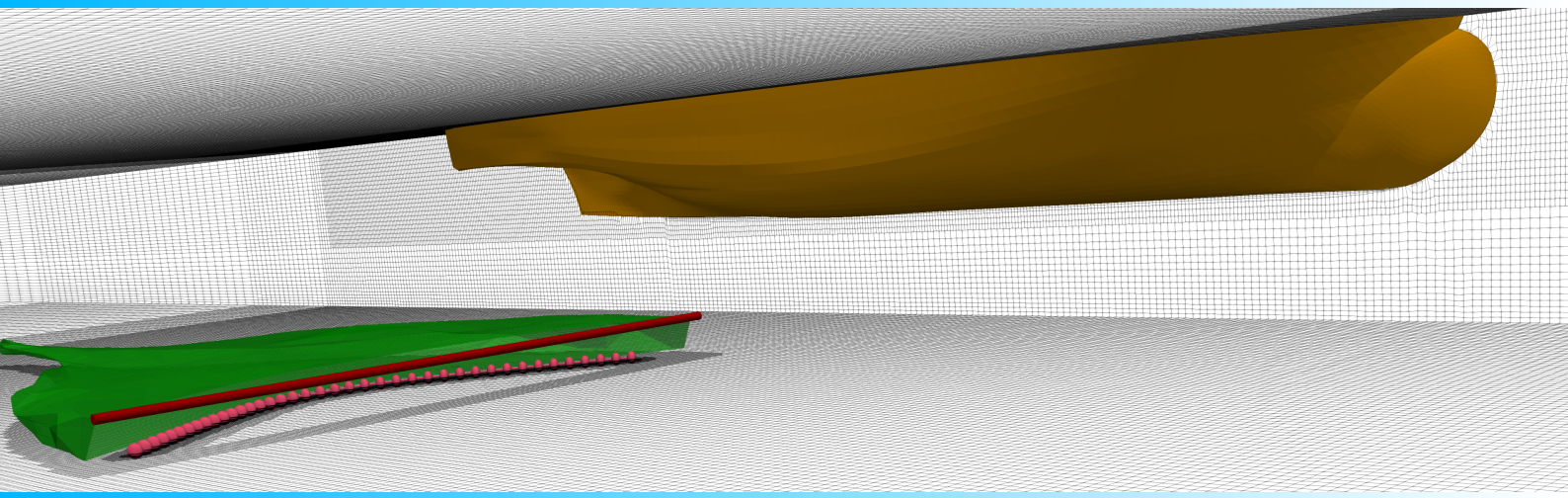
Editors
S. Kosleck, H. Polet & K. Breddermann

Contributions on the Theory of Fishing Gears and Related Marine Systems

Vol. 13



Universität Rostock
Traditio et Innovatio
ILVO

Editors
S. Kosleck, H. Polet & K. Breddermann

Contributions on the Theory of Fishing Gears and Related Marine Systems
Vol. 13

University of Rostock
Faculty of Mechanical Engineering and Marine Technology
Chair of Ocean Engineering
Albert-Einstein-Straße 2
18059 Rostock, Germany

DOI: https://doi.org/10.18453/rosdok_id00005789

Contents

Preface 1

A. TOKAÇ, C. AYDIN, T. ŞENSURAT / TÜRKIYE, E.N. KOSTAK / NORWAY

Comparsion of Dyneema and conventional codend selectivity in Mediterranean bottom trawl 3

J. SANTOS, A. BRÜGER, H. DULZ, D. STEPPUTTIS / GERMANY

Developing and testing benthos release panels in brown shrimp beam trawl fisheries 15

A. SOLDO, N. HERCIGONJA / CROATIA

WinchWatch: Closing the gap between vessel tracking and gear-level fisheries monitoring..... 25

T. SANGEAMWONG, K. EBATA / JAPAN, P. BOONSERM, T. WECHPRASIT / THAILAND

Physical changes in nylon gillnets during soak time in small-scale fisheries, Phuket, Thailand 35

K. YAEGASHI, S. GOMI, K. SUZUKI, T. TAKAGI / JAPAN

Application of state estimation to identify unknown parameters in fishing gear dynamics..... 45

F. BOTTERO, M. GONZÁLEZ / SPAIN

Hydrodynamics of polyethylene knotted diamond mesh netting panels 55

S.-K. KARUMATHIL, A. GOSSET, M. GONZÁLEZ / SPAIN

Motion and Mooring dynamics of a rigid offshore cage: Wave tank experiments and numerical simulation 67

N. HUDA / DENMARK, T. ARAY-SCHMIDT, D. GOSSE / CANADA, M. ABRAHAMSEN-PRSIC / NORWAY, T. VEIGA-MALTA, E. SAVINA, F. G. O'Neill / DENMARK

Experiment and CFD simulation to investigate the effect of ground belt motion with boundary layer profile on the bottom of flume tank 75

K. BREDDERMANN / GERMANY, D. PRIOUR / FRANCE
Close-proximity vessel-gear hydrodynamics: Beam trawls and stow nets.... 83

Preface

The International Workshop on the Development and Evaluation of Maritime Technologies (DEMaT) 2025 was held from 29 September to 2 October 2025 in Oostende, Belgium. The workshop was hosted by ILVO, the Flanders Research Institute for Agriculture, Fisheries and Food, and organized by ILVO, represented by Hans Polet, in collaboration with the Chair of Ocean Engineering at the University of Rostock.

Under the central theme "Technologies to Ensure Sustainable Seafood Production," DEMaT 2025 brought together researchers from engineering and fisheries science to exchange knowledge and discuss recent developments in fisheries technology, fishing gear innovation, marine monitoring systems, aquaculture engineering, and sustainable seafood production. Beyond the presentations themselves, the workshop was particularly marked by intensive and in-depth discussions, creating a highly interactive atmosphere and enabling valuable exchange across disciplinary boundaries.

The scientific programme featured 17 oral presentations covering a broad range of topics, including the reduction of environmental impacts and greenhouse gas emissions in fisheries, advances in fishing gear dynamics and selectivity, hydrodynamic investigations, machine learning applications for fisheries prediction, smart monitoring technologies, and innovations in fisheries management and digitalisation. Ten of the contributions presented at the workshop were selected and submitted as full papers for inclusion in these conference proceedings.

The diversity of topics presented at DEMaT 2025 reflects the interdisciplinary nature of contemporary fisheries and maritime technology research. The workshop highlighted the growing importance of integrating engineering, environmental sciences, digital technologies, and social innovation in order to address current and future challenges in sustainable seafood production and marine resource management.

The editors would like to express their sincere gratitude to all authors, speakers, reviewers, and participants whose contributions ensured the scientific quality and success of the workshop. Special thanks are extended to the organising team at ILVO Oostende for their excellent local organisation and hospitality, as well as to the team at the Chair of Ocean Engineering, University of Rostock, for their continuous support and collaboration.

We hope that these proceedings will provide valuable insights, stimulate further research and cooperation, and contribute to the continued advancement of sustainable maritime technologies and fisheries engineering.

Rostock/Oostende, July 2026
Sascha Kosleck & Hans Polet

COMPARISON OF DYNEEMA AND CONVENTIONAL CODEND SELECTIVITY IN MEDITERRANEAN BOTTOM TRAWLS

Adnan TOKAÇ[1], Celalettin AYDIN[1], Tuğçe ŞENSURAT[2], Enis Noyan KOSTAK[3]
[1]Ege University, Fisheries Faculty, 35100 Bornova, İzmir, Türkiye
[2]İzmir Katip Çelebi University, Fisheries Faculty, İzmir, Türkiye
[3]Norwegian College of Fishery and Aquatic Science, UiT the Arctic University of Norway, Breivika, Tromsø, Norway

Abstract

This study examines the size selectivity performance of a 40 mm knotless square mesh codend constructed from flexible Dyneema netting, compared to traditional codends made of polyethylene (PE) and polyamide (PA) materials in Mediterranean bottom trawl fisheries. Selectivity was evaluated for three commercially important species: red mullet (*Mullus barbatus*), picarel (*Spicara smaris*), and bogue (*Boops boops*). Field trials were conducted in the Eastern Aegean Sea using a commercial trawler and a modified demersal trawl gear setup. Size selectivity was assessed using the hooped covered codend method, and statistical analyses were performed using SELNET software, applying various logistic models with model selection based on the Akaike Information Criterion.

Results indicate that the Dyneema codend demonstrated significantly higher selectivity (L50 values) than traditional codends. For red mullet, the L50 was estimated at 13.03 cm, nearly matching the minimum landing size (MLS), with a selection range (SR) of 1.77 cm. For picarel, L50 and SR were 14.38 cm and 1.09 cm, respectively. For bogue, L50 and SR were 14.62 cm and 1.32 cm. The narrow selection ranges and high R^2 values across species indicate precise and effective size selection.

These findings highlight the superior selectivity of Dyneema codends, supporting their potential as a viable alternative to traditional materials in trawl fisheries. Their use may contribute to reducing juvenile bycatch and enhancing sustainable fishing practices in the Mediterranean. This research was supported by the Ege University Science and Technology Centre (Project No. 2016-SUF-026).

Keywords
Bottom trawl, codend, size selectivity, dyneema, Mediterranean

Introduction
The use of fishing gears and devices that possess selective properties—allowing the escape of undersized fish and juveniles below the minimum landing size—is of critical importance for the conservation of fish stocks and the implementation of sustainable fisheries practices (Armstrong et al., 1990; Tokaç et al., 2020). In other words, a selective fishing gear should retain fish above the first capture size while enabling the escape of those below it.

Bottom trawls are widely employed in demersal fisheries. Since gear selectivity occurs predominantly in the codend section of the trawl, most selectivity studies have focused on this part (Beverton, 1963; Wileman et al., 1996). The type of netting material used in the codend is also a key factor influencing selectivity (Holden, 1971; Tokaç et al., 2004). Traditionally, codends of bottom trawls are constructed from multimonofilament polyethylene (PE) netting; however, the coarse structure of this material tends to reduce selectivity (Tokaç et al., 2004). Moreover, compared to other synthetic fibers, PE is relatively rigid, which often leads to poor knot tightening and knot slippage, resulting in irregular mesh openings in the codend (Tokaç et al., 2004).

In recent years, technological advancements in the textile industry have introduced the potential use of the high-performance polymer fiber "Dyneema®" in fisheries (Tokaç, 2011). Dyneema® fiber, which has been increasingly adopted in fisheries over the last 15–20 years (Tokaç, 2011; Herrmann et al., 2015), is produced using the ultra-high molecular weight polyethylene (UHMWPE) technique and is considered one of the strongest fibers in the world. It is 15 times stronger than steel and approximately 40% lighter than highly durable materials such as aramid (Tokaç, 2011). Trawl nets made from Dyneema® are more durable and significantly lighter than those constructed from polyamide or polyethylene. This reduced weight decreases friction, thereby lowering fuel costs and enabling fishing vessels to operate more quickly and safely (Tokaç et al., 2020). Previous studies indicate that replacing PE codend netting with Dyneema® may have positive effects on size selectivity (Herrmann et al., 2015; Tokaç et al., 2020).

The present study investigated the effect of Dyneema® codend netting on size selectivity for commercially important species such as red mullet (Mullus barbatus), picarel (Spicara smaris), and bogue (Boops boops) in Mediterranean bottom trawl fisheries. For this purpose, trials were conducted using a legally

compliant bottom trawl codend constructed from Dyneema® netting with 40-mm square mesh size, in accordance with the relevant EU, GFCM, and Turkish fisheries regulations. This research represents the first attempt in Turkey to evaluate the selectivity of trawl codends made from Dyneema® netting. The study was supported by the Ege University Scientific Research Projects Coordination Unit under Project No. 16-SÜF-026.

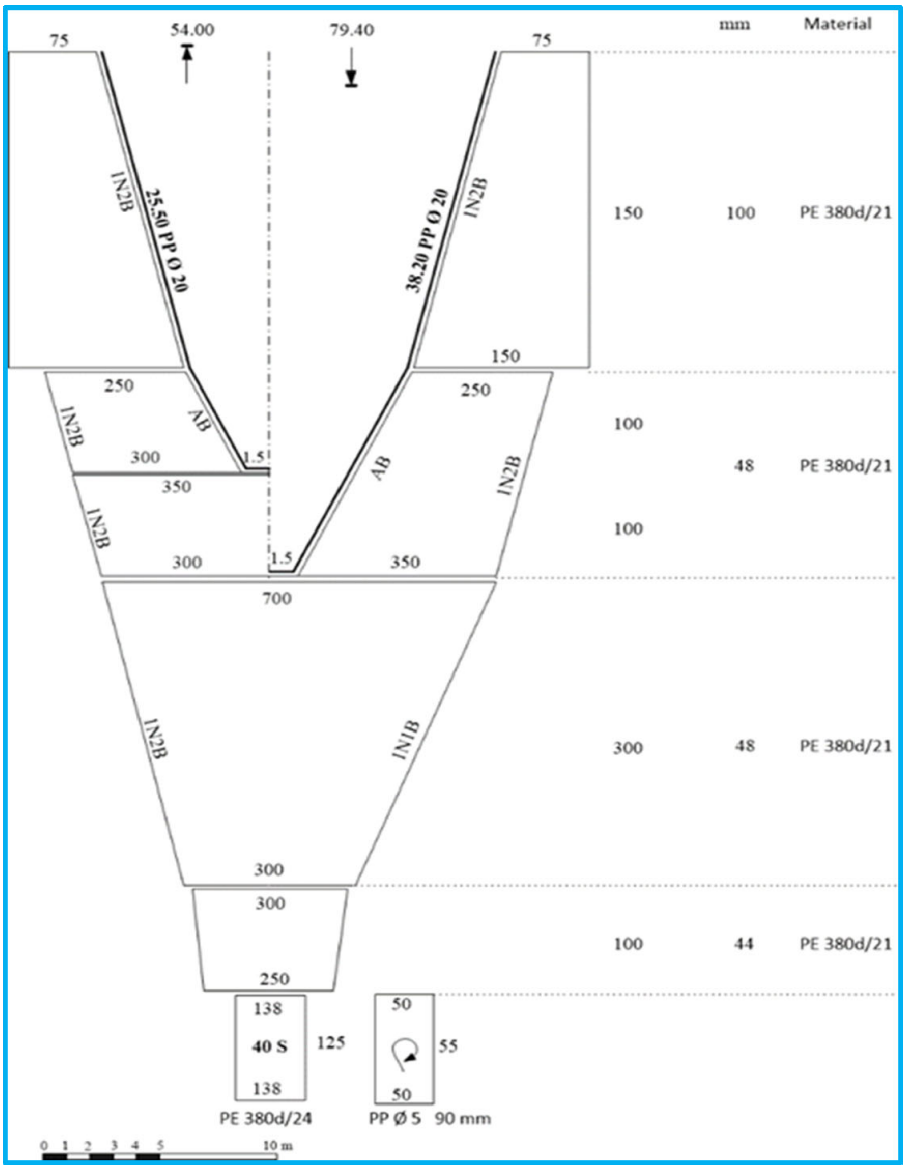


Figure 1
Adaptation of the experimental trawl codend to the commercial trawl net.

Materials and Methods

The field trials were carried out in the Eastern Aegean Sea during the period of February and March 2018. A commercial trawler named “Efsane G” was utilized for the experimental fishing operations. The vessel employed a modified 700-mesh bottom trawl net (Figure 1).

The experimental codend was constructed from knotless Dyneema® netting material The number of meshes on its circumference is 138 meshes (Figure 2). The cover net was made of knotless polyamide (PA) netting with a nominal mesh size of 24 mm and supported by hoops, that 1.9 m in diameter was tied on codend and protective net (Figure 2). The selectivity of the codends was estimated using the hooped covered codend method described by Wileman et al. (1996).



Figure 2
Dyneema trawl codend and hooped covered codend used in the experiments.

Data Analysis

The collected data were analyzed using the SELNET software (Herrmann et al., 2012, 2013). Four different models—Logit, Probit, Gompertz, and Richard—were tested to define the retention probability $r_{av}(l,v)$ for each species. The model exhibiting the lowest Akaike Information Criterion (AIC) value (Akaike, 1974) was selected as the most suitable for the analysis of the selectivity data for each specific species. The selection parameters, L50 (length at 50% retention) and SR (selection range), were estimated using the maximum likelihood method with a logistic equation.

The analyses incorporated the double bootstraps method to account for between-haul variations. This approach is identical to the one described in Millar (1993) and takes both within-haul and between-haul variation into consideration. Each bootstrap resulted in a “pooled” set of data, which then was analyzed using the

identified selection model. Thus, each bootstrap run resulted in an average selection curve. 1000 bootstrap repetitions were conducted to estimate the Efron percentile 95% confidence limits (Herrmann et al., 2012)

Results

The species composition of the catch obtained from the trawl selectivity experiments conducted in this study is presented in Figure 3. Three of the four species for which selectivity was examined—namely red mullet (*Mullus barbatus*), picarel (*Spicara smaris*), and bogue (*Boops boops*)—constituted a significant proportion of the total catch. Species of economic importance accounted for approximately 40% of the total catch, whereas the proportion of discarded and non-marketable species reached up to 60% of the overall catch composition. This alone clearly indicates the necessity of substantial improvements, particularly in terms of selectivity, to ensure the sustainability of this fishery.

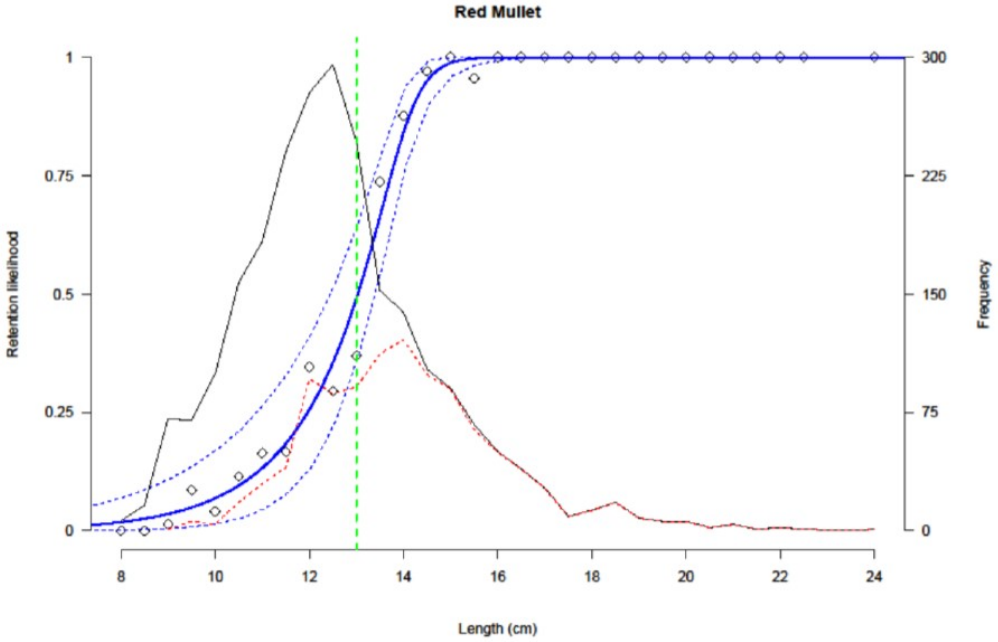


Figure 3
Length frequency distributions and selection curve with confidence limits and observed retention percentages as data points (empty diamonds) of red mullet.

A total of nine valid hauls were conducted using a 40-mm knotless square-mesh Dyneema trawl codend. Both the codend and the cover net were towed for a combined total of approximately 23.5 hours, resulting in a total catch of around 770 kg. Within this total catch, the composition was as follows: red mullet (*Mullus barbatus*) 8.14%, bogue (*Boops boops*) 4.79%, picarel (*Spicara smaris*)

4.76%, European hake (*Merluccius merluccius*) 7.61%, and cephalopods 7.38%. The number of fish caught in the codend and cover net varied among species. The total number of individuals retained in the codend and cover combined was 2,396 for red mullet, 1,723 for bogue, and 2,957 for picarel.

Red mullet selectivity was best described by the Richard model, which showed a good fit (p-value = 0.0007, R^2 = 0.9921). The selectivity curve indicated an L_{50} (length at 50% retention) of approximately 13 cm (13.03) within the confidence interval, with a corresponding SR value (selection range) close to this value (Figure 3). Since the minimum legal landing size for red mullet is 13 cm, these results suggest that the tested trawl codend is suitable for capturing red mullet.

Picarel selectivity was also best described by the Richard model, with a good model fit (p-value = 0.0467, R^2 = 0.9919). The selectivity curve fell within the confidence interval. The L_{50} and SR values were estimated as 14.38 cm and 1.09, respectively (Figure 4). A total of 2,957 picarel were caught, and their length distribution exhibited two peaks at 8.0 cm and 12 cm. No minimum legal landing size is specified for this species in the Turkish fisheries regulations. Previous studies indicate that the first maturity size for picarel occurs at approximately 11.8 cm. Considering this, the tested trawl codend appears highly suitable for picarel.

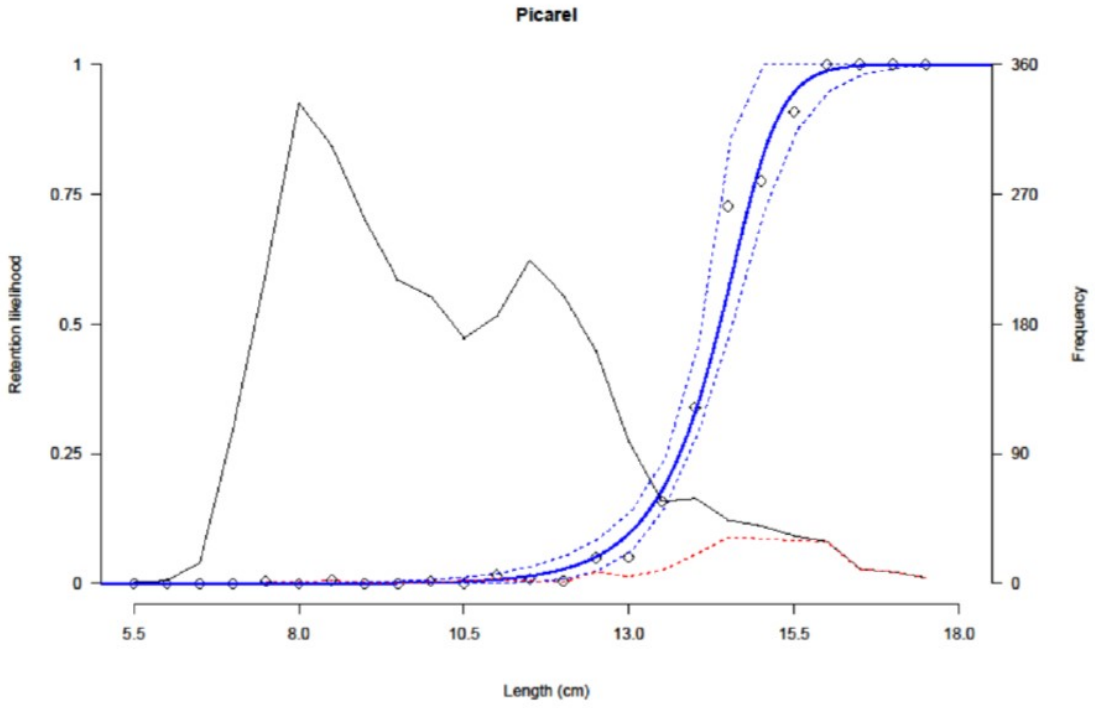


Figure 4
Length frequency distributions and selection curve with confidence limits and observed retention percentages as data points (empty diamonds) of picarel.

Bogue (*Boops boops*) selectivity was best described using the logistic model, which showed a good fit (p-value = 0.1878, $R^2 = 0.9933$). A total of 1,723 bogue individuals were caught, with the majority concentrated in the 11.5 cm length class (Figure 5). The L_{50} and SR values were estimated at 14.62 cm and 1.32, respectively. Although no minimum landing size is specified for this species in Turkey, a 13 cm minimum size limit is recognized internationally

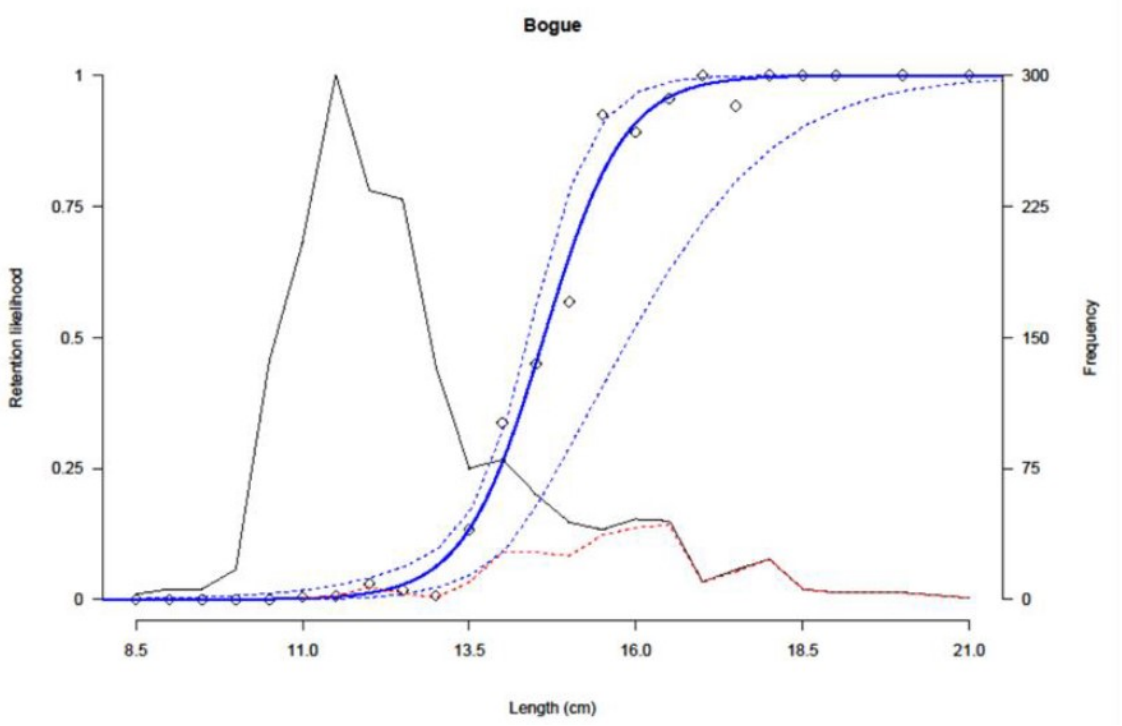


Figure 5
Length frequency distributions and selection curve with confidence limits and observed retention percentages as data points (empty diamonds) of bogue.

Conclusion and Future Steps

This study investigated the selectivity of a knotless Dyneema trawl codend with a nominal mesh size of 40 mm. The research focused on red mullet, picarel, and bogue, with the selectivity parameters and corresponding curves for each species presented in the results section. When the selectivity characteristics of these three species are compared collectively, it is evident that the tested Dyneema trawl codend aligns well with the selectivity models for all three species. Notably, the selectivity curve for picarel exhibits narrower 95% confidence intervals compared to the other two species.

Table 1
Selectivity studies and present work for three diffirent fish species (red mullet, picarel, bogue) in the Mediterranean.

Species	Mesh size (mm)	Mesh Type	Material	n	L50 (cm)	SR	References
Red Mullet	**37.98**	**S knotless**	**Dyneema**	**138**	**13.0**	**1.8**	**Present study**
Red mullet	40	S knotted	PE	150	13.0	1.5	Özbilgin et al., 2011
Red mullet	41.36	S knotted	PE	150	14.1	2.6	Özbilgin et al., 2011
Red mullet	36	S braided	PE	N/A	10.4	3.9	Sarda et al., 2006
Red mullet	40	S knotled	PA/PE	N/A	12.2	2.1	Ordines et al., 2006
Red Mullet	38.65	S knotless	PA	140	10.9	1.4	Sala et al., 2008
Picarel	**37.98**	**S knotless**	**Dyneema**	**138**	**14.38**	**1.1**	**Present study**
Picarel	36	D	PA	200	13.3	1.3	Tokaç et al., 2004
Picarel	40	D	PE	200	12.4	2.4	Tokaç et al., 2004
Picarel	40	D	PA/PE	N/A	9.0	5.1	Ordiles et al., 2006
Picarel	40	S	PA/PE	N/A	17.1	6.9	Ordiles et al., 2006
Picarel	40	D	PE	200	13.5	N/A	Özbilgin et al., 2007
Picarel	44	D	PE	300	7.8	4.7	Eryaşar et al., 2014
Picarel	43.88	D	PE	150	10.18	3.8	Eryaşar et al., 2014
Bogue	**37.98**	**S**	**Dyneema**	**138**	**14.5**	**1.3**	**Present Study**
Bogue	47.57	D	PE	300	6.8	3.1	Eryaşar et al., 2014
Bogue	43.88	D	PE	150	7.6	3.5	Eryaşar et al., 2014

As shown in Table 1, when the L_{50} and SR values corresponding to mesh size are compared with previous studies, the Dyneema trawl codend tested in this study demonstrates favorable selectivity for red mullet, picarel, and bogue, respectively. This results is in parellel with previous study (Herrmann et al, 2015). Full square mesh codend made of 40 mm knotless Dyneema netting could be most useful option for the Mediterranean fisheries.

Due to its structural characteristics, Dyneema® netting is expected to exhibit greater selectivity compared to conventional nylon nets. The selectivity results obtained in this study confirm this expectation. This finding may prompt a reevaluation of the codend materials used in trawl fisheries. From a sustainable fisheries perspective, there is a need for similar studies to be conducted on a larger scale with project-based support to enable the use of more selective netting materials in commercial fishing.

Acknowledgements

We would like to thank the captain and crew of the commercial trawler “EF-SANE G” for their close attention and valuable assistance to the research team during the marine surveys. This study was supported by Ege University BAP Coordination Unit under Project No. 16-SÜF-026. We also extend our gratitude to the Ege University Scientific Research Projects Coordination Office for their support.

References

1. Armstrong, D. W., Ferro, R. S. T., MacLennan, D. N., and Reeves, S. A. – Gear selectivity and the conservation of fish – Journal of Fish Biology, 37, Suppl. A, 1990, 261–262
2. Beverton, R. J. H. – Escape of fish through different parts of a codend – In *The selectivity of fishing gear: Proceedings of joint ICNAF/ICES/FAO special scientific meeting, Lisbon, 1957*, pp. 9–11, International Commission for the Northwest Atlantic Fisheries, 1963
3. Eryaşar, A. R., Özbilgin, H., Gökçe, G., Doğanyılmaz Özbilgin, Y., Saygu, İ., Bozaoğlu, A. S., Kalecik, E. – The Effect of Codend Circumference on Selectivity of Hand-Woven Slack Knotted Codend in the North Eastern Mediterranean Demersal Trawl Fishery – Turkish Journal of Fisheries and Aquatic Sciences, 14, 2014, 463–470
4. Herrmann, B., Sistiaga, M., Nielsen, K. N., and Larsen, R. B. – Understanding the size selectivity of redfish (Sebastes spp.) in North Atlantic trawl codends – *Journal of Northwest Atlantic Fishery Science*, 44, 2012, 1–13.

5. Herrmann, B., Wienbeck, H., Moderhak, W., Stepputtis, D., and Krag, L. A. – The influence of twine thickness, twine number and netting orientation on codend selectivity – *Fisheries Research*, 145, 2013, 22–36.

6. Herrmann, B., Wienbeck, H., Stepputtis, D., Krag, L. A., Feekings, J., and Moderhak, W. – Size selection in codends made of thin-twined Dyneema netting compared to standard codends: A case study with cod, plaice and flounder – *Fisheries Research*, 167, 2015, 82–91.

7. Holden, M. J. (Ed.) – Report of the ICES/ICNAF working groups on selectivity analysis – ICES Coop. Res. Rep., Ser. A, No. 25, 1971

8. Millar, R. B. – Analysis of trawl selectivity studies (addendum): implementation in SAS – *Fisheries Research*, 17(3–4), 1993, 373–377.

9. Ordines, F., Massutí, E., Guijarro, B., and Mas, R. – Diamond vs. square-mesh codend in a multi-species trawl fishery of the western Mediterranean: effects on catch composition, yield, size selectivity and discards – *Aquatic Living Resources*, 19, 2006, 329–338.

10. Özbilgin, H., Tosunoğlu, Z., Tokaç, A., and Metin, G. – Seasonal variation in the trawl codend selectivity of red mullet (Mullus barbatus) – *Turkish Journal of Fisheries and Aquatic Sciences*, 11, 2011, 191–198.

11. Özbilgin, H., Tosunoğlu, Z., Tokaç, A., and Metin, G. – Seasonal variation in the trawl codend selectivity of picarel (Spicare smaris) – *ICES Journal of Marine Science*, 64, 2007, 1569–1572.

12. Sala, A., Lucchetti, A., Piccinetti, C., and Ferretti, M. – Size selection by diamond- and square-mesh codends in multi-species Mediterranean demersal trawl fisheries – *Fisheries Research*, 93, 2008, 8–21.

13. Sardà, F., Bahamon, N., Moli, B., Sardà-Palomera, F. – The use of a square mesh codend and sorting grids to reduce catches of young fish and improve sustainability in a multi-species bottom trawl fishery in the Mediterranean – Sci. Mar., 70, 2006, 347–353

14. Tarım ve Orman Bakanlığı – 6/1 numaralı ticari amaçlı su ürünleri avcılığının düzenlenmesi hakkında tebliğ (Tebliğ No: 2024/20) – T.C. Resmî Gazete, 2024

15. Tokaç, A. – Net Construction and Equipment Techniques (Fisheries II) – Ege University Publications, Faculty of Fisheries, Publication No: 80, Textbook Series No: 40, 2nd edition, Bornova-İzmir, 2011.

16. Tokaç, A., Aydın, C., and Şensurat, T. – Determination of Selectivity of Dyneema Net Material in Demersal Trawl Fisheries: Project No: 16-SÜF-026 Final Report of the General Research Project – Ege University Scientific Research Projects Coordination Unit, 2020.

17. Tokaç, A., Özbilgin, H., and Tosunoğlu, Z. – Effect of PA and PE material on codend selectivity in Turkish bottom trawl – Fisheries Research, 67, 3, 2004, 317–327

18. Tosunoğlu, Z., Aydın, C., and Özaydın, O. – Selectivity of a 50-mm diamond mesh knotless polyethylene codend for commercially important fish species in the Aegean Sea – Journal of Applied Ichthyology, 24, 3, 2008, 311–315
19. Wileman, D. A., Ferro, R. S. T., Fonteyne, R., and Millar, R. B. (Eds.) – Manual of methods of measuring the selectivity of towed fishing gears – ICES Cooperative Research Report No. 215, 1996

DEVELOPING AND TESTING BENTHOS RELEASE PANELS IN BROWN SHRIMP BEAM TRAWL FISHERIES

Juan SANTOS[1*], Annika BRÜGER[1], Henning DULZ[2] & Daniel STEPPUTTIS[1]
[1]Thünen Institute of Baltic Sea Fisheries, Survey and Fisheries Technologies, Alter Hafen Süd 2, Rostock, 18069, Germany
[2]Fischereibetrieb Henning Dulz, Buernstraat 10, Wyk auf Föhr, 25938, Germany

Abstract

In the North Sea brown shrimp beam trawl fisheries, the bycatch of unwanted benthic species is an unsolved issue of increasing concern. To address this issue, German fishers have proposed new gear technologies combining an innovative four-sheet trawl design and Benthos Escape Panels (BEPs), made of large diamond meshes and inserted in the bottom sheet of the trawl. Sea trials testing the performance of three BEP designs varying in dimensions and mounting position were conducted onboard research vessel. The experimental setup used a twin trawl configuration for comparing the catches of four-sheet trawls with and without BEP mounted. Analysis of the resulting paired-gear catch data revealed that mounting BEPs can reduce the bycatch of benthos above 65% in weight when placed in front section of the trawl, while the release efficiency is reduced in ~10 percentage points when placing the BEP at the middle section of the trawl. Mounting BEPS on the front section also reduced bycatch of flatfish species between ~20 and ~50%, which would otherwise have ended up in the codend, even when using the mandatory sieve nets. Catches of marketable brown shrimp were also affected with ~25% average catch losses independently of the BEP design applied. Our results reveal the potential of using simply trawl modifications to reduce the bycatch of benthic species and highlight the importance of collaborative work between fishermen and scientists. Further investigations under commercial and research conditions are being planned with the aim of boosting the optimisation of these technologies for potential commercial uptake.

Keywords

Brown Shrimp, Beam trawl, Bycatch reduction, Benthos, Escape panels

Nomenclature

BEP – Benthos Escape Panel
CC(l) – Catch Comparison curve estimated for brown shrimp

CR(*l*) – Catch Ratio curve derived from CC(l) describing the catch efficiency of a test trawl mounting
iCR – integrative Catch Ratio indicator

Introduction

The development of selective fishing gears is an important management strategy for achieving sustainable commercial fisheries from economic and ecosystem perspectives. In the North Sea beam trawl fisheries targeting brown shrimp, the by-catch of unwanted species is a long-lasting problem. To mitigate bycatch in these fisheries, fishermen are obliged to use either sieve-nets or sorting grids in their trawls to exclude bycatch species before they enter the codend. While these technologies can effectively reduce bycatch (Polet, 2002; Polet et al., 2004; Revill and Holst, 2004), none of them deliver an optimal species separation, particularly with regard to the bycatch of juvenile fish. Catching juvenile fish is not only an ethical issue but also a management challenge, especially in the case of regulated species such as plaice (*Pleuronectes platessa*), for which the fishery has no quota. The bycatch of benthos mix (herein referred to assemblages of invertebrates with low mobility living close to the seabed, shells and other debris) is another unsolved issue with negative implications for the efficiency of the capture process and the catch processing on deck. Once entering the trawl, the benthos mix can cause clogging of the netting and blockages that reduce the sorting efficiency of implemented bycatch reduction devices. Furthermore, the presence of benthos in the catch can make the sorting on deck more difficult and ultimately reduce the quality of the marketable catch fraction. One simple strategy to reduce the bycatch of benthos and flatfish species is to apply large-mesh escape panels in the bottom panel of the trawl (Revill and Jennings, 2005; van Marlen *et al.*, 2005; Wade *et al.*, 2009; Kajikawa *et al.*, 2013). This strategy has been recently adopted by German fishers, and the promising results obtained during initial commercial trials have incentivized a deeper scientific evaluation of the potential of these technologies to improve species selection and catch patterns in brown shrimp fisheries. Based on experimental sea trials conducted in research vessel, this study evaluates the performance of three different BEP designs by addressing the following research questions:

- Can an escape panel installed in the bottom of the trawl be an efficient tool for reducing the bycatch of the benthos mix component, as well as flatfishes and other unwanted fish species in beam-trawl fisheries targeting brown shrimp?
- What is the risk of losing marketable shrimp due to the use of these technologies?
- Can the efficiency of escape panels be related to specific design characteristics or positioning in the trawl body?

Material and Methods

To address the research questions of the study, three different BEP designs made of large diamond meshes (100 mm nominal half-mesh, Table 1) were tested. The initial BEP design was inserted into the lower sheet of the front section of the trawl. The number of free meshes in the front and rear transversal edges of the panel were 53 and 42 respectively, and the panel depth along the longitudinal axis of the trawl was 11.5 meshes. The second design was achieved by covering 8 large meshes on each side of the panel along its longitudinal axis by using small-mesh net strips. Therefore, this modification reduced the number of open meshes by narrowing the width of the original panel. These two designs are hereafter referred to as Front BEP-wide and Front BEP-narrow, respectively (Figure 1). The third BEP design was inserted into the lower sheet of the middle section of the trawl, with 43 and 28 open meshes at the front and rear edges, and with 22.5 open meshes in depth. This third design is hereafter referred to as Mid BEP-wide. Each design was tested one at a time by installing them to a four-sheet trawl (Figure 1). This four-sheet trawl configuration was chosen because it is thought to provide a better control over the positioning of installed selection devices such as BEP's. The mesh sizes of the trawl were representative of those currently used in the fishery, ranging from 27.8 mm stretched mesh size (Fonteyne, 2003) in the front section, to 25.6 mm at the codend (Table 1).

Table 1

Nominal mesh size (half mesh) and measured mesh sizes (stretched mesh size measured according to Fonteyne (2003) of the different trawl sections and BEP designs. Values in brackets represent the standard deviation of the sampled mesh measurements.

	Nominal half mesh [mm]	Measured mesh opening [mm]
Trawl section 1	14	27.8 (0.5)
Trawl section 2	13	24.8 (0.7)
Trawl section 3	13	25.6 (0.7)
Codend	13	25.6 (0.7)
Front BEP-wide/narrow	100	192.9 (1.9)
Mid BEP-wide	100	193.3 (1.6)

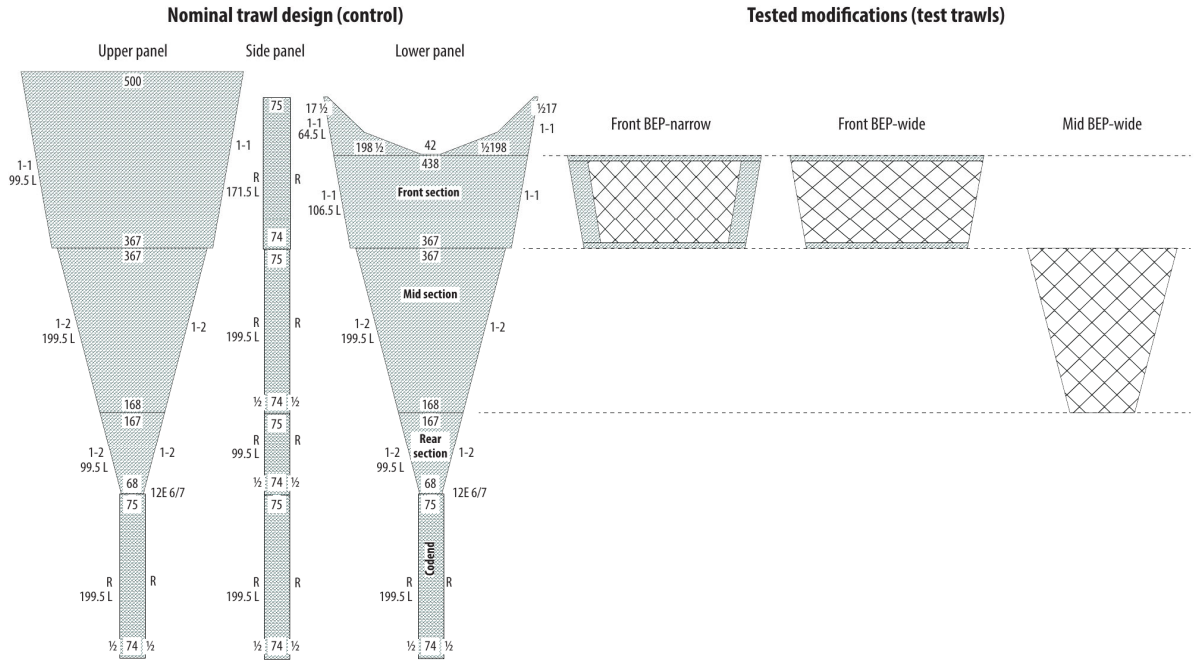


Figure 1
Technical drawing of the four-sheet trawl used during the experimental fishing trials and the three BEP designs tested (one at a time).

The performance of the three BEP designs (Figure 1) was tested during experimental fishing trials on board the German FRV "Solea", between 28 of March and 09 April 2025 in coastal German waters of the Wadden Sea. The tows were conducted during daylight at fishing depths averaging 11.5 m (std.dev = 2.0), the towing speed was set at 3 knots, and the towing duration averaged 36 min (std.dev = 11.0). The experimental design applied was the so-called paired-gear method (Wileman *et al.*, 1996), using the twin-trawl facilities of the vessel. One of the twin trawls mounted the BEP under evaluation (test trawl, *t*). The other trawl remained with the floor sheet in its nominal configuration (control gear, *c*). As the test and control trawls fished simultaneously and in parallel, it was assumed that both encountered the same fish and shrimps' populations, as well as same benthic assemblages during individual hauls. Consequently, the efficiency of the tested BEP designs to reduce bycatch and their potential impact on the catchability of the targeted shrimp was evaluated by quantifying the differences in catches between the two trawls. For the targeted shrimps, differences in catches were evaluated at individual length-classes by estimating catch comparison curves, CC(*l*) (Krag *et al.*, 2014; Santos *et al.*, 2022). Based on catch frequencies at length *l* in the test and control trawl across hauls ($n_{tl} = \sum_{i=1}^{h} n_{til}$ and $n_{cl} = \sum_{i=1}^{h} n_{cil}$, respectively), catch comparison curves describe the share of catches of length *l* in the test trawl relative to the total catch ($n_{tl} + n_{cl}$). Therefore, a value of CC(*l*) = 0.5 would imply equal catch share

among the test and the control gears, suggesting no effect of the tested BEP design on catches. To a more direct quantification of the catch efficiency at length of the test trawl relative to the control trawl, fitted catch comparison curves were derived into catch ratio curves CR(*l*) (Santos *et al.*, 2022). This transformation implies that the value for equal catch efficiency becomes CR(*l*) = 1.0, making the potential gain or loss of catch efficiency in the test trawl easier to interpret. For instance, a value of CC(*l*) = 0.4 is related to 80% catch efficiency of the test trawl relative to the control trawl, and when derived into catch ratio values, it becomes CR(*l*) = 0.8. Therefore, the later suggest a catch loss of 20% due to the BEP effect in the test trawl. To obtain an overall evaluation of the effect of BEPs across individual length classes, we estimated integrative catch ratio estimators (iCR) for the undersized (l<50 mm), marketable (l≥50 mm) and overall catches of the targeted shrimp. For the evaluation of BEP´s performance on fish species, overall iCR were estimated, this due to the limited range of length classes of fish species caught. Interpretation of the magnitude of differences in catches obtained with iCR is equivalent to pointwise values from the estimated CR*(l)* curves. Uncertainties in estimation of CC*(l)*, CR*(l)* and iCR were quantified using a double bootstrap method, in which the process of generating bootstrap data takes into consideration the finite number of shrimp / fishes sampled within-haul as well as the variation naturally occurring between fishing hauls.

Results

The performance of the three BEP designs were successfully tested, resulting in 51 valid hauls collected across designs (Front BEP-narrow = 19 hauls, Front BEP-wide =19 hauls, Mid BEP-wide = 15 hauls). Overall, a very large reduction of the benthos mix component of the catches was observed in the test trawl regardless of the BEP design applied (Figure 1). In particular, the mass of the benthos mix component observed in the control trawl was reduced by ~65% when either of the two Front BEPs was applied to the test trawl (Figure 2). Using the Mid BEP-narrow design delivered a release efficiency on the benthos mix component 10 percentage points below compared to the previous designs (55%). The iCR values obtained for the most abundant fish species in catches and with demersal or benthic habits showed a consistent reduction by more than 20%, regardless of the BEP design used (Figure 3). A significant reduction in catches of plaice and dab, the two most abundant flatfish species in catches, occurred when the BEP was placed in the front section. For dab, its bycatch was reduced to almost 50% with the Front BEP-wide installed. Significant reductions in the bycatch of flounder occurred both at the Front and Mid-section. As for dab, maximum bycatch reduction for this species occurred when using the Front BEP-wide design (58% reduction). In contrast, the bycatch of

whiting, a demersal species with active swimming behaviour, was not affected by the presence of a BEP in the test trawl (Figure 3).

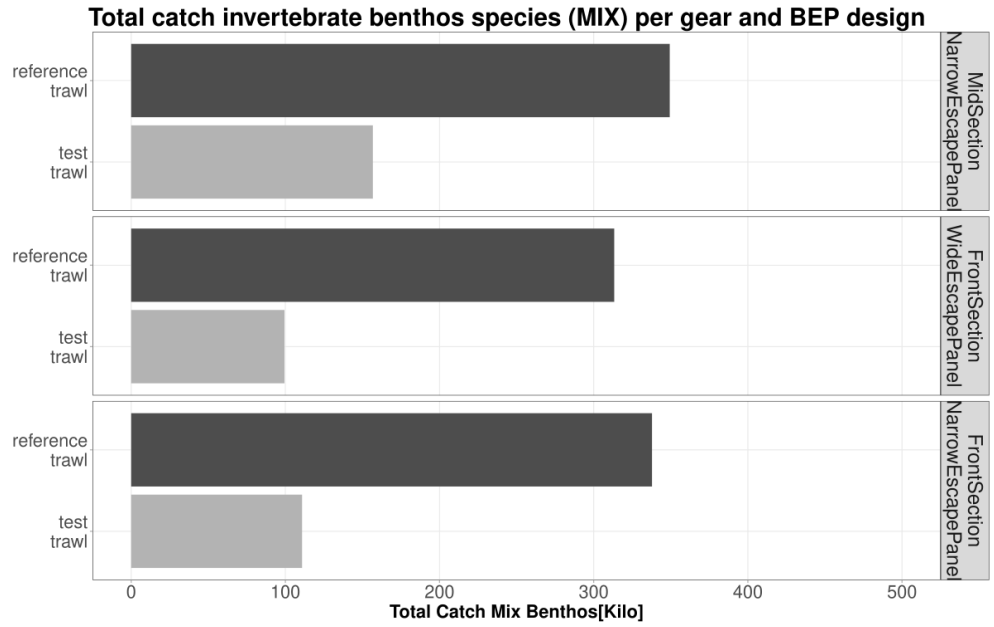


Figure 2
Overall catches (total kilos per trawl pooled across hauls) of the benthos mix observed in the test and control trawl by BEP design tested.

Catches of the targeted shrimp were consistently and significantly affected by the presence of a BEP in the test trawl. Losses of marketable sizes ranged between 22% and 27% depending on the BEP design applied (Figure 4). The reduction in the bycatch of undersized shrimp was in general greater than that of the marketable fraction, especially when the Mid BEP-wide design was applied. In particular, the use of this Mid BEP design resulted in a clear and positive dependency between relative catch efficiency of the test trawl and shrimp length (Figure 5). This nearly linear relationship explains the large discrepancy in the reduction in undersized shrimp catches (~50%) and catch losses of marketable sizes (~27%) obtained with the Mid BEP-wide design (Figure 4). Catch comparison / ratio curves associated to the remaining BEP designs did not show a clear length-dependency on relative catch rates. The lack of overlapping between the pointwise upper confidence limits associated to the average CC(l) and CR(l) curves with the reference lines marking equal catch efficiency among test and control trawls (CC(l) = 0.5 and CR(l) = 1.0 respectively) reveals a lack of support for the hypothesis of equal catch efficiency of control and test trawls for a wide range of lengths.

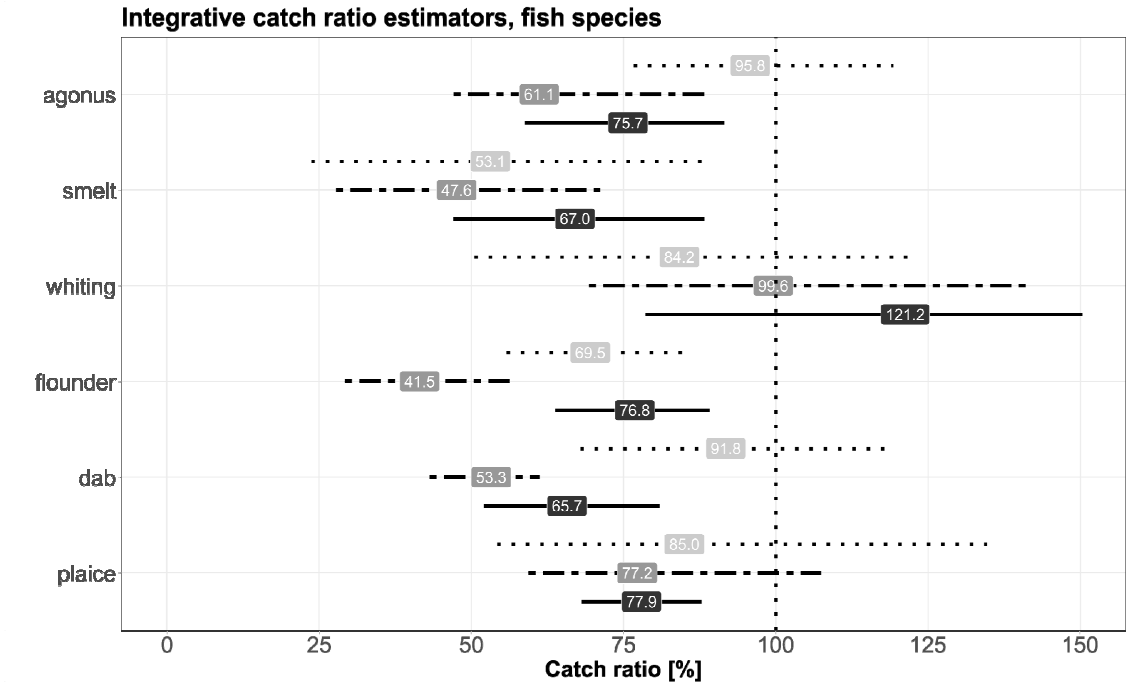


Figure 3
Integrative catch ratio (iCR) for the most abundant fish species in catches by BEP design (black =Front BEP-narrow, dark grey = Front BEP-wide, light grey = Mid BEP-wide). Horizontal bars represent 95% confidence intervals.

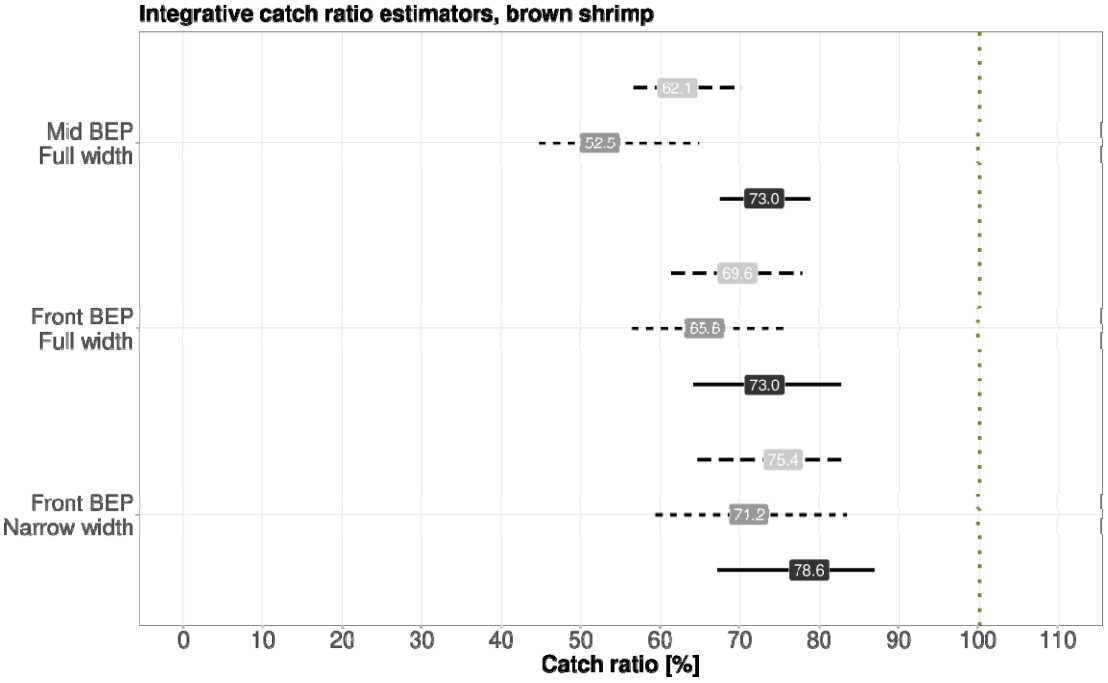


Figure 4
Integrative catch ratio indicators (iCR) for brown shrimp by catch fraction and BEP design (black =Front BEP-narrow, dark grey = Front BEP-wide, light grey = Mid BEP-wide). Horizontal bars represent 95% confidence intervals.

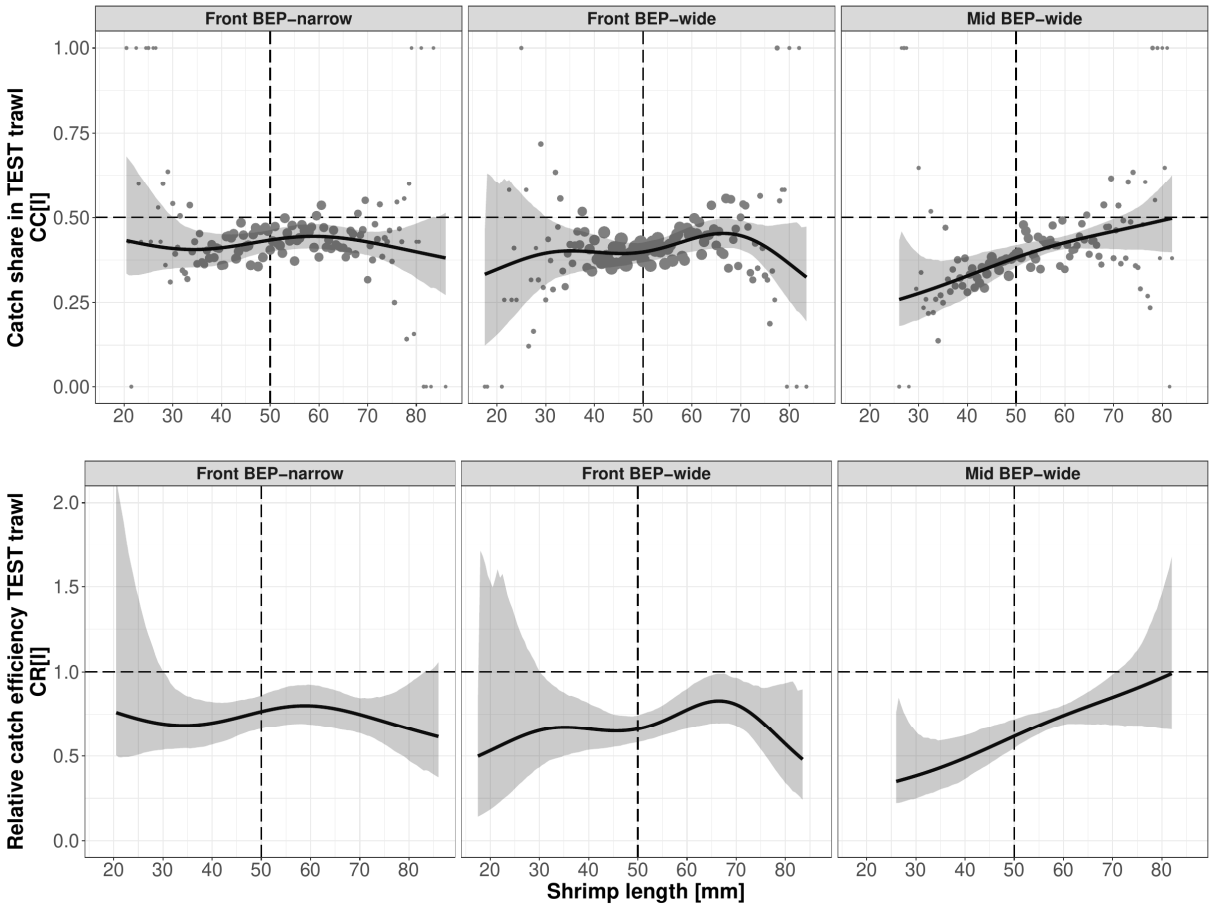


Figure 5
Top row: Average catch comparison curves (CC(*l*)), solid line) estimated for brown shrimp by BEP design. Grey shadowed areas: Pointwise 95% confidence intervals of the estimation. Circles: empirical catch share at length. Horizontal dashed line: value indicating equal catch share among test and control gears. Vertical dashed line: species approximate minimum marketable size (50 mm). Bottom row: Catch ratio curves CR(*l*)) derived from CC(*l*).

Discussion

Our study shows that by inserting benthic escape panels (BEP) into the lower sheet of the trawl, most of the unwanted mix of benthos (formed by benthic invertebrates, shells and other debris) can be excluded shortly after entering the trawl. Comparing the three tested designs reveals that placing a BEP ~10 meshes away from the fishing line results in a greater reduction of benthos mix than positioning it deeper in the mid-trawl section (average ~65% vs ~55% reduction). However, the study did not find clear differences between the Front BEP-wide and BEP-narrow benthos mix reduction. Therefore, no link could be stablished between number of open meshes and amplitude on the transversal axis of the panel on its performance. Bycatch reduction of flatfish species was also detected, and the magnitude of the reduction was found to be dependent on

the species evaluated and the BEP design tested (Figure 3). The average iCR obtained by flatfish species and BEP design suggests that the release of plaice and dab is more likely to happen using Front BEPs while release of flounder occurred significantly in both Front and Mid positions. Therefore, decisions regarding the placement of the BEP in the longitudinal axis of the trawl should take into consideration flatfish species-specific differences in performance and the potential impact of the bycatch of these species on the economic and ecological sustainability of the fishery. Our study also found significant catch losses of targeted brown shrimp by ~25% regardless of the BEP design or the positioning applied. The negative short-term impact of the reported catch losses of targeted shrimp derived from the use of BEPs, without considering the subsequent sorting by any of the implemented selection devices in the fishery, is a major constrain for potential adoption of the current BEP designs in brown shrimp commercial fisheries. Therefore, further efforts are invested to optimize the BEP concept by focusing on improving the catchability of shrimps while keeping the observed bycatch reduction efficiency delivered by the current BEP designs. Such efforts are being made through collaboration between the researchers and the fishermen that initiated and promoted the current investigations on BEP technologies in the German brown shrimp fisheries. Furthermore, this collaborative work will make it possible a deeper evaluation of BEP´s potential considering spatio-temporal variability, and replicability in commercial conditions.

Acknowledgements

The authors would like to thank the “R/V Solea” crew, and the scientific crew for their invaluable contribution to the success of the fishing trials. Special thanks to our Belgian colleague Jasper Van Vlasselaer for joining and help us during the cruise. This work has been partly funded by the Ministry for Energy Transition, Climate Protection, Environment and Nature of the German state of Schleswig-Holstein, through the project Innovationsprogramm Krabbenfischerei Schleswig-Holstein (IPK)

References

1. Fonteyne, R. 2003. Review and evaluation of current mesh measurement methodologies and future perspectives.
2. Kajikawa, Y., Tokai, T., and Hu, F. 2013. Modeling of available size selectivity of the SURF-BRD for shrimp beam trawl. Fisheries Science, 79: 879–894. Springer.
3. Krag, L. A., Herrmann, B., and Karlsen, J. D. 2014. Inferring fish escape behaviour in trawls based on catch comparison data: Model development and evaluation based on data from Skagerrak, Denmark. PloS one, 9: e88819. Public Library of Science.
4. Revill, A. S., and Jennings, S. 2005. The capacity of benthos release panels to reduce the impacts of beam trawls on benthic communities. Fisheries Research, 75: 73–85.
5. Santos, J., Stepputtis, D., Oesterwind, D., Herrmann, B., Lichtenstein, U., Hammerl, C., and Krumme, U. 2022. Reducing cod bycatch in flatfish fisheries. Ocean & Coastal Management, 220: 106058.
6. van Marlen, B., Bergman, M. J. N., Groenewold, S., and Fonds, M. 2005. New approaches to the reduction of non-target mortality in beam trawling. Fisheries Research, 72: 333–345.
7. Wade, O., Revill, A., Grant, A., and Sharp, M. 2009. Reducing the discards of finfish and benthic invertebrates of UK beam trawlers. Fisheries Research: 8.
8. Wileman, D. A., Ferro, R. S. T., Fonteyne, R., and Millar, R. B. 1996. Manual of methods of measuring the selectivity of towed fishing gears. ICES Cooperative Research Report, 215. International Council for the Exploration of the Sea (ICES), Copenhagen, Denmark.

WINCHWATCH: CLOSING THE GAP BETWEEN VESSEL TRACKING AND GEAR-LEVEL FISHERIES MONITORING

Alen SOLDO[1], Nenad HERCIGONJA[1,2]
[1]Department of Marine Studies, University of Split, Split, 21000, Croatia
[2]PRIMARK Fisheries MCS technologies, Croatia

Abstract

Effective fisheries management requires accurate, high-resolution data on fishing effort, gear deployment, and vessel activity. While traditional vessel monitoring systems (VMS) and automatic identification systems (AIS) provide valuable information on vessel position and movement, they fail to capture gear-level operations that define the actual impact on marine ecosystems. The WinchWatch initiative addresses this gap by integrating advanced gear sensors (GearSenz and NetSenz) with onboard data systems and AI-driven analytical tools. This study explores the potential of large-scale sensor deployment for precise effort quantification, spatial micro-planning, and real-time compliance monitoring. Preliminary results from pilot applications in the Adriatic and Mediterranean fisheries demonstrate how sensor-generated data can provide ground truth for AI models, enhance the precision of spatial management tools, and support the transition toward sustainable, transparent, and data-driven fisheries governance. The research also discusses the technical, legal, and ethical challenges of implementing AI and IoT (Internet of Things) solutions in small-scale fisheries.

Keywords

fisheries monitoring, AI, sensor networks, WinchWatch, sustainable fisheries, spatial planning, data-driven management

Introduction

The sustainable management of marine resources depends on understanding how, when, and where fishing occurs. Current global monitoring systems rely largely on vessel-level tracking technologies, such as the Automatic Identification System (AIS) and Vessel Monitoring System (VMS), which provide information about vessel location and movement (Kroodsma et al., 2018). However, these systems do not reveal gear deployment events, fishing depth, or soak time: parameters that directly reflect fishing effort and ecosystem impact.

Recent developments in artificial intelligence (AI), Internet of Things (IoT) devices, and remote sensing technologies have opened new opportunities for fisheries monitoring, control, and surveillance (MCS). AI-powered algorithms can

process vast data streams from satellites, drones, and onboard sensors to identify fishing behavior, detect illegal activities, and predict catch composition (Welch et al., 2024). Yet, AI's performance and reliability depend on the availability of accurate, high-quality datasets for training and validation.

The WinchWatch project was conceived to close this persistent data gap by introducing gear-level sensors capable of recording detailed fishing operations in real time. By synchronizing these sensors with existing VMS data and AI-based analytical platforms, WinchWatch enhances both scientific understanding and management capacity. This study presents the conceptual design and preliminary outcomes of WinchWatch. Specifically, it aims to:

- Demonstrate how mass deployment of gear sensors improves the accuracy of fishing effort estimation;
- Explore the potential of gear-level data as ground truth for AI-based monitoring systems; and
- Discuss the implications of sensor-based monitoring for sustainable fisheries management, spatial planning, and regulatory compliance.

Materials and Methods

System Overview

The WinchWatch system consists of a network of sensors and dedicated software modules designed to monitor fishing effort at the gear level (Fig. 1). Two primary sensor types, GearSenz and NetSenz, were developed to collect operational data from fishing vessels.

GearSenz is attached to the fishing winch and records the exact time, location, and direction of winch rotation (Fig. 2). It counts full cycles of deployment and hauling, transmitting data to the Fisheries Monitoring Center (FMC) at predefined intervals. This enables precise detection of all gear operations, including potentially unregistered or illegal ones. It is mounted on the fishing vessel's winch in a tamper-evident way, so the potential manipulation is made harder and visible.

NetSenz is installed directly on nets to record the time and position of deployment and retrieval (Fig. 3). It also measures and logs into its internal memory, depth and temperature at one-minute intervals, allowing detailed analysis of net use and environmental context. Hence, it can be mounted on the net directly or alternatively on the otter boards (Fig. 4). Mounting on the net provides additional functionality of net authentication. This means that every net can be registered with all its physical characteristics (mesh size, length, width, type, etc.) and then NetSenz enables precise detection of the fishing operation with that exact net, with all its characteristics.

Together, the paired sensors capture both the action (gear use) and context (environmental parameters), creating a robust dataset for fisheries research and management applications (Table 1).

Table 1
Functional overview of GearSenz and NetSenz sensors.

Sensor	Primary Function	Key Parameters	Data Output	Transmission
GearSenz	Detects winch rotation	Time, location, direction, rotation count	Operation cycles	Scheduled to FMC
NetSenz	Detects net deployment/retrieval	Time, position, depth, temperature	Soak time, depth profile	Stored and transmitted

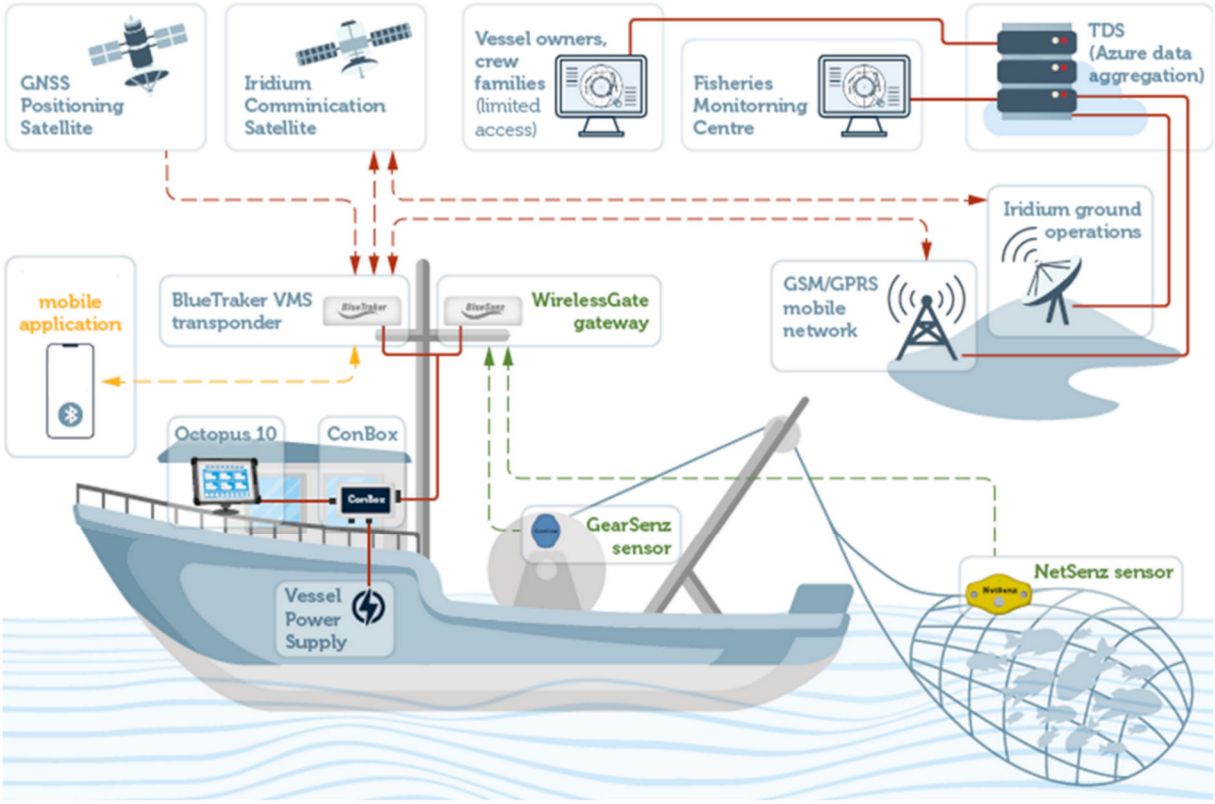


Figure 1
Conceptual overview of the WinchWatch system, showing integration between vessel sensors (GearSenz, NetSenz), onboard VMS, and data analytics tools (Compliance Monitor and Sustainability Planner).



Figure 2
GearSenz mounted of a fishing vessel's winch.



Figure 3
NetSenz mounted on the net.



Figure 4
NetSenz mounted of the otter board (with and without protection bracket).

Software and Data Flow

Two software applications were developed to process and interpret the sensor data:

- WinchWatch Compliance Monitor, a desktop platform that visualizes real-time sensor data, cross-referenced with VMS tracks, allowing fisheries authorities to identify unregistered activities or anomalies in effort distribution.
- WinchWatch Fishing Effort Sustainability Planner, an analytical module that supports spatial planning, allowing managers to define micro-zones of fishing activity and assign individual effort quotas based on real operational data.

Pilot Study

A one-year pilot deployment was conducted on a selected group of fishing vessels operating in the Adriatic Sea. The installation involved the integration of GearSenz and NetSenz units with existing BlueTraker VMS equipment. The

Results and Discussion

Preliminary results obtained from the WinchWatch pilot study demonstrated that mass deployment of gear sensors significantly improves the accuracy of fishing effort estimation. The system precisely detected the timing, location, and duration of each fishing operation, even distinguishing between registered and unregistered nets. Compared to conventional VMS-based estimates, the sensor-derived data provided a finer spatial and temporal resolution of fishing activity, reducing uncertainty in effort assessment.

The innovation that the WinchWatch system introduces is enabling the creation of a precise depth profile of the net underwater. It provides valuable information about the underwater zones in which fishing effort takes place. It enables – quite uniquely – a three-dimensional (3D) fishing effort measurement, cumulative mapping it over time and space, which significantly improves the level of fishing effort assessment compared to methods widely practiced nowadays. Hence, it also helps to distinguish between e.g. washing a net and active fishing operations (Fig. 5).

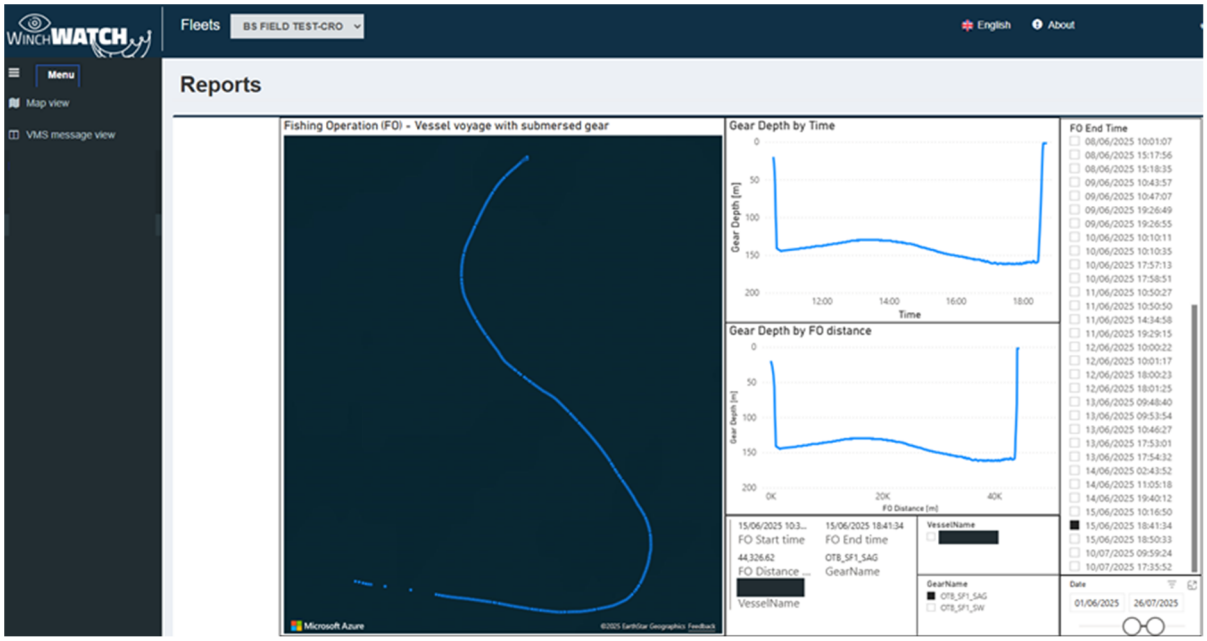


Figure 5
Example of pilot vessel track with overlaid gear operation detections.

Another unique information WinchWatch provides is the possibility to know the exact net (with previously known and registered characteristics) that was used in every single fishing operation. This information brings another couple of new parameters for measuring fishing effort: a) stratification of the fishing effort by the net type, which can be separately measured by the various types of nets; b)

inclusion of net dimensions as a variable in fishing effort measurement i.e. larger net means more fishing effort, similar to the mesh size, etc.
The integration of GearSenz and NetSenz allowed for cross-validation between winch operations and net-specific parameters such as a towing time, depth, and environmental conditions. This dual verification substantially enhances the reliability of data used for both scientific and management purposes.

Furthermore, sensor-derived datasets from WinchWatch serve as valuable "ground truth" for AI systems used in fisheries monitoring. By providing verified records of fishing operations, the system enables machine learning models to better classify vessel behavior and predict fishing events from AIS and satellite imagery. This is particularly relevant in regions where data scarcity and algorithmic bias limit the reliability of automated fisheries surveillance (Alsharabi et al., 2024; Welch et al., 2024). Moreover, the combination of real-time sensor inputs with predictive analytics enhances decision-support tools for fisheries management. AI models trained on WinchWatch data could forecast fishing intensity, assess compliance with spatial restrictions, and even predict bycatch risk under various environmental scenarios (Table 2).

Table 2
Application of WinchWatch data in AI-based fisheries management models.

Application	**Description**	**AI Integration Potential**
Event detection	Identification of gear deployment and retrieval	Training datasets for behaviour classification models
Spatial planning	Mapping fishing intensity and overlap with sensitive habitats	Predictive zoning tools
Compliance monitoring	Detecting unregistered or illegal gear use	Anomaly detection algorithms

The WinchWatch Fishing Effort Sustainability Planner application demonstrated how high-resolution gear-level data can be used to design micro-zones for adaptive spatial management (Fig. 6). By quantifying fishing effort at a sub-regional scale, managers can balance resource utilization and habitat protection more effectively. Preliminary results showed that fishing effort often clusters in narrow zones that are invisible in coarse-scale VMS maps. This new level of detail

facilitates targeted management actions such as temporary closures, rotational access, and real-time effort redistribution.

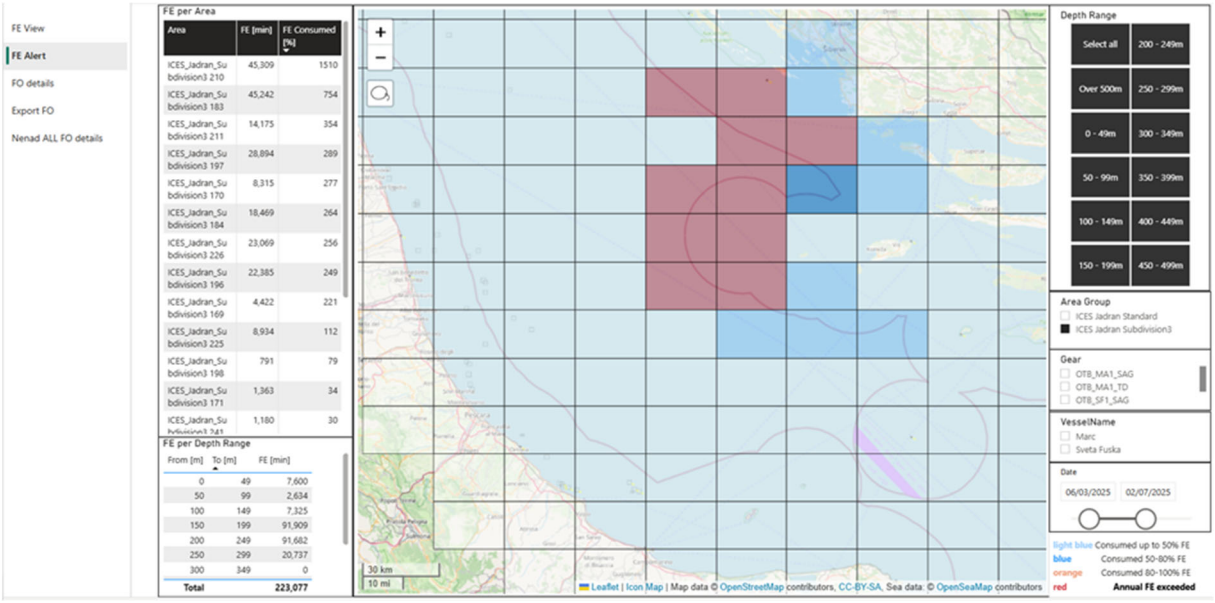


Figure 6
Example of WinchWatch automatic real-time logging and color-coded mapping of fishing effort zonal quotas consumption.

The WinchWatch system demonstrates the feasibility of transitioning from vessel-level to gear-level fisheries monitoring. Its integration with VMS and AI systems represents a major technological step toward real-time, comprehensive observation of fishing activity. The capacity to quantify effort directly from gear operations, rather than inferring it from vessel movement, provides unprecedented accuracy for scientific and policy applications.

Such precision aligns with global efforts to improve data-driven fisheries governance (FAO, 2022). By linking WinchWatch with existing satellite-based surveillance and automated image recognition systems, fisheries authorities can strengthen enforcement against illegal, unreported, and unregulated (IUU) fishing. Additionally, the system's open data architecture allows integration with blockchain-based traceability schemes, facilitating "sea-to-plate" transparency (Zhang et al., 2021). Accurate fishing effort measurement is central to sustainable management, as it underpins stock assessments, quota setting, and spatial planning. WinchWatch offers a methodology for quantifying effort in real time, enabling adaptive management practices such as individual effort quotas and dynamic spatial restrictions. This represents a shift from reactive to proactive governance, consistent with the ecosystem-based approach to fisheries (Hilborn et al., 2015).

In small-scale and coastal fisheries, where data scarcity is most acute, sensor technologies could democratize monitoring by providing affordable, automated

solutions. The WinchWatch Science Kit allows researchers and local cooperatives to participate directly in data collection and analysis, bridging the gap between traditional knowledge and modern analytics. However, equitable access and training remain essential to prevent technological exclusion of smaller operators.

However, it has to be noted that there are still challenges for a full implementation of such a system, as despite its potential, AI and IoT integration in fisheries faces several barriers: a) Data scarcity and bias: Many regions still lack reliable baseline data, which can lead to algorithmic misinterpretation; b) Infrastructure limitations: Poor internet connectivity and power supply constrain real-time data transfer from vessels; c) Socio-economic concerns: Fishers may perceive sensor monitoring as intrusive or a threat to livelihood autonomy; d) Legal and ethical uncertainty: Questions remain about data ownership, privacy, and the admissibility of AI-derived evidence in legal contexts.

Addressing these challenges will require international collaboration to develop shared standards, ethical frameworks, and funding mechanisms that promote inclusion and transparency.

Therefore, future work should focus on: a) Scaling up pilot testing to diverse fisheries and gear types; b) Inviting various scientist groups globally to further research the application scenarios for WinchWatch sensors: deploying WinchWatch Science Kit in their environments; c) Integrating WinchWatch data with AI-driven predictive models for stock and habitat management; d) Developing open-source analytics platforms to foster participatory monitoring; and e) Creating harmonized legal frameworks for sensor data governance.

With further development, WinchWatch could become part of a broader global initiative for smart, sustainable fisheries that combine human expertise with digital intelligence.

In conclusion, WinchWatch initiative demonstrates how the fusion of smart sensors, AI analytics, and real-time data management can revolutionize fisheries monitoring. By capturing fishing effort at the gear level, it provides the granularity needed for accurate scientific assessment, efficient management, and fair enforcement. Beyond its technological innovation, WinchWatch highlights the importance of human-centered design and inclusive policy frameworks that ensure these tools support, not replace, traditional fishing communities. As global fisheries face mounting ecological and economic pressures, systems like WinchWatch offer a pathway toward transparent, adaptive, and evidence-based governance.

References

1. Alsharabi, N., Ktari, J., Frikha, T., Alayba, A., Alzahrani, A.J, Amr jadi and Hamam, H. Using blockchain and AI technologies for sustainable, biodiverse, and transparent fisheries of the future. Journal of Cloud Computing 13, 135, 2024.
2. FAO. The State of World Fisheries and Aquaculture 2022 – Towards Blue Transformation. Food and Agriculture Organization of the United Nations, Rome, Italy, 2022.
3. Hilborn, R., Fulton, E. A., Green, B. S., Hartmann, K., Tracey, S. R., and Watson, R. A. When is a fishery sustainable? Canadian Journal of Fisheries and Aquatic Sciences. 72(9), 2015: 1433-1441.
4. Kroodsma, D. A., Mayorga, J., Hochberg, T., Miller, N. A., Boerder, K., Ferretti, F., Wilson, A., Bergman, B., White, T. D., Block, B. A., Woods, P., Sullivan, B., Costello, C., and Worm, B. Tracking the global footprint of fisheries. Science, 359(6378), 2018: 904–908.
5. Zhang, Y., Liu, Y., Jiong, Z., Zhang, X., Li, B. and Chen E. Development and assessment of blockchain-IoT-based traceability system for frozen aquatic product. Journal of Food Process Engineering, 44(5), 2021.
6. Welch, H., Ames, R.T., Kolla, N., Kroodsma, D.A., Marsaglia, L., Russo, T., Watson, J.T., and Hazen, E.L. Harnessing AI to map global fishing vessel activity. One Earth, 7(10), 2024: 1685–1691.

PHYSICAL CHANGES IN NYLON GILLNETS DURING SOAK TIME IN SMALL-SCALE FISHERIES, PHUKET, THAILAND

Thanakorn SANGEAMWONG[1], Keigo EBATA[1], Phatcharapol BOONSERM[2], Tirapat WECHPRASIT[3]
[1]The United Graduate School of Agricultural Sciences, Kagoshima University, Korimoto 1-21-24, Kagoshima, 890-0065, Japan
[2]Department of Marine Science, Faculty of Fisheries, Kasetsart University, Bangkok, 10900, Thailand
[3]Division of Physics, Faculty of Science and Technology, Thammasat University, Pathum Thani, 12120, Thailand

Abstract

Gillnets are among the most widely used fishing gears in Thailand's small-scale fisheries. Their extensive use underscores the need to assess material durability as a basis for sustainable gear management. This study investigates the physical degradation of nylon (PA) monofilament gillnets used in small-scale blue swimming crab *(Portunus pelagicus)* bottom-set gillnet fishery during varying soak times. Transparent, double-knotted nylon gillnets (diameter 0.3 mm), produced by Thai fishing net manufacturers, were voluntarily contributed by fishers. Mesh sections were collected on four dates: September 1 (new nets), and 7, 13, and 19, 2024. These samples were categorized by cumulative soak time into four groups: 0 (new), 6, 12, and 18 days. Field observations revealed that fishers in the study area typically replace their gillnets approximately every 18–20 days after initial deployment. Tensile strength was evaluated using a universal tensile testing machine, and surface degradation was examined using light microscopy and scanning electron microscopy (SEM). Results demonstrated a significant decline in tensile strength and strain at break with increasing soak time ($p < 0.05$). The tensile strength decreased from 669 MPa (day 0) to 654 MPa (day 12) and 627 MPa (day 18). Similarly, strain at break reduced from 0.37 to 0.21 and 0.12, respectively. Microscopic observations revealed visible discoloration and surface cracking beginning as early as day 6. SEM images showed that fragmentation and material detachment were evident after 12 days of immersion. This is the first study in Thailand examining the physical degradation of fishing gear materials. The results contribute to sustainable gear management and inform the development of biodegradable alternatives, which are not yet commercially available in the country.

Keywords
Small-scale fisheries, Nylon monofilament gillnet, Soak time, Phuket, Thailand

Introduction
Small-scale fisheries (SSFs) are a cornerstone of coastal livelihoods and food security throughout Southeast Asia. In Thailand, SSFs account for the majority of the country's fishing fleet and employ thousands of households, contributing not only to local subsistence but also to national seafood production and exports (Sangeamwong et al., 2025). Among the wide variety of gears used, nylon bottom-set gillnets are particularly common in small-scale crab fisheries. Their popularity stems from their low cost, widespread availability, and effectiveness in capturing target species such as the blue swimming crab (*Portunus pelagicus*), which represents one of the most valuable export commodities in Thailand. Despite these benefits, the use of nylon gillnets has raised growing concerns related to gear loss, ghost fishing, and long-term marine plastic pollution (Grimaldo et al., 2019). Gillnets, especially those made from synthetic polymers like nylon, are highly durable under marine conditions. Lost or discarded nets can continue to trap marine organisms for extended periods, a phenomenon widely recognized as ghost fishing (Pham et al., 2014; Min et al., 2020). This issue has significant ecological and socio-economic consequences, as it leads to unnecessary mortality of commercially important species, damages benthic habitats, and reduces the income of coastal fishers. Globally, attention has therefore shifted toward the development and adoption of alternative materials for fishing nets that are less persistent in the marine environment (Le Gué et al., 2024).

Biodegradable polymers, including polybutylene succinate co-adipate-co-terephthalate (PBSAT), have been promoted as a promising substitute to conventional nylon (Grimaldo et al., 2020). Laboratory and field studies in several countries have demonstrated that PBSAT-based nets can degrade more rapidly in seawater, thereby reducing the long-term risks of ghost fishing and marine debris (Grimaldo et al., 2018). While these advances are encouraging, the adoption of biodegradable netting is still at an early stage, and substantial knowledge gaps remain. A key issue is that most evaluations of net materials have been performed under controlled laboratory conditions, often focusing on unused nets. Although such tests guided by international standards such as ISO 1806:2002 provide essential insights into the tensile strength and elongation of netting materials, they do not fully reflect the changes that occur during actual fishing operations. In practice, nets are exposed to repeated soaking, hauling, abrasion, and environmental variability, all of which can alter their physical and mechanical properties. Properties such as breaking strength, elongation at break, and knot stability are not static; they deteriorate progressively with soak time and repeated use. Understanding

these changes is crucial, as they directly influence catch efficiency, gear selectivity, and the economic lifespan of the gear (Grimaldo et al., 2020).

The Thai context is particularly noteworthy. Despite being one of the largest seafood exporters globally and a regional leader in small-scale fishing, Thailand has not yet introduced biodegradable netting materials such as PBSAT into its fisheries. To date, there is no published research examining either the performance of PBSAT gillnets or even the baseline degradation patterns of nylon nets under local fishing conditions. This absence of knowledge is striking, given the importance of blue swimming crab fisheries to Thailand's economy and the heavy reliance of small-scale fishers on nylon gillnets. Without a fundamental understanding of how nylon nets change during actual soak times, it is impossible to evaluate the potential benefits or trade-offs of transitioning to biodegradable alternatives in the future.

This study was designed to address the above gaps by systematically investigating the physical changes that occur in nylon gillnets during soak time under small-scale fishery conditions in Ao Por, Phuket. Specifically, the study focused on evaluating tensile strength, elongation, and surface degradation of nylon nets across soak durations. By applying standardized tensile tests in combination with microscopic surface observations, the research provides a detailed account of how nylon nets deteriorate with repeated soaking, offering insights into both material performance and fishery implications. The contributions of this study are threefold. First, it provides the first empirical dataset on nylon gillnet degradation under field-relevant soaking conditions in Thailand, thereby filling a critical gap in local fisheries science. Second, it establishes a baseline for future evaluations of biodegradable alternatives such as PBSAT, allowing for direct comparisons of performance under identical fishing conditions. Third, the findings have immediate policy relevance, offering evidence that can inform discussions on mesh-size regulations, net replacement intervals, and the potential integration of alternative materials into Thailand's small-scale fisheries. More broadly, the research underscores the importance of linking material science with fisheries management, highlighting how gear technology influences both fishing efficiency and sustainability.

Material and Methods

Experimental gillnets

The fishing grounds were located off the coast of Ao Por, Phuket province, around 8°02'– 8°07' N and 98°28' – 98°29' E, which is a frequently used fishing ground for small-scale blue swimming crab *(Portunus pelagicus)* bottom-set gillnet fishery. For this study, net samples were voluntarily provided by fishers who supplied sections of net damage while removing target species and aquatic

organisms. All samples were derived from the same set of gillnets. Fishers provided gillnet specimens on September 1 (initial deployment of new gillnets), 7, 13, and 19, 2024, which is during the peak season of blue swimming crab gillnet fishery (June–October). Fishers utilize transparent double-knotted 0.3 mm nylon (PA) monofilament gillnets. According to the fishers, the operational lifespan of these nets averages 18–20 days before replacement becomes necessary. We classified the samples into four groups based on cumulative soaking time: 0 (new), 6, 12, and 18 days. Net samples were prepared for analysis by selecting forty intact single-mesh samples from each soaking time group. The actual mesh sizes were measured using a Vernier calliper without applying tension to the mesh. The mean mesh size ± standard deviation of the samples was 116.4 ± 1.4 mm.

Mechanical properties of the gillnets

Mechanical properties of the nylon gillnet samples, specifically tensile strength and elongation at break, were measured using a universal testing machine. All specimens were tested under wet conditions, corresponding to soaking durations of 0, 6, 12, and 18 days. Before testing, net samples were immersed in tap water at 20 ± 2 °C for at least 12 h without the use of wetting agents, in accordance with ISO 1806:2002 (ISO, 2002).

Assessment of gillnet damage

Monofilament and knot segments were randomly taken from gillnet samples supplied by local fishers to assess material degradation under different soaking periods. Initial inspection of physical damage was carried out with a stereomicroscope, while detailed surface morphology of samples was examined using a Scanning Electron Microscope (SEM).

Data analysis

An independent-samples t-test was employed to evaluate mean differences in netting samples across soaking durations (0, 6, 12, and 18 days). All tests were conducted as two-tailed, enabling detection of differences in either direction, with the significance level set at $\alpha = 0.05$. Prior to conducting pairwise comparisons, linear associations among the four soaking groups were examined to ensure that the observed variation was consistent with the expected trend. This approach allowed us to distinguish whether degradation patterns reflected systematic changes across soaking periods rather than random variation between independent samples (Sala et al., 2004).

Results

At day 0 (new net), the tensile strength of nylon monofilaments was significantly higher ($p < 0.05$) than that observed after 6, 12, and 18 days of soaking. A

noticeable decline began after 6 days, with tensile strength decreasing from 669 MPa at day 0 to 654 MPa at day 12 and further to 627 MPa at day 18 (Fig. 1).

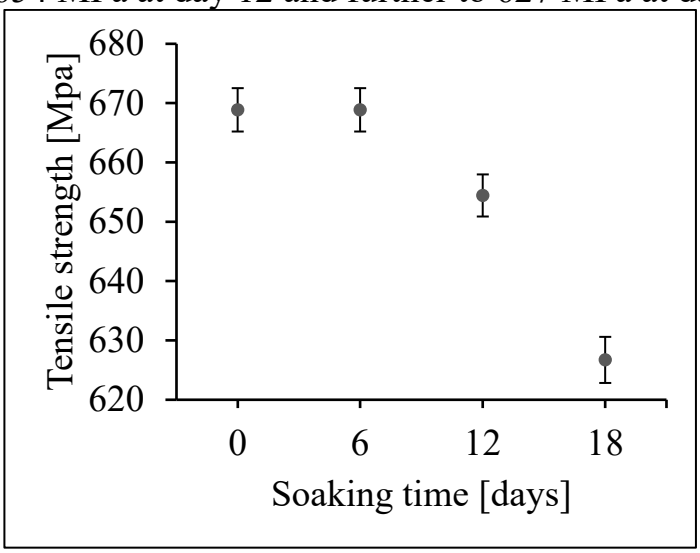


Figure 1
Changes in tensile strength of nylon (PA) monofilament gillnet samples across different soaking durations. Data points represent mean values, with error bars showing standard deviations.

The strain at break in new nets (0 days soaking) was significantly higher ($p < 0.05$) compared with nets soaked for 6, 12, and 18 days. A clear decline was evident after 6 days, with values decreasing from 0.37 at 0 days to 0.21 at 12 days and further to 0.12 at 18 days (Fig. 2).

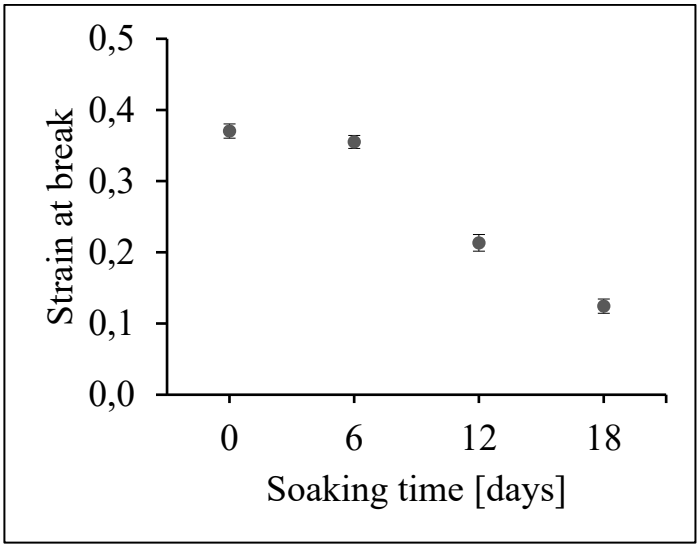


Figure 2
Changes in strain at break of nylon (PA) monofilament gillnet samples across different soaking durations. Data points represent mean values, with error bars showing standard deviations.

Light microscopy observations revealed rapid discoloration of nylon (PA) monofilament gillnets (Fig. 3). Within 6 days of soaking, the original clear appearance had noticeably faded, with filaments exhibiting a faint yellow or nearly colorless tone. In addition, initial surface cracks began to emerge after approximately 6 days.

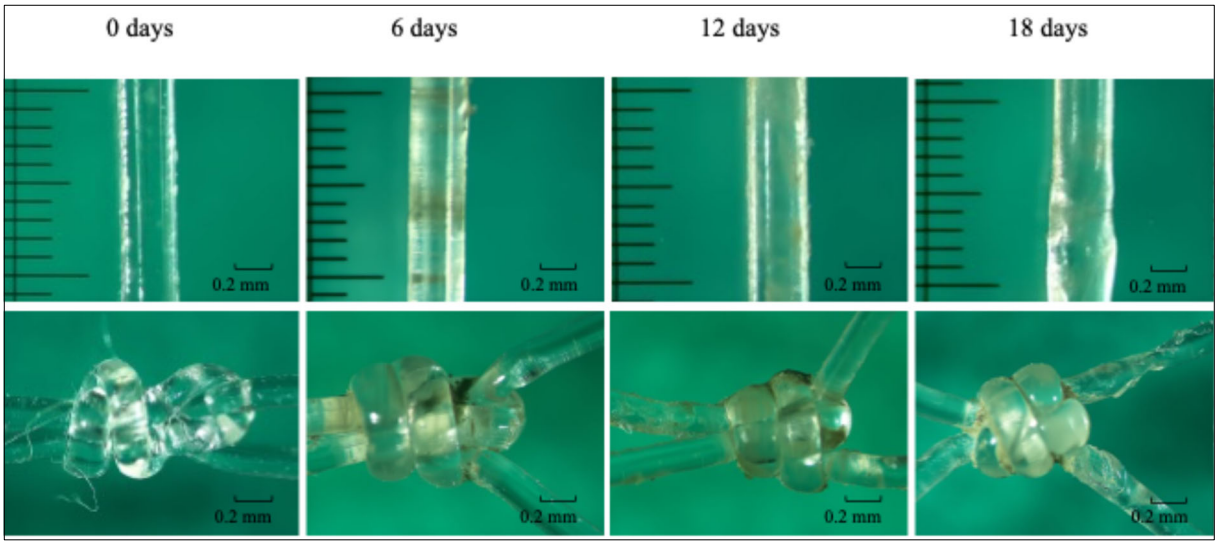


Figure 3
Light microscopy images of nylon (PA) monofilament gillnet samples after different soaking durations, showing progressive changes in color and surface condition.

Scanning Electron Microscopy (SEM) revealed that new nylon (PA) monofilaments had relatively smooth surfaces with only minor scratches, likely originating from the manufacturing process (Fig. 4). After 12 days of soaking, noticeable surface damage was evident, including cracks and localized ruptures, which suggest progressive physical wear on the filaments.

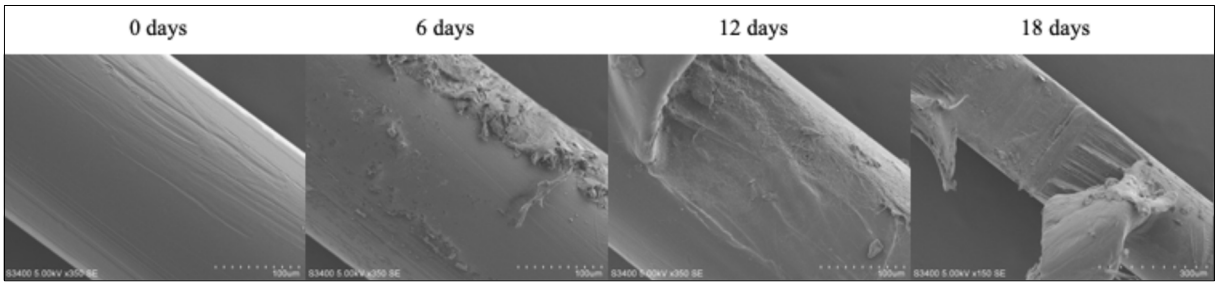


Figure 4
SEM micrographs showing surface characteristics of nylon (PA) monofilament gillnet samples across different soaking durations.

Discussion

This study provides the first systematic dataset on the physical changes of nylon (PA) gillnets under field-relevant soak durations in a small-scale blue swimming crab bottom-set gillnet fishery in Ao Por, Phuket. By integrating standardized tensile testing, elongation analysis, light microscopy, and scanning electron microscopy (SEM), we demonstrated that significant physical deterioration of nylon nets occurs within two weeks of immersion. The decline in tensile strength was gradual, whereas strain at break declined sharply, indicating that nets became markedly more brittle with extended soak time. Complementary microscopic observations revealed early signs of color fading and crack initiation by day 6, progressing to more pronounced surface damage by day 12. Taken together, these results delineate a clear timeline of wear and damage, with practical implications for the durability, selectivity, and sustainability of gillnet use in small-scale fisheries. Beyond their immediate relevance for Ao Por, these findings establish a crucial baseline for evaluating future biodegradable alternatives such as PBSAT, which are not yet introduced in Thailand.

The tensile strength of nylon monofilaments decreased steadily with soak duration. Although the relative decline (~6% over 18 days) may appear modest, it is statistically significant ($p < 0.05$) and highly relevant from an operational perspective. In fishing practice, gillnets are subject to dynamic stresses, including hauling loads, wave action, and snagging on the seabed. Even a small reduction in tensile capacity at the filament level increases the likelihood of local breakage in knots or mesh segments, which represent the weakest structural points of the gear (ISO, 2002; Kim et al., 2016). The pattern observed here mirrors reports from other marine gear studies, where tensile degradation of synthetic fibers often occurs more gradually than elongation loss but is still operationally decisive (Sala et al., 2004). The correspondence between our laboratory results and fishers' reported practice of replacing nets approximately every 18–20 days suggests that the observed tensile decline is ecologically and economically meaningful. In other words, gear replacement intervals chosen by local fishers are not arbitrary but reflect an adaptive response to the measurable reduction in net strength.

In contrast to tensile strength, strain at break showed a much sharper decline. Nets exhibited extensibility of 0.37 in new condition, which decreased to 0.21 at day 12 and further to 0.12 at day 18. This represents a reduction of ~43% and ~68% over 12 and 18 days, respectively. The sharp loss of extensibility indicates that nylon filaments became substantially more brittle during immersion. The reduction in elongation capacity is operationally critical because extensibility governs mesh dynamics. Gillnets function by ensnaring crabs or fish as they attempt to pass through mesh openings; adequate flexibility allows meshes to adapt to the

morphology of captured organisms, improving selectivity and reducing gear breakage. A loss of extensibility thus compromises both efficiency and durability. Brittle meshes are more likely to rupture under sudden shocks, such as when hauling nets in rough seas or when larger-than-target organisms strike the gear. The decoupling between relatively modest reductions in tensile strength and dramatic reductions in strain at break suggests that the dominant mechanism is not simple fiber weakening but rather surface-initiated micro-damage that curtails elongation capacity. This interpretation is strongly supported by the microscopic evidence described below.

Light microscopy revealed that visible deterioration began as early as 6 days of soaking, when net filaments lost their clear coloration and appeared faint yellow or translucent. At the same time, small surface cracks became visible. These observations correspond precisely with the point at which strain at break began to decline significantly, indicating that visual changes in color and micro-cracking are early warning indicators of mechanical degradation. From a practical perspective, this suggests that low-cost visual inspection of nets, using handheld magnifiers or stereoscopes, may provide fishers with a simple tool to monitor gear quality in the field. Identification of early-stage surface cracking could guide proactive gear maintenance or timely replacement, thereby reducing losses from catastrophic tearing and minimizing the risk of ghost fishing caused by lost nets (Pham et al., 2014).

SEM observations provided valuable insight into the surface condition of nylon filaments across soak durations. New nets displayed smooth surfaces with only minor scratches, likely originating from the manufacturing process. After 12 days of soaking, localized cracks and ruptures were observed on the filament surface. While these features indicate physical damage, it is important to emphasize that they do not necessarily represent chemical degradation of the polymer. The current study did not assess changes in molecular structure, and therefore conclusions about material degradation at the chemical level cannot be drawn. Future work should incorporate spectroscopic techniques such as ATR-FTIR to examine potential alterations in polymer bonds and confirm whether observed surface damage corresponds to true degradation (Min et al., 2020). Alternatively, the cracks and ruptures documented here may also result from operational stresses, particularly when fishers forcibly remove entangled crabs from the nets. Thus, the SEM results should be interpreted cautiously as evidence of surface damage rather than conclusive proof of material degradation.

Although the findings provide important insights, several limitations should be acknowledged. Only one nylon monofilament type was tested, leaving potential variability among manufacturers and filament diameters unexplored. In addition,

no chemical or crystallographic analyses were conducted, restricting the conclusions to surface-level physical wear rather than confirming molecular degradation. Finally, the study did not directly examine the relationship between net degradation and fishing performance, such as CPUE or gear selectivity, which remains a critical avenue for future research. These limitations underscore the importance of interdisciplinary follow-up studies that integrate material science, chemistry, and fisheries ecology to provide a more comprehensive understanding of gillnet performance (Grimaldo et al., 2019; Sangeamwong et al., 2025).

Acknowledgements

We gratefully acknowledge the financial support for this research provided by The Asahi Glass Foundation, Japan. We sincerely thank Somkiat Pichiyut, a small-scale fisher from Ao Por fishing community, Phuket Province, Thailand, for his kind contribution of used nylon (PA) monofilament bottom-set gillnets for this study. Many thanks to Dr Tomoko Yamamoto, Kagoshima University, for assisting with advice and assistance in preparing nylon (PA) gillnet samples for use with the stereo microscope. We also greatly appreciate Alisa Pattarapisitporn, Saga University, for valuable advice and support in analyzing monofilament gillnet samples using the scanning electron microscope (SEM) techniques in this study. We would also like to thank Chitchanok Sangeamwong, National Electronics and Computer Technology Center, Thailand, for guidance in analyzing photographic data, calibrating object sizes in microscope images, and visualizing data from microscope photography.

References

1. Grimaldo, E., Herrmann, B., Jacques, N., Kubowicz, S., Cerbule, K., Su, B., Larsen, R., and Vollstad, J. – The effect of long-term use on the catch efficiency of biodegradable gillnets – Marine Pollution Bulletin, 161, 2020
2. Grimaldo, E., Herrmann, B., Vollstad, J., Su, B., Moe-Føre, H., and Larsen, R.B. – Comparison of fishing efficiency between biodegradable gillnets and conventional nylon gillnets – Fisheries Research, 213, 2019, 67–74
3. Grimaldo, E., Herrmann, B., Vollstad, J., Su, B., Moe Føre, H., Larsen, R. B., and Tatone, I. – Fishing efficiency of biodegradable PBSAT gillnets and conventional nylon gillnets used in Norwegian cod (*Gadus morhua*) and saithe (*Pollachius virens*) fisheries – ICES Journal of Marine Science, 75, 6, 2018, 2245–2256
4. ISO 1806, 2002. Fishing Nets – Determination of Mesh Breaking Force of Netting. International Organization for Standardization, 6 p. https://www.iso.org/standard/28360.html
5. Le Gué, L., Savina, E., Arhant, M., Davies, P., Dumergue, N., and Vincent, B. – Influence of knot strength on the mechanical performance of a biodegradable gillnet – Scientific Reports, 14, 1, 2024

6. Kim, S., Kim, P., Lim, J., An, H., and Suuronen, P. – Use of biodegradable driftnets to prevent ghost fishing: physical properties and fishing performance for yellow croaker – Animal Conservation, 19, 2016, 309–319
7. Min, K., Cuiffi, J.D., and Mathers, R.T. – Ranking environmental degradation trends of plastic marine debris based on physical properties and molecular structure – Nature Communications, 11, 2020
8. Pham, C.K., Ramirez-Llodra, E., Alt, C.H.S., Amaro, T., Bergmann, M., Canals, M., Company, J.B., et al. – Marine litter distribution and density in European seas, from the shelves to deep basins – PLoS One, 9, 2014
9. Sala, A., Lucchetti, A., and Buglioni, G. – The change in physical properties of some nylon (PA) netting samples before and after use – Fisheries Research, 69, 2, 2004, 181–188
10. Sangeamwong, T., Ebata, K., Boutson, A., Leenawarat, D., Anraku, K., and Archdale, M.V. – Logbook-based assessment of blue swimming crab *(Portunus pelagicus)* gillnet fishery: a case study of small-scale fishing communities in Laem Phak Bia, Phetchaburi, Thailand – Fisheries Science, 2025

APPLICATION OF STATE ESTIMATION TO IDENTIFY UNKNOWN PARAMETERS IN FISHING GEAR DYNAMICS

Kengo YAEGASHI[1], Shintaro GOMI[2], Katsuya SUZUKI[3], Tsutomu TAKAGI[4]
[1]Hokkaido University, Graduate School of Env. Science, A-410, N10W5, Kita-ku, Sapporo, Hokkaido, 060-0810, Japan
[2]Hokkaido University, Faculty of Fisheries Sciences, 214, 3-1-1 Minato-cho, Hakodate, Hokkaido, 041-8611, Japan
[3]Nitto Seimo Co.,Ltd., 14-14 Ichimonji-cho, Fukuyama, Hiroshima, 721-0953, Japan
[4]Hokkaido University, Faculty of Fisheries Sciences, E310, 3-1-1 Minato-cho, Hakodate, Hokkaido, 041-8611, Japan

Abstract

Controlling the behavior of fishing gear underwater is essential for selectivity on fishing gear and achieving sustainable fisheries. However, such control has been difficult because it is almost impossible to observe the behavior clearly underwater. Therefore, numerical simulations have been developed to visualize and analyze the behavior. We have developed a simulation system called the NaLA (Net shape and Load Analysis) system, which is useful for simulations of several fishing gears. However, simulation systems rely on approximations of physical parameters such as hydrodynamic coefficients because it is almost impossible to measure these parameters accurately. To overcome this problem, we have developed a new system for controlling the behavior of fishing gear and estimating unknown parameters using state estimation techniques based on the NaLA system. In this study, we attempted to estimate unknown parameters, such as the length of warp and the size of floats on trawl nets, which are required for realizing control, and tried to control the shape of some fishing gears. Furthermore, in order to maintain stable production of passive fishing gear, we estimated a diameter of the mooring line to be large enough not to break during disasters such as typhoons and rapid tidal currents. These results are valuable and can suggest how to control the behavior of fishing gear as fishers desire. This state estimation system is applicable to any variables and parameters as long as they are described as physical quantities in the system model.

Keywords

Netting, fishing gear, numerical simulation, data assimilation

Nomenclature

M_i – Mass
$\Delta M_{i,k}$ – Added mass
i – The number of mass point
$\boldsymbol{C}_{i,k}$ – Inertia transformation matrix
$\boldsymbol{a}_i$ – Acceleration vector
$\boldsymbol{T}_i$ – Tension force vector
$\boldsymbol{F}_{i,k}$ – Hydrodynamic force vector
$\boldsymbol{W}_i$ – Gravitational force vector
$\boldsymbol{B}_i$ – Buoyant force vector
$\boldsymbol{z}_t$ – Augmented state vector
$\boldsymbol{f}$ – Function of a system model
$\boldsymbol{x}_t$ – State vector
$\boldsymbol{\theta}_t$ – Unknown parameter vector
$\boldsymbol{v}_t$ – System noise vector
$\mathbf{Q}$ – Covariance matrix of system noise
$\boldsymbol{y}_t$ – Observation vector
$\mathbf{H}$ – Observation matrix
$\boldsymbol{w}_t$ – Observation noise vector
$\mathbf{R}$ – Covariance matrix of observation noise
$\hat{\boldsymbol{w}}$ – Deviation of observation noise
$\boldsymbol{V}$ – Covariance matrix of state
L – Load capacity
r – Radius

Introduction

The productivity of fisheries and aquaculture has been increasing, and accordingly, problems of fisheries that we should resolve urgently, such as overfishing and bycatch, have also increased. Providing solutions for these challenges is essential to realizing sustainable fisheries. One of the solutions would be control the shape of the fishing gear during operation because its shape is considerably crucial to the amount of fish caught. However, it is still difficult to control the shape of the fishing gear underwater as clearly observing its behavior is hardly possible. Hence, research on attempts to control the behavior of fishing gear has been limited. For instance, (Hu *et al.*, 1994) had experiments to investigate the characteristics of midwater trawl for controlling. (Umeda, 1991) attempted to introduce a theory of control engineering to the field of fishing gear in order to control the dynamics of midwater trawl. They were only focused on the specific fishing gears, and the second one was limited to two dimensions. Therefore, as a starting point, an accurate numerical simulation system is required to visualize and analyze the

behavior of the fishing gear in order to achieve control. (Lee *et al.*, 2005) developed a numerical simulation system for understanding the movement of fishing gear. In addition to this, (Lee, 2002) suggested the requirement of controlling the fishing gear using the numerical simulation system and Fuzzy logic. (Takagi *et al.*, 2004) developed a numerical simulation system called the NaLA system (Net shape and Load Analysis system), and (Gomi *et al.*, 2021) attempted to control a net geometry underwater using the NaLA system by integrating a data assimilation method. However, there are still some challenges in terms of controlling the behavior of the fishing gear using numerical simulations. One reason for this is that numerical simulations rely on approximations that can be organized into two types. One comes from describing a physical phenomenon as a discretized model or from numerical computation methods. Another is from approximations of specific physical parameters, such as hydrodynamic coefficients, that are hardly possible to measure directly and precisely. The accuracy of the latter is essential for the accuracy of numerical simulations. Thus, we have developed a new system by integrating a data assimilation method based on the NaLA system in order to provide a solution to these challenges. Data assimilation is a well-known method, which is based on Bayesian inference, in the field of meteorology and control engineering. In this paper, we show how the integrated NaLA system can control the behavior of the fishing gear and estimate the unknown parameters that are required for realizing the control and stability of the passive fishing gear.

Numerical model

The NaLA system is a numerical simulation system developed by (Takagi *et al.*, 2004), and this can calculate and visualize the behavior of the fishing gear. This system is based on the Lumped-Mass model with describing nets of the fishing gear as mass points and spring bars, as shown in Figure 1. In this model, the equation of the motion of mass point i can be expressed as follow:

$$\left(M_i + \sum_{k=1}^{2} \left[\boldsymbol{C}_{i,k} \, \Delta M_{i,k} \, \boldsymbol{C}_{i,k}^{\mathrm{T}} \right] \right) \boldsymbol{\alpha}_i = \boldsymbol{T}_i + \sum_{k=1}^{2} \left[\boldsymbol{C}_{i,k} \, \boldsymbol{F}_{i,k} \right] + \boldsymbol{W}_i + \boldsymbol{B}_i \tag{1}$$

where M_i and $\Delta M_{i,k}$ are the mass and the added mass of the mass point i, respectively. $\boldsymbol{C}_{i,k}$ is the inertia transformation matrix that allows the body-fixed coordinates system to change into the absolute coordinates system. $\boldsymbol{\alpha}_i$ is the acceleration vector of the mass point i. $\boldsymbol{T}_i$ and $\boldsymbol{F}_{i,k}$ are the tension force vector and the hydrodynamic force vector, respectively. $\boldsymbol{W}_i$ and $\boldsymbol{B}_i$ are the gravitational force vector and the buoyant force vector, respectively.

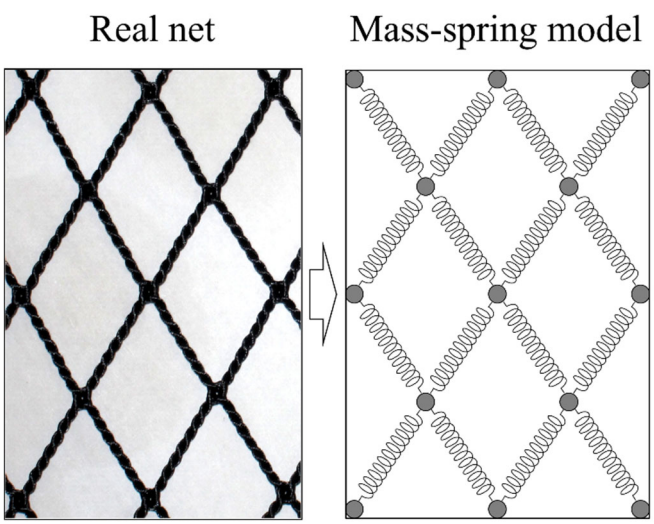


Figure 1
A schematic diagram of expressing a real net as mass-spring model in Lumped-Mass model.

Data assimilation

Data assimilation is a method for controlling and estimation, and its motivation is to improve the accuracy of numerical simulation by assimilating observational data. In other words, data assimilation allows the state to be controlled with satisfying the observational data. In addition to this, it can simultaneously estimate the unknown parameters that are to change in order to realize the control with using an augmented state. A system model and an observation model are required in data assimilation methods. A system model represents state transition in the simulation model, thus, is expressed in this study as follows:

$$\boldsymbol{z}_t = \boldsymbol{f}(\boldsymbol{z}_{t-1}) + \boldsymbol{v}_t \tag{2}$$

where $\boldsymbol{f}$ represents the NaLA system dynamics. $\boldsymbol{z}_t$ is the augmented state vector at time t given by:

$$\boldsymbol{z}_t = \begin{pmatrix} \boldsymbol{x}_t \\ \boldsymbol{\theta}_t \end{pmatrix} \tag{3}$$

where $\boldsymbol{x}_t$ is the state vector and $\boldsymbol{\theta}_t$ is the unknown parameter vector. $\boldsymbol{v}_t$ in the equation (1) is called the system noise vector, which is distributed as a Gaussian distribution $\mathcal{N}(\mathbf{0}, \mathbf{Q})$ and $\mathbf{Q}$ is a covariance matrix. On the other hand, the observation model is described in this study as follows:

$$\boldsymbol{y}_t = \mathbf{H}\boldsymbol{z}_t + \boldsymbol{w}_t \tag{4}$$

where $\boldsymbol{y}_t$ is the observation vector, and $\mathbf{H}$ is called an observation matrix, which is applicable only when the observation system is assumed linear. $\boldsymbol{w}_t$ is called the observation noise vector, which follows a Gaussian distribution $\mathcal{N}(\mathbf{0}, \mathbf{R})$ and $\mathbf{R}$ is a covariance matrix. In this study, we introduced ensemble Kalman filter (EnKF) (Evensen, 1994) to the NaLA system because EnKF is applicable to the nonlinear system model such as the NaLA system. In EnKF, each ensemble member is updated by the gain called Kalman gain. The update equations for each ensemble member i are as follows:

$$\boldsymbol{z}_{t|t}^{(i)} = \boldsymbol{z}_{t|t-1}^{(i)} + \boldsymbol{K}_t(\boldsymbol{y}_t + \hat{\boldsymbol{w}}_t^{(i)} - \mathbf{H}\boldsymbol{z}_{t|t-1}^{(i)}) \tag{5}$$

$$\boldsymbol{K}_t = \boldsymbol{V}_{t|t-1}\mathbf{H}^{\mathrm{T}}(\mathbf{H}\boldsymbol{V}_{t|t-1}\mathbf{H}^{\mathrm{T}} + \mathbf{R}_t)^{-1} \tag{6}$$

$t \mid t-1$ expresses that left t means this variable at time t, and right $t-1$ means this variable is conditioned on $\boldsymbol{y}_{1:t-1}$ that is observation from time 1 to time $t-1$. $\hat{\boldsymbol{w}}$ expresses a deviation of observation noise. $\boldsymbol{V}$ is a covariance matrix of the state $\boldsymbol{x}$.

Net models and analysis

To simplify the problem, we used a simple trawl net model, which is shown in Figure 2. The length of the warp is 100 m. The radius of the float is 0.065 m and the radius of the sinker is 0.021 m. We assumed that this trawl model is at a scale of 1:5 relative to the real net and applied the Froude's law. Therefore, the speed of uniform flow of 0.230 m s^{-1} in this simulation is equivalent to the speed of 0.514 m s^{-1} (1.0 knot) in practice. First, we attempted to control the height of the trawl to an arbitrary value, which is called a target value, with estimating the radius of the center float or the center sinker. Figure 3 shows the position of the height that is controlled and the positions of the target parameters. Second, the length of the warp is estimated with controlling the depth of the position of the two floats next to the one in the red circle in Figure 3.

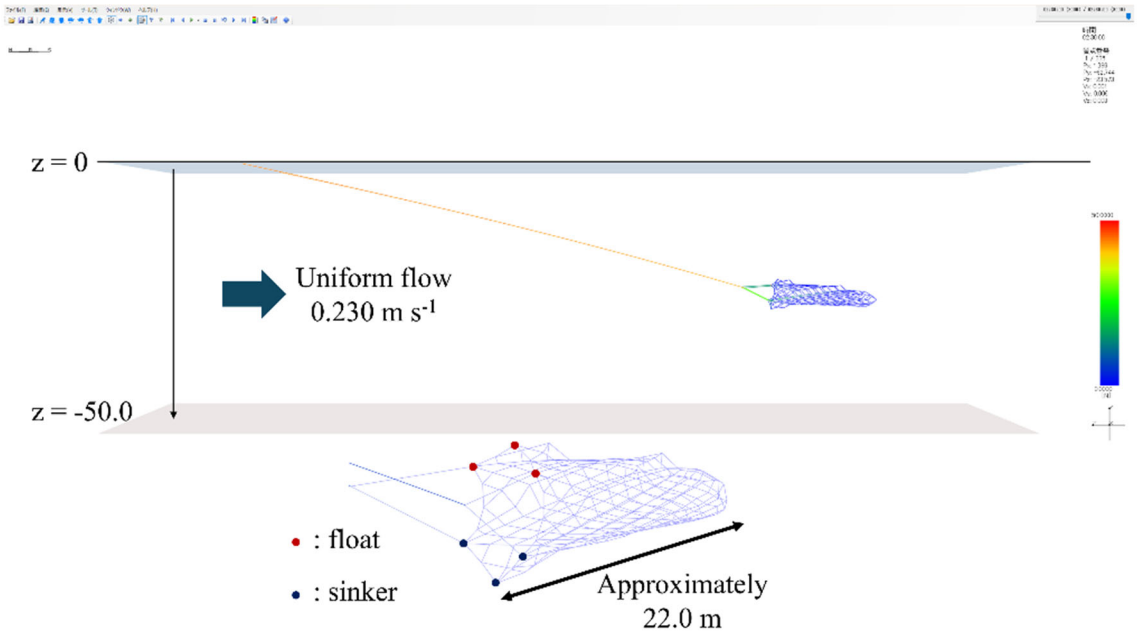


Figure 2
The simulation domain and the simple trawl net model.

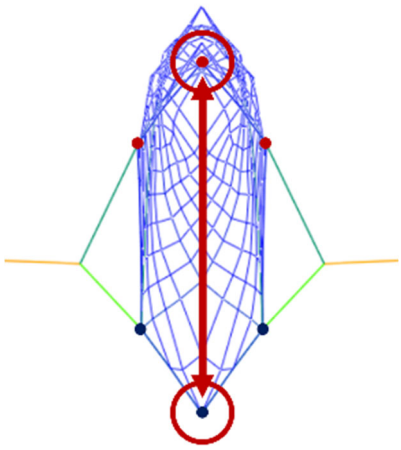


Figure 3
The position of the height controlled and the positions of the float and the sinker where these radii are estimated.

Finally, we attempted to estimate the radii of the mooring lines of a setnet to be large enough not to break during the rapid tidal currents. Figure 4 shows the set net used in simulation and illustrates the bars estimated their radii, which enclosed in black circles. In this estimation, the state values were set as tensile stress, and we applied a function in order to set the target value at each time step because the load capacity of the mooring line varies with the radius. The equation that we used for setting the target value as follows:

$$L = 330163r^2 + 1545.8r \tag{7}$$

where L is the load capacity (kN) and r is the radius (m) of the mooring line. Equation (7) was obtained by regression of the material standards. Additionally, we set a safety factor to 2 in order to ensure that the state is sufficiently safe. In this case, the current speed was set to 0.772 m s^{-1} (1.5 knots) assuming that rapid tidal current occurs.

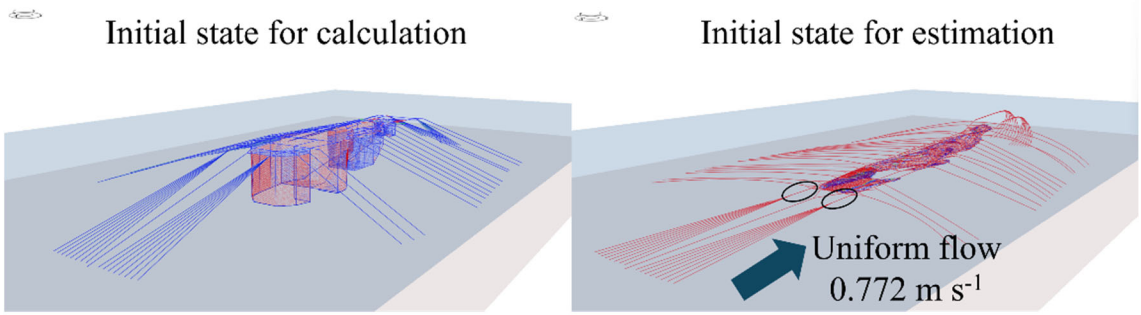


Figure 4
Initial state for calculation and for estimation of the setnet.

In all of the cases, we used 20 ensemble members. Then, in estimation of the radii of the float and the sinker, we set the standard deviation to 1.00×10^{-3} for both system noise and observation noise. Additionally, considering taking time to converge at the value of parameter, time interval of filtering was set as 500 steps. In the case of estimation of the warp length, the standard deviation for the system noise was set to 0.01, and the one for the observation noise was set to 1.00×10^{-3}. Moreover, interval of filtering for the trawl depended on time interval of filtering, which was 1000 steps, and when the difference of between the state and the target value is still larger than 0.1. On the other hand, interval of filtering for the setnet depended on time interval of filtering, which was 50 steps, or when the difference of the tension from the previous step satisfied the threshold that was 0.03 kN as convergence. Then, the standard deviation for both noise in this case is the same as the case of estimation of the radii of the float and the sinker.

Results and discussion

We set the target value of the height to 6.50 m in estimation for both the float and the sinker. Then, the initial values of radii of the float and the sinker are 6.48×10^{-2} m and 2.09×10^{-2} m, respectively. Figures 5 and 6 show that the height is controlled by estimating the radii of the float or sinker.

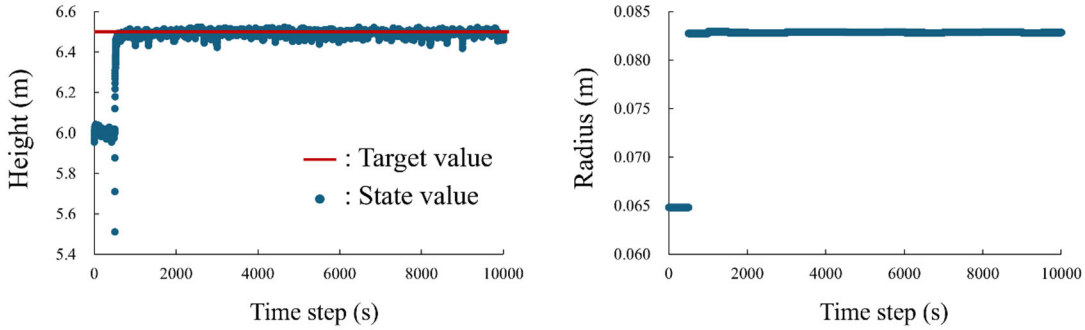


Figure 5
On the left, the time series of the height controlled to the target value. On the right, the time series of the estimated radius of the float.

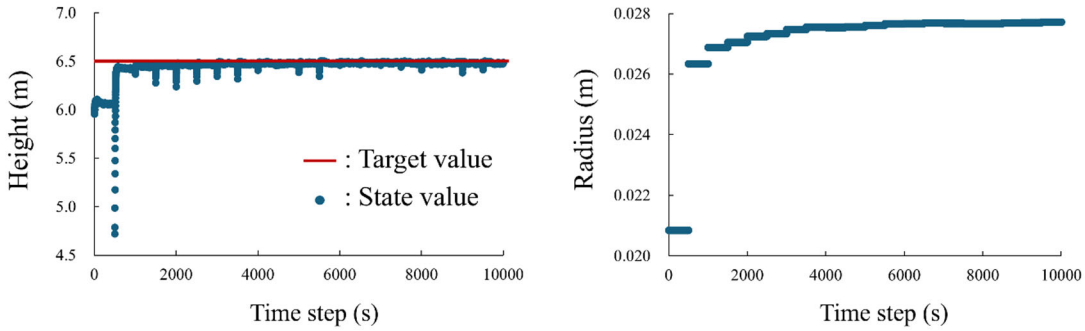


Figure 6
On the left, the time series of the height controlled to the target value. On the right, the time series of the estimated radius of the sinker.

The means of the state over the range from time step 6000 to 10000, which can be considered to be convergence, are 6.50 m and 6.49 m for the case of the float and the sinker, respectively. Moreover, their standard deviations are 1.08×10^{-2} m and 7.65×10^{-3} m, respectively. Therefore, each state value is in good agreement with the target value. The fluctuations of the state are considered to be due to numerical errors. In the case of estimating the length of the warp as well, the state is in good agreement with the target value that is set as -10.0 m, as shown in Figure 7.

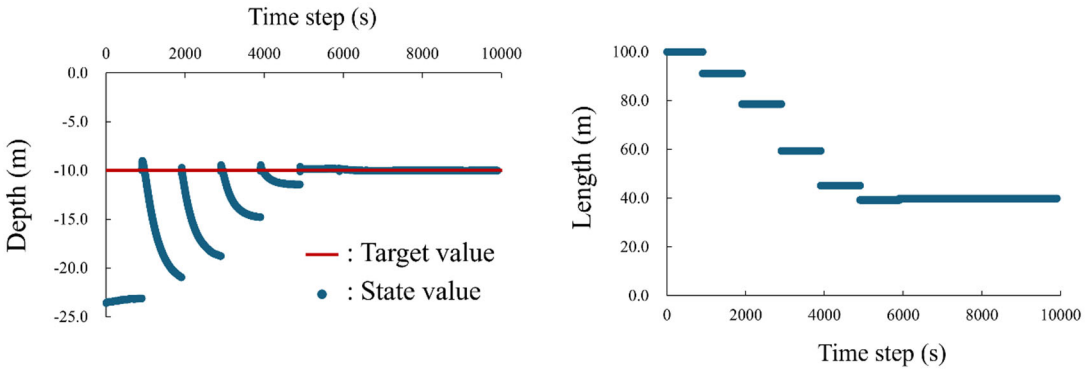


Figure 7
On the left, the time series of the depth controlled to the target value. On the right, the time series of the estimated length of each warp.

The mean of the state over the range from time step 8000 to 10000, which can be considered to be convergence, is -9.98 m and its standard deviation is 6.52×10^{-3} m. In the case of estimating of the radii of the mooring lines, the results are also in good agreement with the variable target values. Figure 8 shows that the state is controlled to the target values that vary with the estimated radius. Then, the mean of the state over the range from time step 400 to the end, which can be considered to be convergence, is 59.8 MPa and its standard deviation is 0.1 MPa. In addition to this, the mean of parameter, whose initial value is 1.90×10^{-2} m, over the same range is 3.44×10^{-2} m and its standard deviation is 3.14×10^{-5} m.

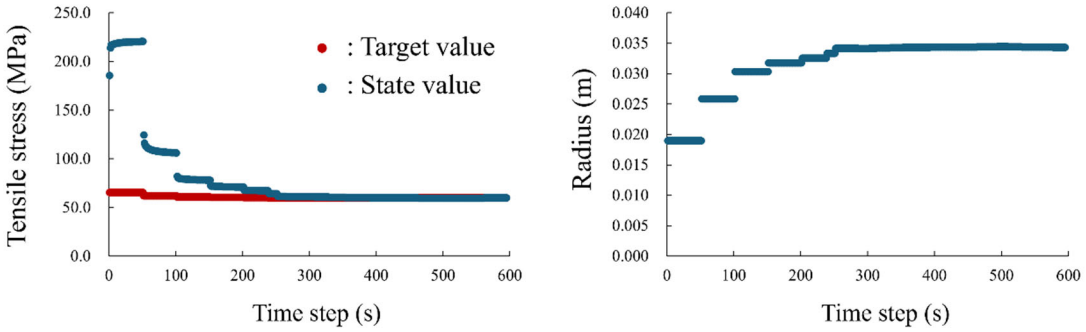


Figure 8
On the left, the time series of the tensile stress controlled to the target values. On the right, the time series of the estimated radius of the mooring line.

Conclusion and future work

Our proposed system allows the parameters to be estimated in order to realize control of the state toward the target values. Furthermore, a notable feature of this system is that it is easy to apply to any variables and parameters as long as they are described as physical quantities in the model. This would make it easy to

control the behavior and shape of the fishing gear underwater. Hence, this system is valuable for selectivity on fishing gear and achieving sustainable fisheries. As future work, we will continue to develop this system in order to introduce it to an actual operation, moreover, we aim to provide real-time control.

Acknowledgements

This research was supported by JSPS Grant-in-Aid for JSPS Fellows Grant Number 25KJ0471.

References

1. Hu, F., Matuda, K., and Sato, K., Characteristics of Dynamic Control of Midwater Trawl System in Field Experiments. Nippon Suisan Gakkaishi 60, 1994.
2. Umeda, N., An Optimal Regulator for a Midwater Trawl System, Bulletin of National Research Institute of Fisheries Engineering. National Research Institute of Fisheries Engineering, 1991, p. 10.
3. Lee, C.-W., Lee, J.-H., Cha, B.-J., Kim, H.-Y., and Lee, J.-H., Physical modeling for underwater flexible systems dynamic simulation. Ocean engineering 32 (3-4), 2005, 331-347.
4. Lee, C.-W., Dynamic analysis and control technology in a fishing gear system. Fisheries Science 68 (sup2), 2002, 1835-1840.
5. Takagi, T., Shimizu, T., Suzuki, K., Hiraishi, T., and Yamamoto, K., Validity and layout of “NaLA”: a net configuration and loading analysis system. Fisheries Research 66 (2-3), 2004, 235-243.
6. Gomi, S., Takagi, T., Suzuki, K., Shiraki, R., Ogino, I., and Asaumi, S., Controlling a fishing net geometry underwater using a data assimilation method. Applied Ocean Research 106, 2021, 102467.
7. Evensen, G., Sequential data assimilation with a nonlinear quasi-geostrophic model using Monte Carlo methods to forecast error statistics. Journal of Geophysical Research: Oceans 99 (C5), 1994, 10143-10162.

HYDRODYNAMICS OF POLYETHYLENE KNOTTED DIAMOND MESH NETTING PANELS

Francisco BOTTERO, Manuel GONZÁLEZ
Universidade da Coruña, Campus Industrial de Ferrol, Laboratory of Mechanical Engineering, Ferrol, 15403, A Coruña, Spain

Abstract

Research on fishing netting, particularly diamond mesh netting used in trawling, remains unexplored. Despite its widespread use, there is a lack of detailed understanding of its hydrodynamic behaviour under varying mesh geometries, material properties, and operational conditions. Most existing studies focus on simplified mesh types, overlooking complex interactions that are crucial in real-world trawling operations.
This study presents a detailed experimental study of the drag and lift coefficients of this type of netting. Experiments were conducted in a towing tank using seven different netting samples. In addition to commonly studied parameters such as solidity, angle of attack, and flow speed, two factors specific to diamond mesh netting were also considered: mesh opening and mesh orientation (T0 or T90). These, along with other geometric and mechanical aspects, such as twine diameter, mesh size, and twine stiffness, play a critical role in netting performance and selectivity. More than 1500 experimental data points were generated, covering solidities from 0.09 to 0.77.
Our main findings are: (i) the empirical formulae available for the drag and lift of the netting showed significant discrepancies with the experimental observations, especially for solidities above 0.3; (ii) the outline drag and lift coefficients are linear concerning the solidity, which contradicts most published empirical formulae; (iii) drag in the T0 orientation is less than in the T90 orientation, while the lift is greater. Finally, new empirical formulae for drag and lift based on linear regression of experimental data were proposed, with excellent goodness of fit.

Keywords

Diamond mesh, hydrodynamics, solidity, empirical formulae, trawl fishing gear

Introduction

Towed fishing gears, such as trawls, are the most important gear in marine fishing in terms of the weight and value of the catches. Trawl netting typically features a knotted diamond mesh morphology, usually made from polyethylene (PE). The comprehension of the hydrodynamic characteristics of the netting is crucial for making effective modifications and improvements in the design of fishing gear,

enhancing capture efficiency, and reducing environmental impact [4], [6]-[8]. In addition, it serves to develop realistic computational models that simulate netting behaviour during fishing operations, avoiding costly and time-consuming sea trials [9], [14], [15].

The standard method for characterising the hydrodynamics of the netting involves experimentally measuring the drag and lift coefficients on a flat rectangular netting panel. This approach is labour-intensive and requires specialised facilities. To minimise the dependence on experimental testing, researchers use experimental data to develop empirical formulae based on the netting solidity S. A significant amount of research related to the measurement of forces and modelling of hydrodynamic coefficients has been published in the last decades [2], [10]-[13], [17], [19].

Most of the experimental work done to measure hydrodynamic forces on netting has been focused on aquaculture netting, with square meshes and thin twines, and often knotless. However, there is a notable absence of studies that address the hydrodynamics of knotted diamond mesh netting made of thick PE twines, such as those typically used in towed fishing gear. This netting has important physical and operational differences with the aquaculture netting, in terms of thickness and surface roughness of the twines, shape and size of the knots, variable shape of the mesh, etc. Hence, empirical formulas based on experimental data from aquaculture netting might yield erroneous results when extrapolated to PE diamond mesh netting used in trawl gear. In this work, a detailed experimental study of the drag and lift coefficients of this kind of netting is presented.

Empirical formulae for drag and lift coefficients

Most empirical formulae express the drag and lift coefficients as a function of the solidity S of the netting, defined as the ratio of the solid area of the netting panel A_s to its outline area A_{out} (the area of the bounding rectangle):

$$S = A_s/A_{out} \tag{1}$$

Solidity is a parameter that offers a quick assessment of the density of a netting panel but does not convey information about its morphology. Nevertheless, it is widely employed in existing formulations due to its high level of generality. It can be calculated in two ways: (i) experimentally, by analysing digital images of the netting; (ii) using analytical expressions based on the nominal dimensions of the netting, such as mesh size l_m and twine diameter d_t. Although the experimental method is more precise, it is also more complicated, and therefore most authors use analytical expressions.

Another important aspect that needs to be clarified is the hydrodynamic coefficient, defined as:

$$C = 2F/\rho v^2 A \tag{2}$$

where F is the hydrodynamic force on the object (drag or lift), ρ is the mass density of the fluid, v is the relative flow speed between the object and the fluid, and A is the reference area. Two choices were found in the literature regarding the reference area A: the outline A_{out} and the solid A_s area of the netting panel. To distinguish them, we will use C_D^{out} and C_L^{out} for drag and lift coefficients that use the outline area A_{out}, and C_D^s and C_D^s for coefficients that use the solid area A_s. This distinction implies a simple scale change in the coefficients, which are related by the solidity of the netting:

$$C_D^{out}/C_D^s = C_L^{out}/C_L^s = S \quad (3)$$

This inherent flexibility in the interpretation of hydrodynamic coefficients underscores the importance of clarity and consistency in the reporting methodologies.

Table 1 summarises the formulae available in the literature, with their key features and the assumptions made to derive them. Further details can be found in [3]. The models have been developed for square meshes with thin-diameter twines, in contrast to what happens with trawl fishing netting analysed in the present study. The range of solidities used to derive the models is quite limited, with minimum values around 0.05 - 0.1 and maximum values around 0.2 - 0.3.

Table 1

Summary of empirical formulae for drag and lift coefficients of netting proposed by different authors.

Author	*Coefficients*	*Mesh shape*	*Knot effect*	*Variables*	*Solidity range*
Milne [12]	C_D^s	Diamond, square	Yes	S	0.067 - 0.200
Aarsnes [1]	C_D^{out}, C_L^{out}	Square	No	S, α	n/a
Løland [11]	C_D^{out}, C_L^{out}	Square	No	S, α	0.130 - 0.317
Zhan [19]	C_D^s, C_L^s	Square	No	S, α, v	0.128 - 0.223
Fridman [5]	C_D^s	n/a	No	S, v^b	n/a
Balash [2]	C_D^{out}	Square	Yes	S, v^b	0.051 - 0.235

Some models only provide the drag coefficient in netting oriented perpendicular to the flow. Strekalova [16] analysed the variation of the drag coefficient for ropes at different angles of attack, and proposed that the drag coefficient at an angle α ($\mathrm{C_{D_\alpha}}$) can be calculated from the drag coefficient at $\alpha = 90°$ ($\mathrm{C_{D_{90}}}$) as:

$$\mathrm{C_{D_\alpha}} = \mathrm{C_{D_{90}}} \sin^3(\alpha) \quad (4)$$

This correction could be applied to models that do not consider α variation.

Materials and methods

Experimental setup

Seven samples of new high-density polyethylene (HDPE), single twine braided, knotted diamond mesh netting have been tested, as detailed in Table 2.

Table 2
Main characteristics of the tested netting samples: twine diameter d_t, nominal mesh size l_m and number of meshes in the normal and tangent directions, m_N and m_T, according to Figure 2. d_t and l_m are expressed in mm.

Netting	d_t	l_m	m_N	m_T	d_t/l_m
redline–3.2–160	3.2	160	4	5	0.020
redline–4–100	4	100	6	8	0.040
redline–4–120	4	120	5	6	0.033
redline–5–100	5	100	6	8	0.050
redline–5–120	5	120	5	6	0.042
tp–pe–4–80	4	80	8	10	0.050
tp–pe–5–70	5	70	8	10	0.071

Experiments aimed at measuring the drag and lift forces on the netting samples were conducted at the towing tank of the Research Centre for Naval and Industrial Technologies of the University of A Coruña, using a testing device specifically designed and manufactured for this research (Figure 1).

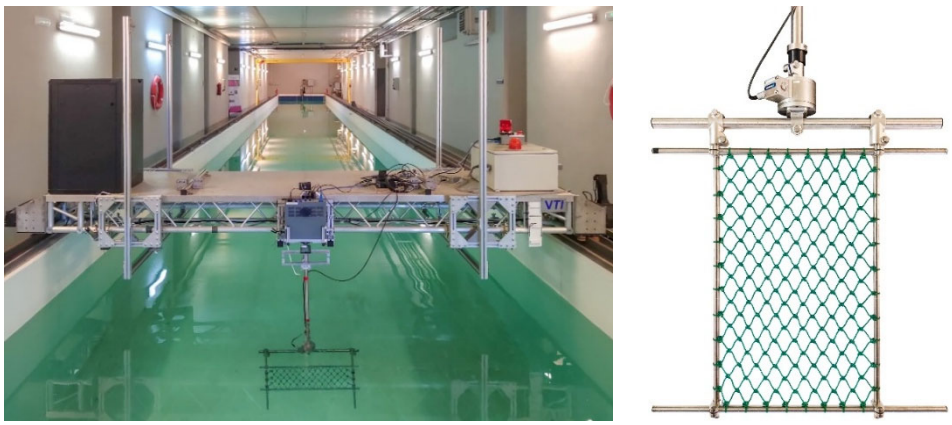


Figure 1
On the left, the towing tank and netting testing device mounted on the towing carriage. On the right, a detail of the frame used to hold the samples.

The test consists of towing the frame at a constant speed and with a certain angle of attack and measuring the drag and lift forces with and without the netting sample mounted on it (two runs are required for each test), so forces on the netting are calculated by subtraction. A preliminary study was carried out to determine

the optimal waiting time between consecutive runs to return the body of water to a calm state and avoid disruptions that could affect the results.

Factors affecting hydrodynamics of netting

The effect of mesh opening on the shape of diamond mesh netting is shown in Figure 2, along with the standard tangent T and normal N directions in this kind of netting. Unlike square meshes, diamond meshes can open or close depending on the forces acting on them, thus modifying the dimensions of the netting panel. Also, meshes are not symmetric, so it is easy to almost completely close the meshes by pulling in the N direction, but it is very difficult to achieve this by pulling in the T direction. Mesh opening λ is defined as the ratio between the tangent l_{mT} and nominal l_m mesh sizes.

$$\lambda = l_{mT}/l_m \ = \sin(\phi) \tag{4}$$

In general, an increase in mesh opening results in a larger outline area A_{out} while the solid area A_s remains virtually the same, leading to a decrease in solidity. Therefore, the solidity of diamond mesh netting is not constant but varies with mesh opening. High-resolution digital images of the netting were acquired, and image analysis software was employed to calculate solidity as the ratio of netting pixels to the total number of pixels in the image, denoted as S^{exp} to distinguish from the solidities obtained by analytical expressions.

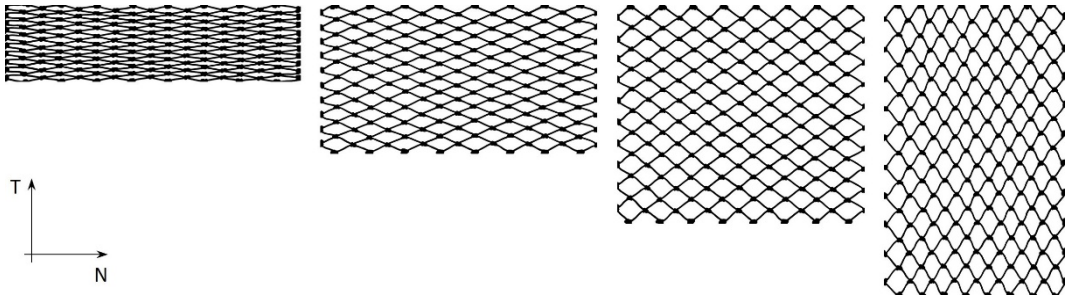


Figure 2
Effect of mesh opening λ on the shape of diamond mesh netting, for λ = 0.2, 0.4, 0.6 and 0.8 (left to right). Photographs of the tp-pe-4-80 sample at $\alpha = 90°$.

Another important aspect of diamond mesh netting is its orientation, either T0 or T90. At $\alpha = 0°$, the T0 orientation corresponds to the N-direction of the netting being parallel to the water flow, while in the T90 orientation, the T-direction of the netting is aligned with the water flow.

Parametric study

To study the effect of the aforementioned factors on the hydrodynamics of diamond mesh netting, an experimental parametric study summarised in Table 3 was conducted. Mesh opening λ could adopt values between 0 and 1, but practical experience shows that values of $\lambda > 0.2$ or $\lambda > 0.8$ are difficult to achieve due to

the stiffness of knots and twines. The variation of α is automated in our experimental setup, so a fine grid was taken for this parameter: 9 sample points in steps of 10°. Regarding the fluid speed v, three sample points were taken from 0.5 to 1.5 m/s. Higher speeds were not used to avoid exceeding the capacity of the force sensor.

Table 3
Parameters and sample points in the experimental parametric study.

Parameter	*Values*
Orientation	T0, T90
Mesh opening λ	0.2, 0.4, 0.6, 0.8
Angle of attack α(°)	90, 80, 70, 60, 50, 40, 30, 20, 10
Speed v	0.5 1.0 1.5

Results and discussion

Solidity

As expected, the experimental solidity S^{exp} decreases with mesh opening in a non-linear way for $\lambda < 0.6$; beyond that point, solidity remains almost constant (Figure 3). Solidity for $\lambda = 0.2$ is approximately 2.35 times greater than for $\lambda = 0.6$ for all netting samples. No results are shown for the tp-pe-5-70 sample with $\lambda \geq 0.8$ because that netting is so stiff that we could not achieve that level of mesh opening. Measured solidities range from 0.09 to 0.77. It is noteworthy to mention that many of the measured solidities are outside the ranges used in the literature to derive the empirical formulae.

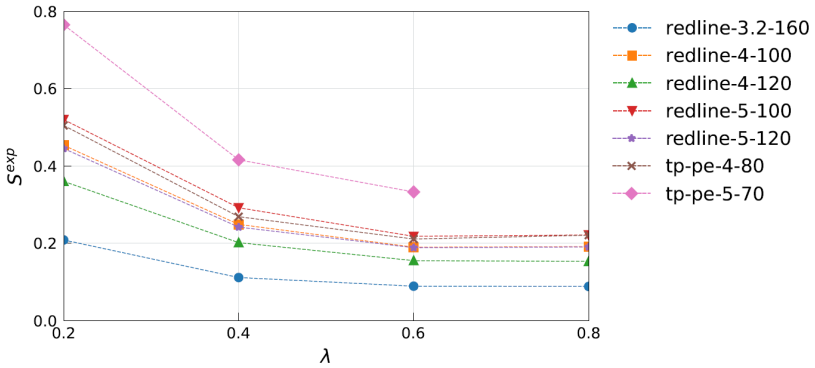


Figure 3
Experimental solidity S^{exp} as a function of mesh opening λ.

Drag coefficient for angle of attack $\alpha = 90°$

Figure 4 plots the drag coefficient C_D as a function of the measured solidity S^{exp}. Although in theory, the results for T0 and T90 should be identical at $\alpha = 90°$,

small differences can be seen due to measurement errors. Both the outline C_D^{out} and the solid C_D^s drag coefficients are represented. C_D^{out} exhibits a clear linear relationship with solidity across all netting samples, mesh openings, flow speeds, and over the full solidity range (0.09 - 0.77). A simple linear regression yields a coefficient of determination $R^2 = 0.98$ and the following model:

$$C_{D_{90}}^{out} = -0.0923 + 1.4682\, S \quad (5)$$

The model is not valid for $S < 0.08$, for example, it predicts zero drag at $S = 0.063$, a minor limitation since such low solidities are rare in this kind of netting. When dividing C_D^{out} by S^{exp} to obtain the solid drag coefficient C_D^s (Equation 3), the relationship with the solidity is no longer clear. Therefore, C_D^s is not a suitable parameter to study the hydrodynamics of this type of netting. From here on, the hydrodynamic coefficients based on the outline area will be used to present the experimental results. A clear trend between drag coefficient and Reynolds number is challenging to establish based on the experimental results.

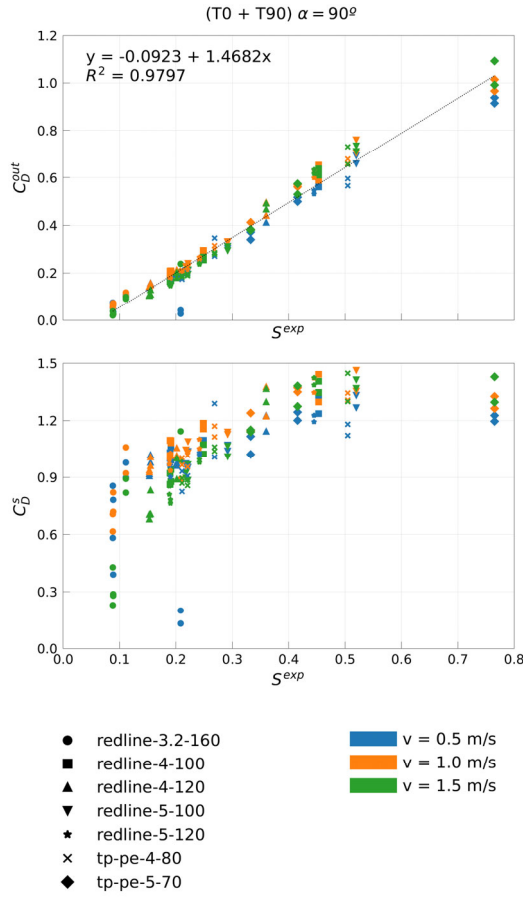


Figure 4
Drag coefficient for $\alpha = 90°$ as a function of S^{exp} at different speeds.

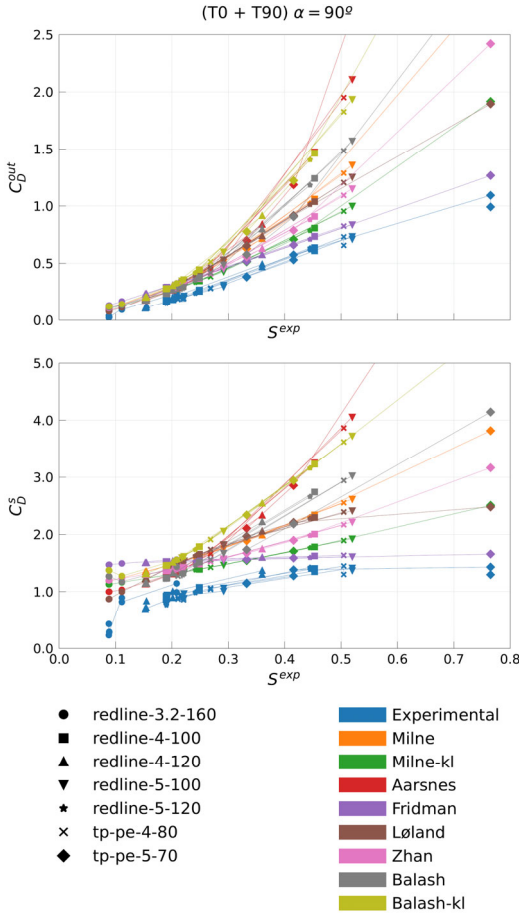


Figure 5
Comparison between experimental data and formulae (kl = knotless).

As shown by Figure 5, none of the existing formulae provides a good fit for the experimental data obtained for knotted diamond mesh netting. While for low solidities some of them seem close to the data, they diverge as solidity increases.

Drag and lift for angles of attack $\alpha < 90$

For a speed of 0.5 m/s, the drag and lift coefficients show fluctuations in all tests and, in many cases, have no clear trend. This effect is even more pronounced for the lift coefficients. Hence, data associated to this speed is omitted. Additionally, data for 1 m/s is excluded because it closely resembles that of 1.5 m/s. Therefore, the analysis will focus on the maximum forward speed of trawling.

Beginning with the drag coefficient, it usually exhibits a steady increase until it reaches a maximum value at $\alpha = 90°$. T0 and T90 orientations show clear differences. Coefficients are higher for the T90 orientation, with some exceptions. As the mesh opening increases, the coefficients tend to equalize, being higher for T0 when the opening reaches 80%. Regarding the lift coefficients, values are usually higher for T0 than T90 orientations, except for openings of 80%. It is important to note that the lift increases until it reaches a peak around 45°. However, for T0 orientations this value tends to 50° as the opening approaches 20%, while for T90 orientations it shifts closer to 40° as the opening increases.

The linear correlation of the hydrodynamic coefficients with solidity at different angles of attack is remarkable. In general, the goodness of fit is exceptionally good, but it gets worse as the α decrease.

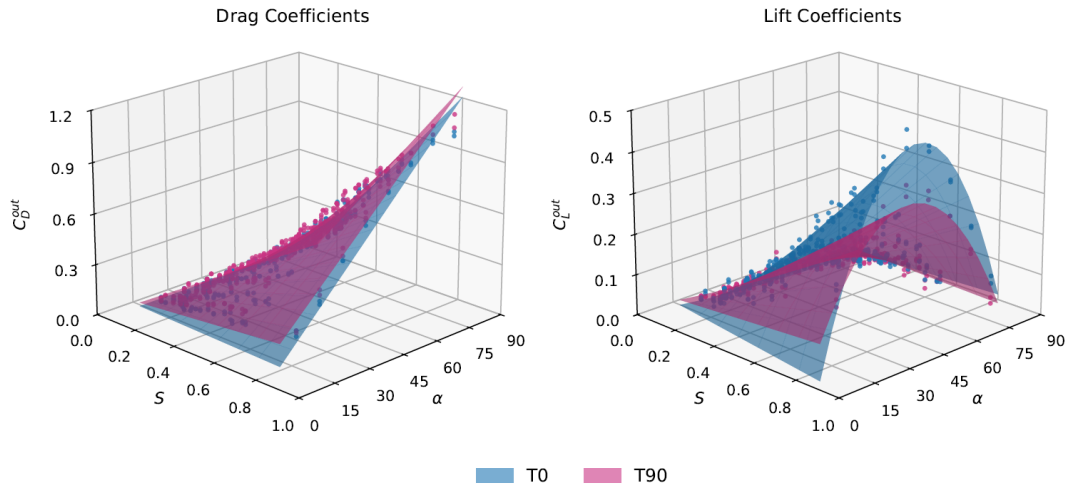


Figure 6
Experimental data and regression model of drag and lift outline coefficients.

All the aspects mentioned can be observed in the 3D plot of Figure 6, which shows the hydrodynamic coefficients as a function of the experimental solidity and the

angle of attack, for both orientations at a flow speed of 1.5 m/s. The regression model used is also plotted alongside the experimental data.

Comparison with formulae from other authors

Figure 7 compares the empirical regression model with the empirical formulae derived by other authors for $S = 0.4$ and 0.8. For both coefficients, the lower the solidity the more accurate the formulae, this happens because they were initially stated for low solidity netting. Therefore, their divergence at higher solidities is unsurprising. Consequently, their comparison with experimental values primarily serves to highlight the absence of an empirical formula capable of accurately predicting the behaviour of high-solidity netting.

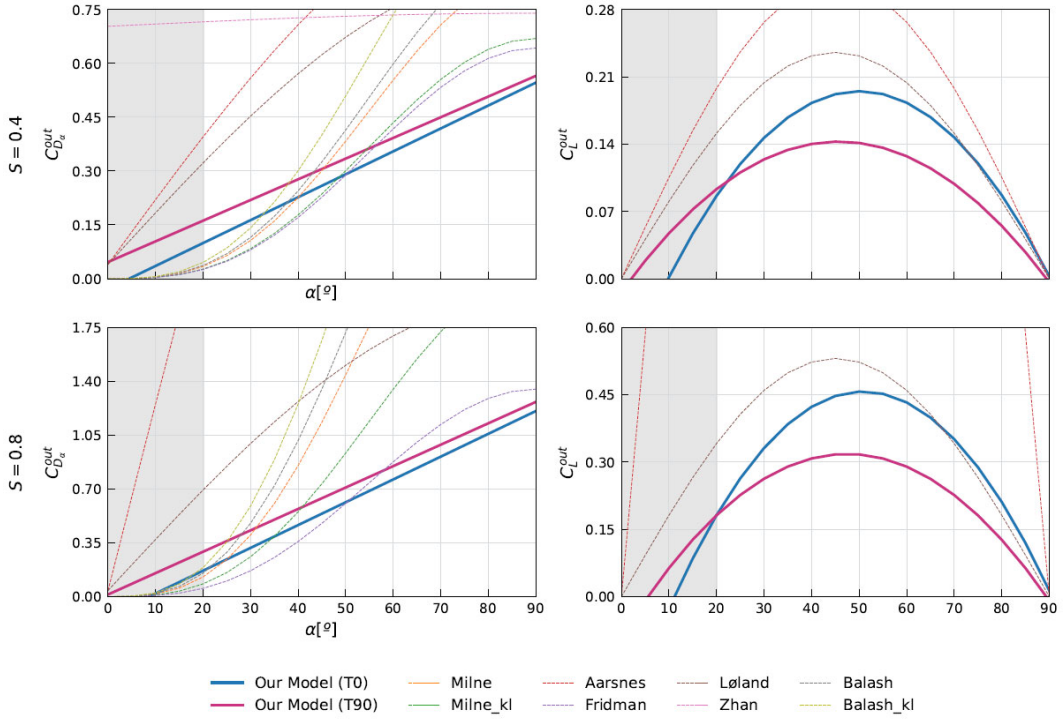


Figure 7
Comparison between the regression model and different authors formulae. Our model is not valid for angles of attack under 20° (shaded in grey).

This study has some limitations derived from the experimental setup, which does not allow to measure accurately the drag and lift at speeds $\leq 0.5\, m/s$, due to vibrations in the towing carriage, and at angles of attack, $< 20°$, where the shadow effect occurs and a special setup is required [18]. The findings underscore that empirical formulae to predict drag and lift of a particular kind of netting need to be derived from experimental data for that netting, to consider its morphology, material and other factors that may affect its hydrodynamics.

References

1. Aarsnes, J., Rudi, H., Loland, G., 1990. Current forces on cage, net deflection. In: Engineering for Offshore Fish Farming. Thomas Telford.
2. Balash, C., Colbourne, B., Bose, N., Raman-Nair, W., 2009. Aquaculture net drag force and added mass. Aquacultural Engineering 41, 14–21.
3. Bottero, F., Gonzalez, M., 2025. Hydrodynamics of polyethylene knotted diamond mesh netting panels. Ocean Engineering 326, 120793.
4. Burgaard, K.B., Carstensen, S., Fuhrman, D.R., Saurel, C., O'Neill, F.G., 2023. Using hydrodynamics to modify fishing performance of a demersal fishing gear. Fisheries Research 268, 106831.
5. Fridman, A.L., Danilov, Y., 1987. Ob Osobennostyah Soprotivleniya Rybolovnoi Seti. Rybolovnoe Hozyajstvo 6.
6. Herrmann, B., 2005. Modelling and simulation of size selectivity in diamond mesh trawl cod-ends. Ph.D. thesis. Aalborg University, Department of Production.
7. Herrmann, B., Wienbeck, H., Moderhak, W., Stepputtis, D., Krag, L.A., 2013. The influence of twine thickness, twine number and netting orientation on codend selectivity. Fisheries Research 145, 22–36.
8. Kennelly, S.J., Broadhurst, M.K., 2021. A review of bycatch reduction in demersal fish trawls. Reviews in Fish Biology and Fisheries 31, 289–318.
9. Lee, J., Lee, C.W., Choe, M.Y., Lee, G.H., 2011. Applying fishing-gear simulation software to better estimate fished space as fishing effort. Fisheries and Aquatic Science 14, 138–147.
10. Løland, G., 1991. Current forces on and flow through fish farms. Ph.D. thesis. Norwegian University of Science and Technology (NTNU).
11. Løland, G., 1993. Current forces on, and water flow through and around, floating fish farms. Aquaculture International 1, 72–89.
12. Milne, P., 1972. Fish and Shellfish Farming in Coastal Waters. Fishing News (Books) Ltd.
13. Patursson, Ø., Swift, M.R., Tsukrov, I., Simonsen, K., Baldwin, K., Fredriksson, D.W., Celikkol, B., 2010. Development of a porous media model with application to flow through and around a net panel. Ocean Engineering 37, 314–324.
14. Priour, D., 2009. Numerical optimisation of trawls design to improve their energy efficiency. Fisheries Research 98, 40–50.
15. Priour, D., De La Prada, A., 2015. An experimental/numerical study of the catch weight influence on trawl behavior. Ocean Engineering 94, 94–102.
16. Strekalova, V., 1964. O Zakone Izmeneniya Sil Soprotivleniya Elementa Trosa. Kaliningradskoe Knizhnoe Izdatel'stvo 18.

17. Tang, M.F., Dong, G.H., Xu, T.J., Zhao, Y.P., Bi, C.W., Guo, W.J., 2018. Experimental analysis of the hydrodynamic coefficients of net panels in current. Applied Ocean Research 79, 253–261.
18. You, X., Hu, F., Takahashi, Y., Shiode, D., Dong, S., 2021. Resistance performance and fluid-flow investigation of trawl plane netting at small angles of attack. Ocean Engineering 236.
19. Zhan, J., Jia, X., Li, Y., Sun, M., Guo, G., Hu, Y., 2006. Analytical and experimental investigation of drag on nets of fish cages. Aquacultural Engineering 35, 91–101.

MOTION AND MOORING DYNAMICS OF A RIGID OFFSHORE CAGE: WAVE TANK EXPERIMENTS AND NUMERICAL SIMULATIONS

Sarath-Krishnan KARUMATHIL, Anne GOSSET, Manuel GONZÁLEZ
Universidade da Coruña, Campus Industrial de Ferrol, Ferrol, A Coruña, 15403 Spain

Abstract

This work presents an experimental–numerical study of the hydrodynamic response of an offshore aquaculture cage, focusing on cage motions and mooring interactions in regular waves. The numerical model couples a two-phase flow solver in OpenFOAM with MoorDyn for dynamic mooring simulation and uses an overset dynamic mesh to resolve the rigid-body motion of the cage.

Validation experiments were carried out in a wave tank with a rigid circular cage (initially without netting panels) held by four mooring lines anchored to the basin floor. Regular waves with three different amplitudes and two periods were generated. Cage motions were tracked using passive optical markers and motion-capture cameras, and the resulting data was compared with numerical predictions. The results demonstrate that the coupled solver can reproduce the key motion characteristics and mooring responses of a rigid offshore cage in waves.

Work is underway to measure tensions in mooring lines and compare them with numerical results. Future work plans to test and simulate a flexible cage instead of a rigid one.

Keywords

Aquaculture cages, Mooring dynamics, computational simulations

Introduction

The growing global demand for fish, combined with constraints on nearshore farming capacity, has accelerated the expansion of aquaculture into offshore environments, where stronger waves, currents, and wind forces prevail. These energetic conditions subject cage structures and mooring systems to complex hydrodynamic loads, increasing the importance of reliable design tools and accurate performance prediction. Offshore aquaculture systems must maintain structural integrity and stock containment under extreme sea states, requiring a thorough understanding of the combined effects of environmental impacts and structural response of the aquaculture systems. Numerical modelling has become an

essential approach for investigating these interactions, enabling the detailed analysis of force distributions, motion characteristics, and mooring behaviour. In particular, Computational Fluid Dynamics (CFD) techniques are increasingly employed to simulate hydrodynamic loading and optimize cage designs for offshore deployment.
An offshore cage system consists of several interdependent subsystems: (i) a floating collar, typically fabricated from high-density polyethylene (HDPE), providing buoyancy and structural compliance; (ii) sinkers or sinker tubes to stabilize cage geometry; (iii) a mooring system comprising anchors and lines to constrain the motions; and (iv) netting panels enclosing the rearing volume. While numerous studies have examined the interactions between individual components or limited subsystem combinations, fully coupled numerical models capable of resolving the complete hydrodynamic–structural behaviour of the system are only beginning to emerge.

The present work contributes to bridging this gap through the development and validation of a coupled CFD–mooring simulation framework for an offshore aquaculture cage. The numerical model integrates a two-phase flow solver in OpenFOAM with MoorDyn for dynamic mooring analysis, employing an overset dynamic mesh to capture rigid-body cage motion. Validation experiments were conducted in a wave tank using a scaled rigid circular cage without netting panels, held in position by four mooring lines anchored to the basin floor. Regular waves with three amplitudes and two periods were generated, and cage motions were recorded using passive optical markers tracked by motion-capture cameras. The predictions of numerical simulation are confronted to experimental data in terms of motion characteristics and mooring responses of the rigid cage in regular waves.

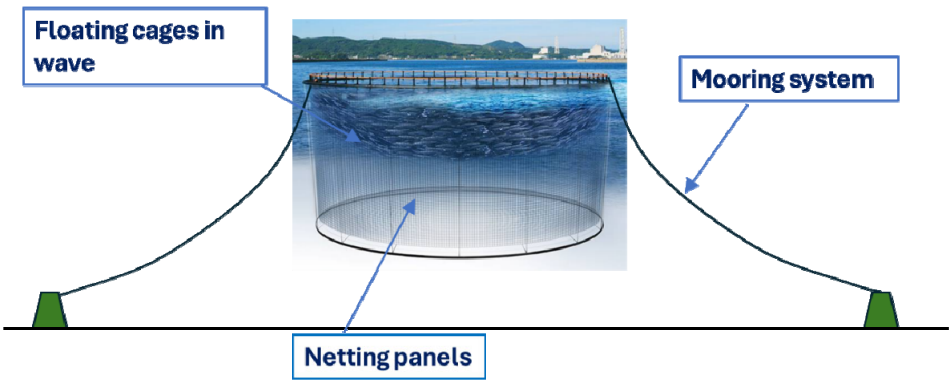


Figure 1
Components of a gravity type offshore aquaculture cage.

Numerical methodology

The computational framework employed in this study is based on *OpenFOAM*®, the open-source finite volume C++ libraries designed for solving partial differential equations arising from fluid dynamics. Specifically, the solver *interFoam* is utilized, which is designed for incompressible, immiscible, two-phase flows. In the turbulent regime, the solver resolves the incompressible, unsteady Reynolds-Averaged Navier–Stokes (RANS) equations for two immiscible fluids (air and water), along with a Volume of Fluid (VOF) method for free surface capturing. Wave generation and absorption within the computational domain are implemented via relaxation zone techniques, which mitigate undesired wave reflections at domain boundaries.

In the initial phase of the study, the floating collar is modelled as a rigid body. While this assumption may not be valid under highly energetic sea states, it provides a reasonable first-order approximation for analysing the coupled hydrodynamic processes in the system. The rigid body dynamics are simulated using *OpenFOAM*'s sixDoFRigidBodyMotion solver, which computes translational and rotational motion with six degrees of freedom. This solver integrates the rigid body equations of motion under the influence of hydrodynamic forces and moments.

Maintaining mesh quality is critical in simulations involving large structural motions. The overset meshing technique is selected for the present study, as it provides superior capability for unrestricted body motion while maintaining numerical stability and solution accuracy. In this method, the floating body is enclosed within a moving mesh block that overlaps with a stationary background mesh. Solution variables are exchanged across the overlapping region via interpolation, ensuring continuity. This technique offers greater flexibility for large and complex motions.

Accurately modelling mooring systems in offshore aquaculture remains challenging, largely due to the limited availability or uncertainty of key physical properties such as axial stiffness, elasticity, and damping characteristics. In the absence of well-defined material and configuration data, model development often relies on iterative calibration, where both physical parameters and numerical settings are refined through trial-and-error procedures.

MoorDyn (Hall and Goupee, 2015) adopts a lumped-mass formulation, discretizing each mooring line into interconnected nodes that account for axial tension, weight, hydrodynamic drag, and seabed interaction. This approach is well suited for capturing large displacements and nonlinear dynamic behaviour in mooring lines associated with floating offshore structures.

In the present study, MoorDyn was selected for the fully coupled simulation of a moored aquaculture cage under combined wave and current loading, owing to its open-source implementation and established compatibility with the overset dy-

namic mesh solver (*overInterDyMFoam*) in *OpenFOAM*. As demonstrated by Mi et al. (2024), this coupling enables bidirectional force exchange between the mooring lines and the floating structure, thereby supporting high-fidelity fluid–structure interaction simulations of offshore aquaculture cages.

Experimental Campaign

An experimental campaign was carried out to generate validation data for the numerical simulations and to study the hydrodynamic behaviour of a rigid offshore aquaculture cage under controlled wave conditions. The tests were conducted in a wave basin equipped with a multi-flap wavemaker capable of generating both regular and irregular waves. For this study, only regular waves were considered, with three combinations of wave amplitude and two combinations of period chosen to represent a range of wave steepnesses relevant to offshore aquaculture applications.

The physical model consisted of a rigid circular cage representing the floating collar of a full-scale structure (Figure 2). With a diameter of 1 m and a height of 0.4 m, it represents a real cage with a model scale of 1:25. The cage was moored using four synthetic lines arranged symmetrically and fixed to anchors on the basin floor. The mooring configuration was scaled to maintain appropriate stiffness and restoring characteristics at model scale.

The motion of the cage was recorded using a motion-capture system composed of passive reflective markers placed at several points on the collar. These markers were tracked by an array of infrared cameras positioned around the basin, providing six-degree-of-freedom time series of cage motions (surge, sway, heave, roll, pitch, and yaw).

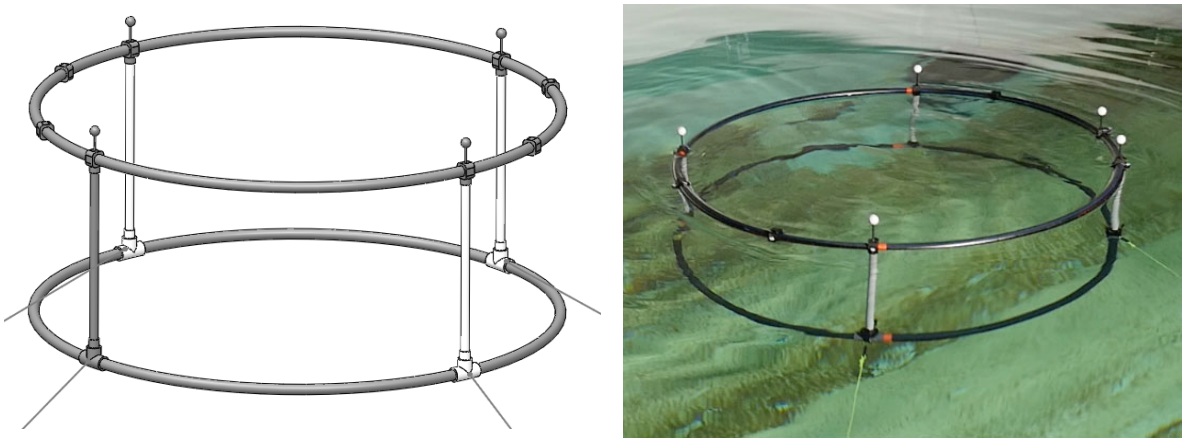


Figure 2
Computer design of the physical model (left) and real model in the wave basin (right).

All measurements were synchronised with the wave maker signal to enable direct phase-resolved comparison with numerical results. This dataset forms the basis for validating the coupled numerical solver by comparing predicted cage motions with experimental observations across the tested wave conditions.

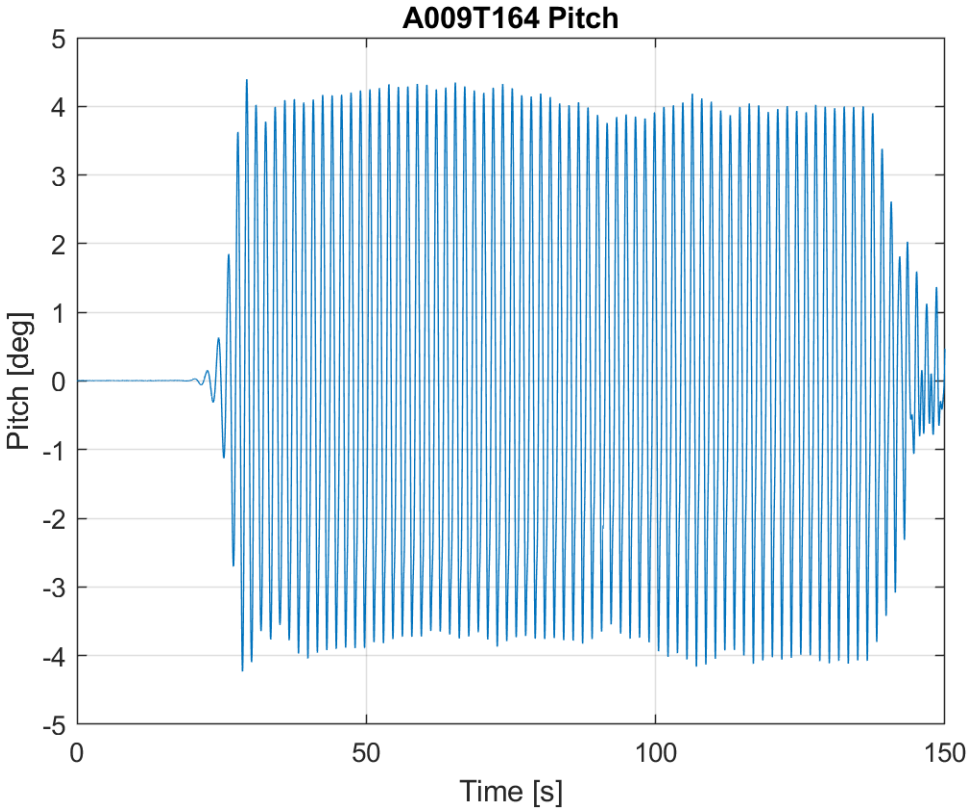


Figure 3
Captured pitch motion of the rigid collar cage under a regular wave of amplitude 9 cm and period 1.64 seconds.

Results

The dynamic response of the rigid circular cage subjected to regular wave forcing was quantified in terms of pitch, roll, yaw and translational (X, Y, Z) motions.

The **pitch response** (Figure 3) was identified as the dominant motion mode. After an initial transient, the cage quickly reached steady-state oscillations with amplitudes of approximately ±4.5° (for amplitude 9 cm and period 1.64 seconds). The response was strongly periodic, reflecting the influence of the incoming waves, and remained stable throughout the test duration. These results confirm that wave excitation primarily excites pitch motions in the cage system.

The **roll response** was found to be minimal compared to pitch. The oscillations did not exceed ±0.15°, and the signal exhibited higher-frequency fluctuations superimposed on the wave period, producing a slightly irregular envelope. The

small roll amplitudes demonstrate that the cage maintained lateral stability under the imposed wave conditions, and that roll contributed negligibly to the overall dynamics.
In contrast, the **yaw response** displayed a markedly different behaviour. Instead of remaining centred around zero, the cage experienced slow-varying drift motions, with peak yaw angles reaching approximately 3.2° for the wave amplitude 9 cm and period 1.64 seconds. The translational responses revealed that surge and heave were the dominant motion components, with strong periodic oscillations induced by the incident waves. Surge also exhibited a gradual drift, while sway was characterized primarily by slow-varying lateral excursions of smaller magnitude. Together, these results indicate that the cage motion is strongly affected by wave-induced vertical-plane dynamics, with lateral displacements playing a secondary role. Similar behaviour was observed in other test cases for amplitudes of 5 cm and 7 cm with periods of 1.64 s and 1.92 s.

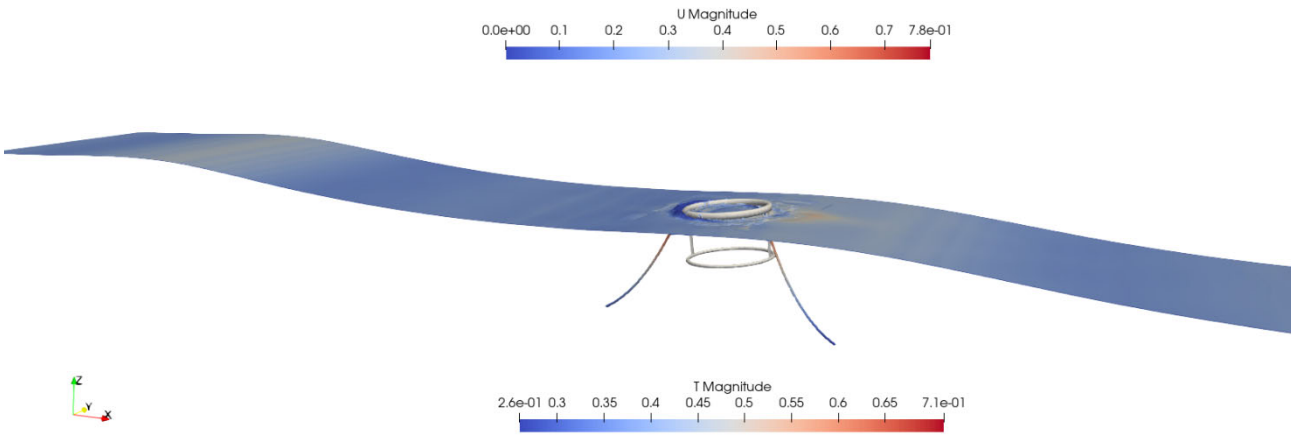


Figure 4
Numerical model of the rigid cage with mooring restraints under regular waves.

Numerical simulations were conducted using the coupled CFD–MoorDyn framework to evaluate the hydrodynamic response of the rigid circular cage under regular wave forcing. The model incorporated a two-phase flow solver in *OpenFOAM* for wave–structure interaction and *MoorDyn* for dynamic mooring line behaviour, with rigid-body motions captured through an overset dynamic mesh. The simulations captured the key features of cage dynamics under wave forcing, with pitch and heave dominating the response and roll remaining negligible. Surge oscillations, yaw drift, and sway excursions were also reproduced, albeit with somewhat smaller magnitudes than observed experimentally. While these preliminary comparisons indicate encouraging consistency between nu-

merical and physical results, a thorough validation against the experimental dataset is still required and will be addressed in the following stages of the study.

Conclusions and future work

This work presented an experimental–numerical study of the hydrodynamic response of a rigid circular aquaculture cage under regular wave forcing. The experiments showed that cage dynamics are dominated by pitch and heave oscillations, with surge also significant, while sway and yaw were mainly characterized by slow drift and roll remained negligible. The coupled CFD–MoorDyn model reproduced the main motion features, particularly in the vertical plane a thorough validation work is in progress.
Future work will focus on measuring and comparing mooring line loads, extending the analysis to flexible floating collars, and incorporating net panels to better capture the hydrodynamic–structural interactions of scaled cage systems.

Acknowledgements

The authors would like to thank the Interreg EU project SISdATA (EAPA_0040/2022) for funding and supporting this project.

References

1. Hall, M., Goupee, A., 2015. Validation of a lumped-mass mooring line model with DeepCwind semisubmersible model test data. Ocean Eng. 104, 590–603. https://doi.org/10.1016/j.oceaneng.2015.05.035
2. Mi, S., Avital, E.J., Williams, J.J.R., Chatjigeorgiou, I.K., 2024. Development of a novel multi-component coupled numerical model for aquaculture systems in OpenFOAM. Appl. Ocean Res. 151, 104146. https://doi.org/10.1016/j.apor.2024.104146

EXPERIMENT AND CFD SIMULATION TO INVESTIGATE THE EFFECT OF GROUND BELT MOTION WITH BOUNDARY LAYER PROFILE ON THE BOTTOM OF FLUME TANK.

Nurul Huda*[1], Tomas Araya-Schmidt[2], Daniel Gosse[2,] Mia Abrahamsen-Prsic[3], Tiago Veiga-Malta[1], Esther Savina[1], Finbarr G O'Neill[1]

[1]Technical University of Denmark, National Institute of Aquatic Resources, Section for Fisheries Technology, 9850 Hirtshals, Denmark

[2] Centre for Sustainable Aquatic Resources, Fisheries and Marine Institute, Memorial University of Newfoundland, NL A1C 5R3 St. John's, Canada

[3] SINTEF Ocean AS, Department of Ships and Ocean Structures, 0614 Oslo, Norway

Abstract

Accurate scale modelling of demersal trawl in the flume tank is essential for development of sustainable demersal towed fishing gear. However, the current modelling approaches often neglect the dynamic interaction between the gear and the seabed. This study investigates the potential of using flume tank ground belt motion to replicate seabed contact effects in scale models. We conducted a series of experiments under two conditions: flume tank without net models, flume tank with net models, and CFD simulations of flume tank without net models. The focus was on analysing how varying the belt ground speed relative to the water flow influences the boundary layer characteristics near the bottom of the tank.

Velocity distribution at specific heights were measured for different combinations of belt and water flow speeds. In addition, CFD simulations were carried out to as a prediction tool of boundary layer profile near the bottom of flume tank. The results from both experiments and CFD simulations show that running the flume tank ground motion slower and faster than water flow speed significantly modifies the bottom boundary layer. This modification, in turn, affects the tension load distribution in the trawl, as observed in the net model experiments.

These findings suggest that controlled ground belt motion can serve as a viable method to simulate realistic bottom contact in flume tank experiments, thereby enhancing the fidelity of scale modelling for demersal trawl gear development.

Keywords

flume tank, ground belt motion, demersal trawl, CFD, boundary layer

Introduction

Flume tanks have played a vital role in the design and development of fishing gears. These facilities allow us to test small scale model trawls to predict key parameters such as shape, geometric dimensions, towing load, and even fuel consumption before the gear is manufactured in the full scale (Winger et al., 2006). In contrast to real world conditions, where the gear is towed by a vessel, in the flume tank, we keep the gear still while the water is circulated and the bottom of the tank is moved at the same speed as the current speed. This setup creates a steady, controlled and repeatable environment which is ideal for experimental testing.

In actual fishing operations, especially when targeting demersal species, trawl gear encounters various types of seabeds, from rock to hard sand to soft mud. Huda et al., (2025) demonstrated that softer seabed sediments tend to increase the spread and towing load of demersal trawls. Changes to the gear geometry can affect the herding area and influence the trawl's effectiveness in capturing target species, while the towing load influences the fuel consumption and carbon emission during fishing operation (Kaykaç et al., 2017; O'Neill et al., 2018). Notably, current flume tank testing methods do not account for seabed sediment types and hence do not predict their effect.

Given that research has shown that the interaction between fishing gear and seabed sediments can significantly alter the efficiency and environmental footprint of fishing operations (Eigaard et al., 2016; Paradis et al., 2021), this represents a significant knowledge gap which may limit our ability to modify or design gears that will reduce bycatch, minimize environmental impact and improve fuel efficiency (Aydın & Tosunoğlu, 2011; Maynou et al., 2021).

In this paper we investigate a new flume tank test methodology, where instead of keeping the ground belt speed the same as the current speed, we tested the gear by running the ground belt speed slower and faster than the current speed. We consider how this affects the towing load and the gear geometry and discuss how this approach may be used to model the effect of different seabed sediment types. To further understand this effect, we measured the flow speed at different heights and longitudinal positions in the boundary layer close to the ground belt. Additionally, we conducted CFD simulations as a prediction tool of boundary layer at the bottom of flume tank.

Methods

Small scale demersal trawls test with various current and ground belt speeds

To investigate the effect of ground belt speed on the towing load and the trawl geometry, a 1:10 small scale demersal trawl was tested in the Flume Tank North Sea A/S in Hirtshals, Denmark with 4 current speeds: 0.25, 0.4, 0.55, and 0.7 m/s (Figure 1). At each current speed, instead of running the ground belt speed equal to current speed, the ground belt speed was set to run at five different speeds: 0, 0.25, 0.4, 0.55, and 0.7 m/s, which resulted in 20 combinations of current and ground belt speed.

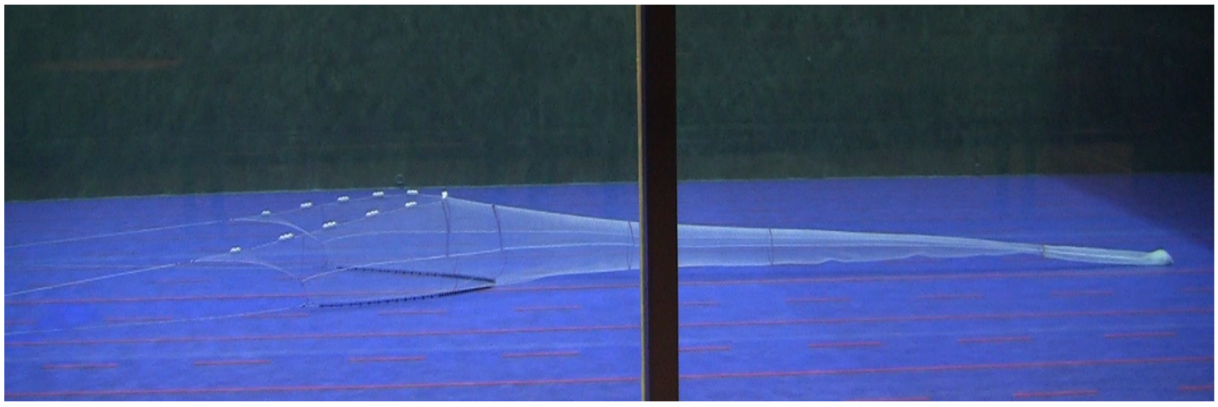


Figure 1
1:10 Trawl scale model used in flume tank test Hirtshals

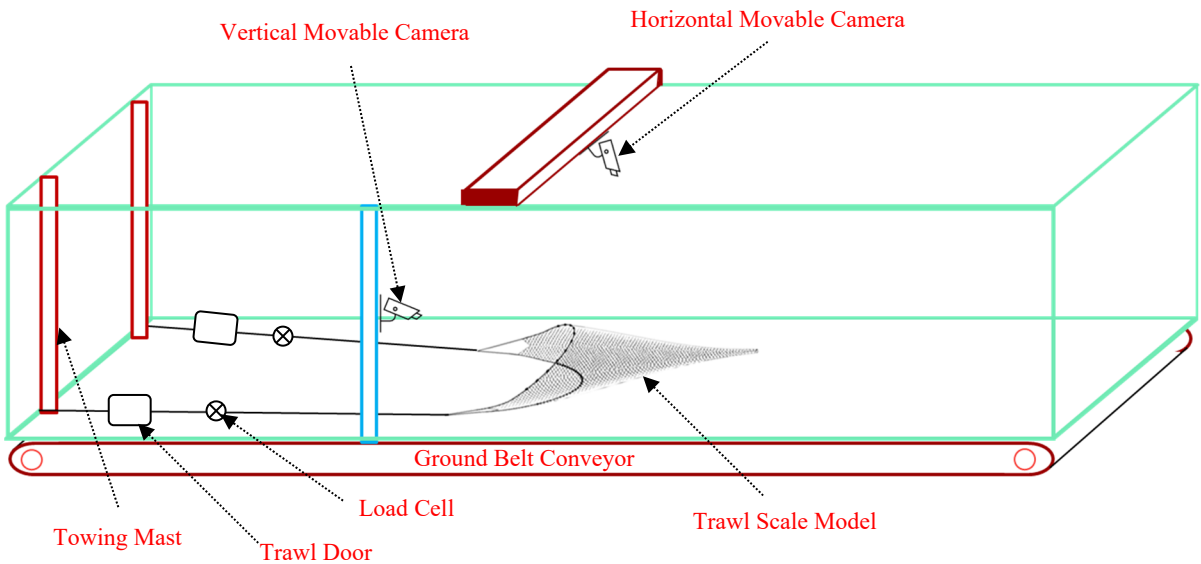


Figure 2

Small scale model flume tank test layout

The warp tensions were recorded using Futek tension loadcells located between the trawl door and the fishing gear. The rigging comprised 2.42 m lower bridles,

2 m sweep ropes, 0.185 m backstops, and 4 m warp lines from trawl door to towing mast as illustrated on Figure 2. The geometry of trawl (headline height, wing spread, and door spread) was recorded using movable camera.

Flume tank boundary layer measurement

The boundary layer was investigated at current speeds 0.5 m/s and four ground belt speeds: 0, 0.25, 0.5, and 0.7 m/s. A magnetic-inductive flowmeter (Figure 4) measured current speed at heights 2, 5 and 20 cm from the ground belt at a central position, 12.25 m from the front of the ground belt (Figure 3).

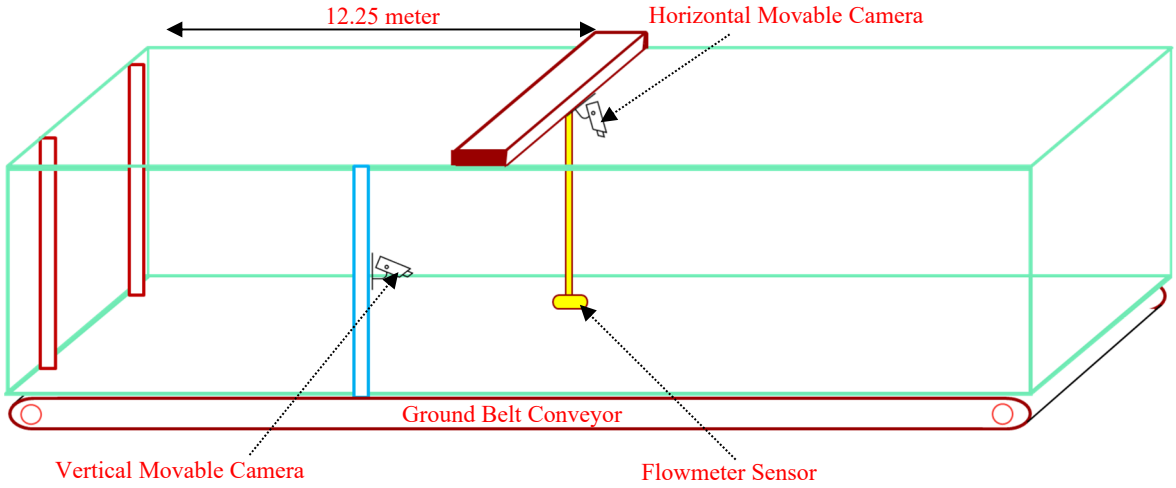


Figure 1
Boundary layer measurement layout

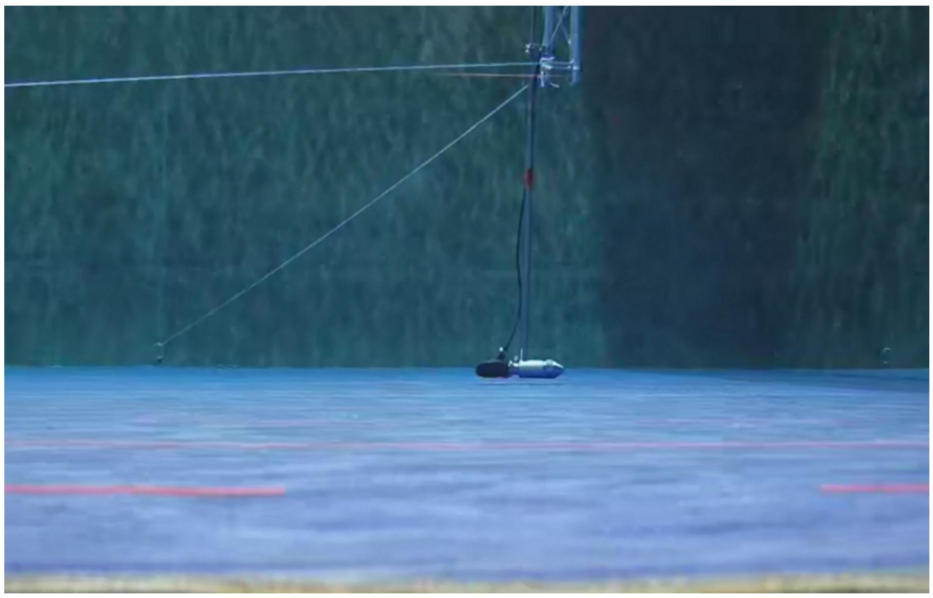


Figure 2
Flowmeter used for boundary layer measurement in flume tank Hirtshals

Computational Fluid Dynamic (CFD) simulation of flume tank to predict boundary layer

A 2D computational fluid domain was built, 21.3 m long and 2.7 m height, reflecting the dimensions of the North Sea Flume Tank. The ANSYS Fluent program with K Omega SST solver was used. The fluid domain consisted of 50000 structured quadrilateral mesh, with concentrated small cells near the bottom of the flume tank. The mesh is shown in Figure 5. Boundary condition of the tank bottom was "no slip condition" with moving wall motion to simulate ground belt speed with range 0, 0.25, 0.5, and 0.7 m/s with uniform current speed inlet 0.5 m/s and atmospheric pressure at outlet.

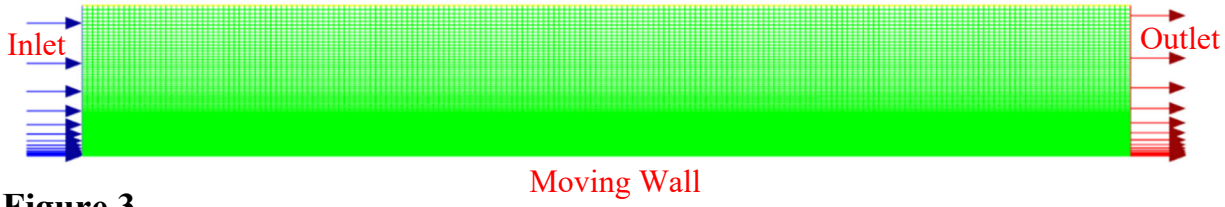


Figure 3
CFD boundary condition set up of flume tank

Results

Testing small scale demersal trawl with various current and ground belt speed

Figure 6 shows the load and trawl headline height during the tests with the current speed ranging from 0.25 to 0.7 m/s and the belt speed ranging from 0.0 to 0.7 m/s. The load increases and the headline height decrease with increasing ground belt speed. Meanwhile Figure 7 shows how the wing spread, and the door spread increase with the increase of ground belt speed.

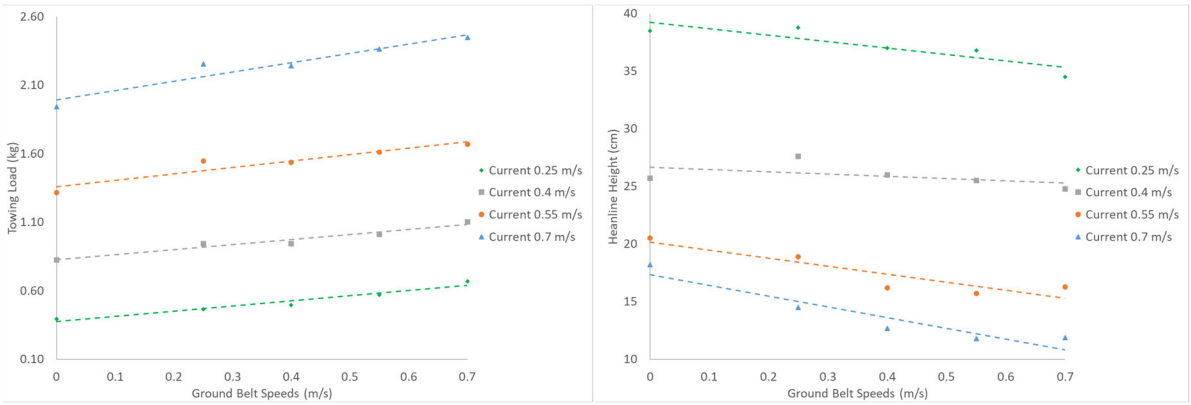


Figure 4
Towing load and headline height results

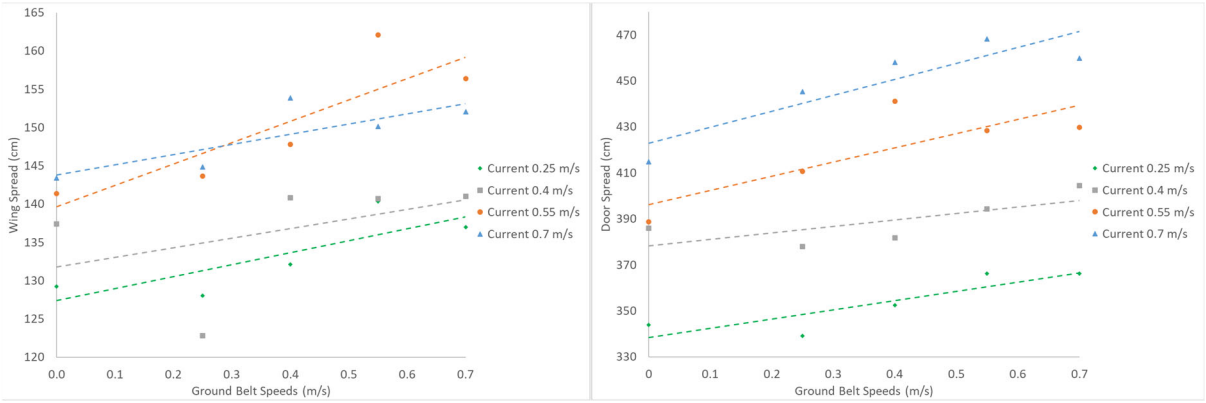


Figure 5
Trawl spread geometry results

Boundary layer measurements

The measured boundary layer velocity profiles and the results of the CFD simulations are illustrated in Figure 8. The profiles are presented as a function of the fluid velocity against the height above the ground plane (in meter), up to 0.2 m. Eight distinct curves correspond to different belt speed 0, 0.25, 0.5, and 0.7 m/s on same current speed 0.5 m/s as shown in Figure 8. The flume tank measurements are represented by solid line while the CFD measurements are the dashed lines.

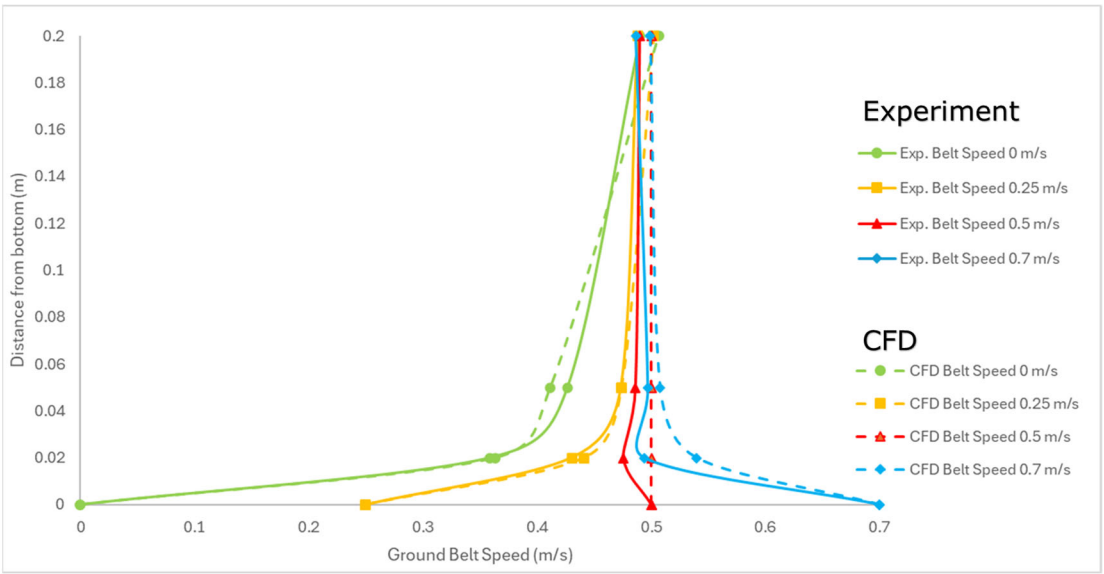


Figure 6
Boundary layer profile near bottom of flume tank

Discussion and conclusion

The flume tank test results of 1:10 small scale demersal trawl have confirmed that there are increases in load, wing spread, door spread and reduction in headline

height as ground belt speed increase. Huda et al. (2025) find similar changes to the load and geometry during sea trials with a full-scale gear when moving from hard sand to softer, muddier sediments.
These results suggest that there is a possibility to model the effect of towing on different sediment types by modifying the ground belt speed in the flume tank.

The boundary layer experiment shows that as the ground belt speed increases, the boundary layer thickness decreases up to the point when the belt and current speed are the same and the boundary layer effectively disappears. When the belt speed exceeds the current speed a boundary layer reappears, and its thickness increases as the belt speed increases.

These results may explain the increase in drag with increasing belt speed observed in the scale model trials as the ground gear and the lower netting panels will experience an increase of velocity (within the boundary layer) as the belt speed increases.

We believe the results of this study will improve the development of sustainable towed fishing gears that reduce bycatch and environmental impact.

Acknowledgements

The research works has received funding from the BlueBio Cofund and is part of the project Reducing environmental impact and greenhouse gas emissions in commercial fisheries (RightFish).

References

1. Aydın, C., & Tosunoğlu, Z. (2011). Evaluation of Sorting Grids for Deepwater Rose Shrimp (Parapenaeus Longirostris) in the Eastern Mediterranean Demersal Trawl Fishery. *Journal of Applied Ichthyology*. https://doi.org/10.1111/j.1439-0426.2011.01897.x
2. Eigaard, O. R., Bastardie, F., Breen, M., Dinesen, G. E., Hintzen, N. T., Laffargue, P., Mortensen, L. O., Nielsen, J. R., Nilsson, H. C., O'Neill, F. G., Polet, H., Reid, D. G., Sala, A., Sköld, M., Smith, C., Sørensen, T. K., Tully, O., Zengin, M., & Rijnsdorp, A. D. (2016). Estimating seabed pressure from demersal trawls, seines, and dredges based on gear design and dimensions. *ICES Journal of Marine Science*, *73*, i27–i43. https://doi.org/10.1093/icesjms/fsv099
3. Huda, N., Veiga-Malta, T., Savina, E., & O'Neill, F. G. (2025). The impact of ground gear weight and sediment type on the towing resistance and geometry of demersal trawl fishing gears. *ICES/FAO Working Group on Fishing Technology and Fish Behaviour (WGFTFB25)*, 138–138. https://doi.org/10.17895/ices.pub.30231325

4. Kaykaç, M. H., Düzbastılar, F. O., Zengin, M., Süer, S., & Rüzgar, M. (2017). Untitled. In *Turkish Journal of Fisheries and Aquatic Sciences*. https://doi.org/10.4194/1303-2712-v17_5_06
5. Maynou, F., García-de-Vinuesa, A., Martínez-Baños, P., Sánchez, P., & Demestre, M. (2021). Relative Catch Performance of Two Gear Modifications Used to Reduce Bycatch of Undersized Fish and Shrimp in Mediterranean Bottom Trawl Fisheries. In *Marine and Coastal Fisheries*. https://doi.org/10.1002/mcf2.10178
6. O'Neill, F. G., Summerbell, K., & Ivanović, A. (2018). The contact drag of towed demersal fishing gear components. *Journal of Marine Systems*, *177*, 39–52. https://doi.org/10.1016/j.jmarsys.2017.08.002
7. Paradis, S., Goñi, M. A., Masqué, P., Durán, R., Arjona-Camas, M., Palanqués, A., & Puig, P. (2021). Persistence of Biogeochemical Alterations of Deep-Sea Sediments by Bottom Trawling. *Geophysical Research Letters*. https://doi.org/10.1029/2020gl091279
8. Winger, P. D., DeLouche, H., & Legge, G. (2006). Designing and testing new fishing gears: The value of a flume tank. *Marine Technology Society Journal*, *40*(3), 44–49. https://doi.org/10.4031/002533206787353240

CLOSE-PROXIMITY VESSEL-GEAR HYDRODYNAMICS: BEAM TRAWLS AND STOW NETS

Karsten BREDDERMANN[1], Daniel PRIOUR[2]

[1]GEOMAR Helmholtz Centre for Ocean Research Kiel, RD4, 1-3, Wischhofstrasse, Kiel, 24148, Germany
[2]Ifremer, RDT Research and Technological Development, Plouzané, 29280, France

Abstract

This study presents a methodological framework for analyzing the close-range hydrodynamic interaction between fishing vessels and fishing gear - specifically beam trawls and stow nets - using Fluid-Structure Interaction (FSI) simulations with OpenFOAM and FEMNET. In many coastal shrimp fisheries, the beam trawl is operated in close proximity to the vessel, making the interaction between the ship-induced flow and the net or trawl structure potentially a key factor influencing gear performance and bycatch patterns.

Similarly, stow nets are also deployed in close proximity to the vessel but differ in their mode of operation: both the net and the vessel are anchored, and the gear is driven by tidal or riverine currents. As a passive alternative to beam trawling, stow nets offer very low fuel consumption. Understanding the flow dynamics and structural responses in such configurations is essential for evaluating their efficiency and viability.

The paper outlines the modelling setup, assumptions, and simplifications applied in the simulations, and presents initial results demonstrating key interaction effects. This work lays the foundation for further investigations into gear performance, ecological impact, and sustainable fishing practices through high-fidelity numerical modelling.

Keywords

FEMNET, OpenFOAM, vessel-gear interaction, numerical modelling, partitioned approach

Introduction

As the demand for sustainable fishing practices grows, there is increasing pressure to minimize fishing's environmental impact, particularly in Marine Protected Areas (MPAs). The European Union (EU) and the United Kingdom (UK) are considering or implementing bans on bottom trawling in these regions, posing challenges for coastal fisheries that rely on such practices. To address these challenges, there is a need for alternative fishing methods that reduce ecological damage while ensuring the economic viability of fishing communities.

One of the main concerns in sustainable fishing is bycatch. Minimizing bycatch is essential for achieving more sustainable practices, and understanding the interactions between fish and fishing gear is a crucial step toward this goal. Specifically, hydrodynamics may play an important role in triggering fish behaviour, influencing their interaction with fishing gear. Fish possess specialized sensory organs, such as the lateral line, which allow them to perceive and respond to hydrodynamic stimuli, including flow patterns like vortex streets, tip vortices, and bow waves, as well as critical flow properties such as pressure gradients, vorticity, and acceleration ([4], [3]). If the reactions of fish to these stimuli were better understood, hydrodynamic studies of gear could inform future designs and techniques to reduce bycatch.

In addition to ecological concerns, the need to reduce operational costs, particularly fuel consumption, is driving interest in passive fishing gear. Stow nets, for example, offer a potential alternative to beam trawls, as they rely on natural currents instead of vessel-powered propulsion, significantly reducing energy costs. Stow nets are anchored close to the ship, similar to some beam trawl fisheries, where the gear is operated in close proximity to the vessel. The close interaction between the ship and the gear could serve as a "design variable" that influences the hydrodynamics of passive gear, potentially leading to more efficient fishing practices. For beam trawl fisheries, identifying the hydrodynamic field could help understand bycatch patterns—such as localization and potentially the species involved—once fish behaviour in relation to hydrodynamics is better understood. This paper presents a framework for analyzing the hydrodynamic interaction between fishing vessels and gear and identifies hydrodynamic fields in the vessel-gear configuration to inform gear placement and future designs.

Methods

Software used

In previous work [2], we developed an open-source framework for simulating flexible net structures in currents by coupling a structural solver with a viscous flow solver in a partitioned fluid–structure interaction (FSI) scheme.

The net structure is modelled with FEMNET [10, 11, 12, 13], (http://femnetting2.free.fr), a finite element code capable of representing flexible netting, cables, and rigging under hydrodynamic and structural loads. It accounts for elasticity, bending, buoyancy, and fish catch pressure, and solves for quasi-static equilibrium and dynamic analyses of the structure.

The surrounding fluid is simulated with OpenFOAM [6, 7, 8], using snappyHexMesh for discretization and extensions to automate case generation from FEMNET. The netting is represented by a porous-medium approach [1], which constitutes a simplification of the actual net geometry, with the corresponding coefficients calculated according to the formulas given in [5].

The coupled solution process starts from an initial shape prediction of the net structure using FEMNET. The flow field is then solved in OpenFOAM, and the resulting velocity or pressure distribution is mapped to the FEMNET discretization. The updated net shape is calculated using FEMNET's quasi-static equilibrium algorithms, making the present implementation applicable to quasi-static scenarios. The coupling procedure involves repeated data exchange between the solvers and is continued until a converged solution is obtained. Outputs from both solvers are visualized in ParaView [9].

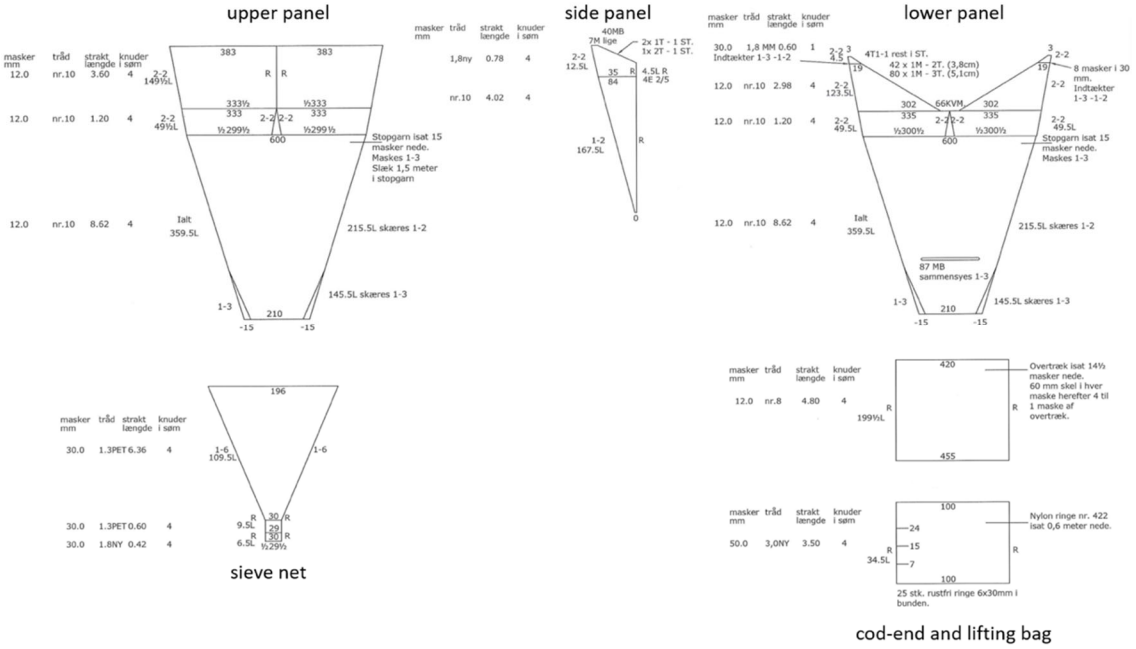


Figure 1
Net plan.

Nets
The first test object is a beam trawl with a beam width of approximately 9.5 m. The clearance between the seafloor and the underside of the beam is 0.55 m, and the beam itself has a diameter of 0.125 m. The netting plan is shown in Figure 1; nearly all panels use a full mesh size of 24 mm. The headline measures 9.6 m in length, while the fishing line is 12.6 m long and fitted with a bobbin line comprising 40 bobbins of 200 mm diameter each. For the present simulations, the trawl shoes, lifting bag netting, and sieve net were neglected.

The stow net corresponds to the beam trawl described above, but without the bobbin line. All other dimensions and netting specifications remain unchanged.

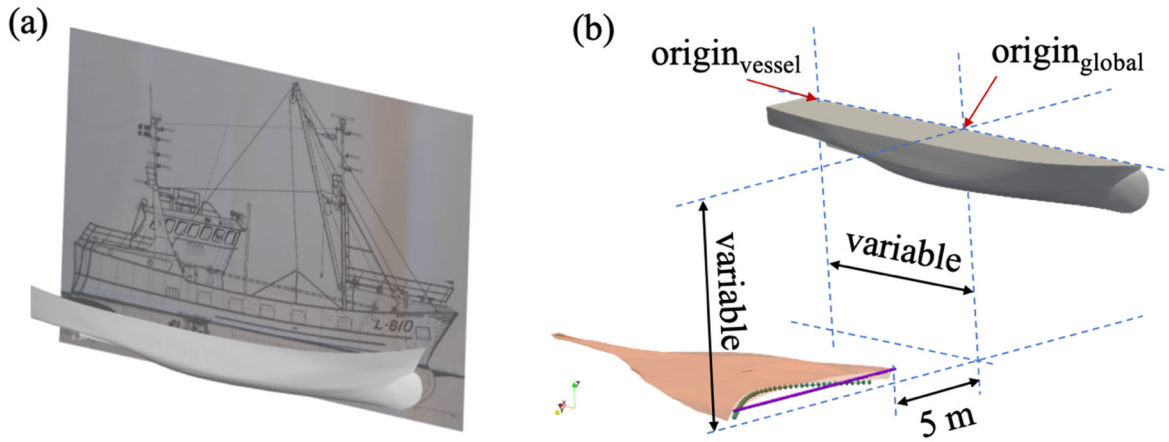


Figure 2
FreeCAD model of the hull of the fishing vessel.

Fishing Vessel
The fishing vessel considered is a beam trawler with an overall length of approximately 22 m, a breadth of 6 m, and a draught of about 2 m, Figure 2 (a). The hull geometry was derived from the general arrangement plan, modeled in FreeCAD, and exported in .stl format for subsequent use in snappyHexMesh. The propeller and Kort nozzle were not included in the model.

Computational Set Up
The computational domain was defined with a symmetry plane coinciding with the vessel's midship plane. The beam trawl was positioned alongside the vessel at a fixed transverse distance of 5 m (Figure 2 (b)). Due to the use of the symmetry plane, the setup effectively represents a net deployed on both sides of the vessel. The longitudinal position of the vessel relative to the trawl was fixed but should be varied in future investigations. The water depth was set to 10 m, 6 m, and 4 m

in separate cases. For each configuration, the beam, bobbin line, and vessel were modelled as fixed to one another, while the netting was free to deform.
To reduce computational cost and improve numerical stability, a free water surface was not considered. Instead, the top boundary was treated as a symmetry plane, effectively creating a double-hull configuration with the vessel hull truncated at the waterline. At the inlet boundary, a uniform flow velocity of 1.5 m/s was prescribed. The outlet boundary was defined by a static pressure of 0 Pa, and all remaining boundaries were assigned zero-gradient conditions.

Results and Discussion

Figure 3 depicts the pressure distribution on the symmetry plane and a plane parallel to the ground but 0.05 m above it. The pressure distribution shows the expected pattern around the ship. A high-pressure region develops at the bow (stagnation point) followed by a gradual transition to a low-pressure region amidships. From theory a pressure recovery is expected in the stern region. However, due to the flow separating in the stern region the pressure increase is not as distinct as expected.

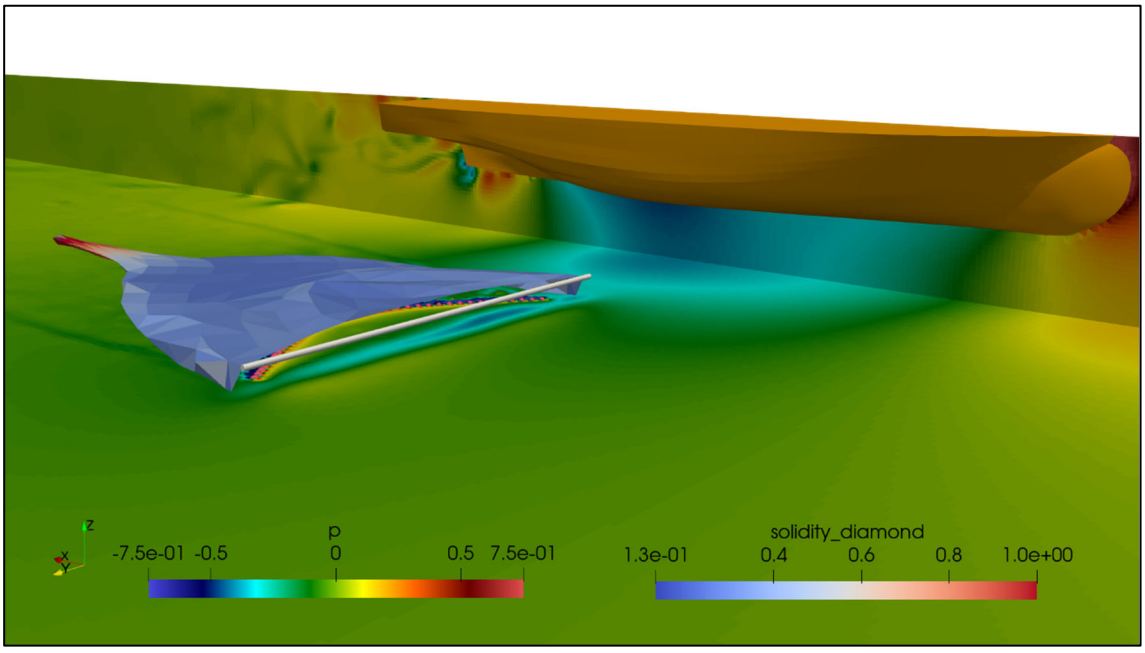


Figure 3
Kinematic pressure (p/ϱ, in m^2/s^2) contour plot on the symmetry plane and a plane 0.05 m above ground. Depth: 4 m, beam trawl configuration. The nets surface depicts the meshes solidity.

For the beam trawl and stow net a low-pressure zone forms beneath the beam as the flow is constricted and accelerated due to the beam. Visible also is that the midship low-pressure region expands in the net entrance area affecting the net

side closer to the ship. In front of the bobbins there is an increase in pressure again since the flow is blocked by the bobbins. Figure 4 presents a velocity contour plot on the same planes. Distinctive is the unsteady wake developing behind the ship and bobbin line. In reality, the ship's wake is expected to differ, as the influence of the propeller, duct and rudder has been omitted. Nevertheless, it becomes apparent that the flow patterns behind the ship will be unsteady. This holds true for the stow net case also, since flow will also separate from the hull. If these unsteady pressure/ velocity fluctuations have positive or negative effects on the catch cannot be judged since no information is available to the knowledge of the authors which relates pressure or flow fluctuations to behaviour patterns.

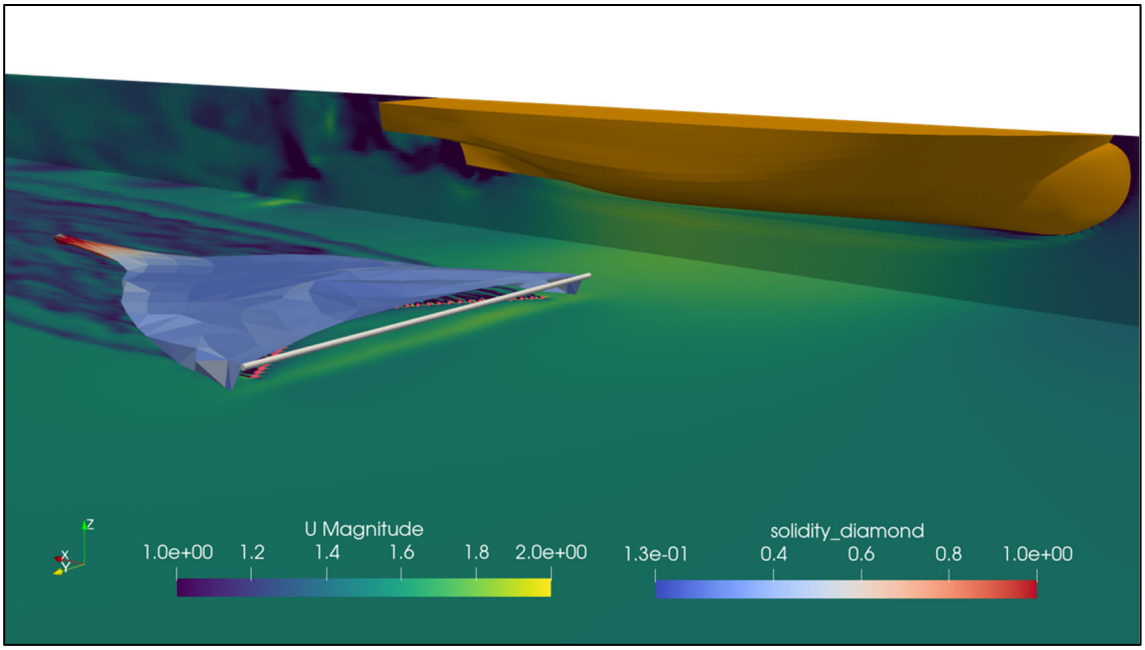


Figure 4
Velocity contour plot (in m/s) on the symmetry plane and a plane 0.05 m above ground. Depth: 4 m, beam trawl configuration.

To judge the effect of the proximity of the ship to the net the flow rate through the area below the beam is used and can be interpreted as a proxy for the flow into the net. In Figure 5 the relative flow rate into the net is given dependent on the depth over ground. The relative flow rate is calculated by

$$\lambda = \frac{Q_{sim}}{Q_0} = \frac{Q_{sim}}{A_{bb} \cdot v_{in}} \quad (1)$$

where Q_{sim} is the volume flow rate through the area below the beam determined by the simulations, v_{in} the inlet flow velocity, and A_{bb} the area below the beam down to the ground.
The net's longitudinal position is amidships. Smaller depths imply that the net is closer to the ship. It becomes apparent that with increasing proximity, the flow

into the net increases due to the higher velocity and lower pressure region amidships. The stow net exhibits a slighter higher flow rate into the net since no bobbins obstruct the flow. Whether this finding holds true for other longitudinal positions is the subject of ongoing investigations.

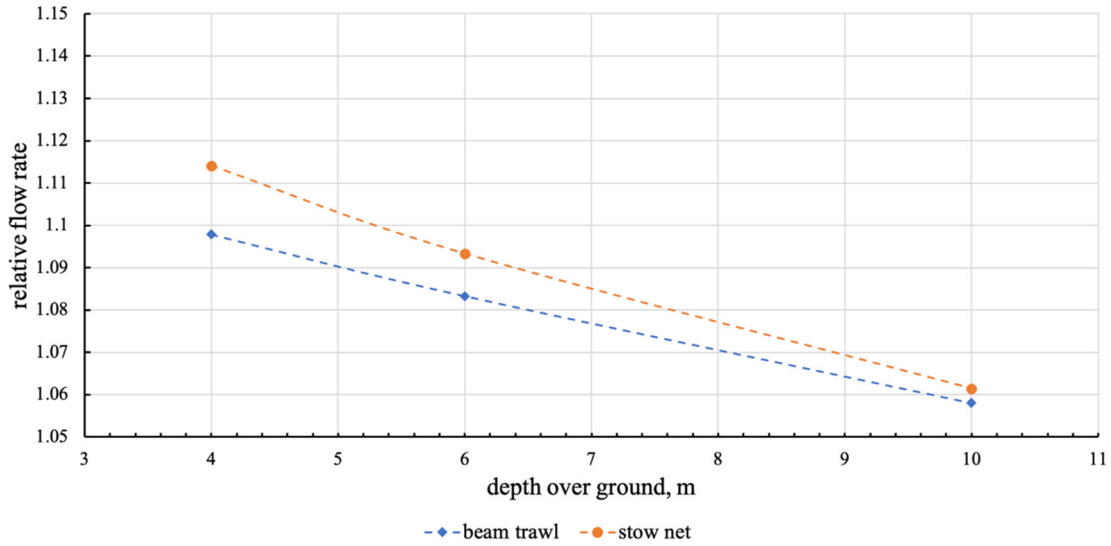


Figure 5
Relative volume flow rate entering the net based on the undisturbed flow velocity and area below the beam.

Conclusion

Analysis of the relative flow rate into the net shows that proximity to the hull significantly influences inflow, with smaller depths leading to higher flow rates as a result of the intensified low-pressure region amidships. Stow nets exhibited slightly higher inflow than beam trawls, since no bobbins obstructed the flow. These findings indicate that the vessel-gear configuration can act as an important design parameter for passive gear systems.

The implications are twofold. From an ecological perspective, understanding how hydrodynamic conditions shape fish–gear interactions could contribute to reducing bycatch once behavioural responses to unsteady flow and pressure fluctuations are better understood. From an operational perspective, proximity effects may offer opportunities to optimize gear placement for higher efficiency in passive fisheries, with stow nets emerging as a promising low-energy alternative to beam trawls. Future work should focus on extending these analyses to different longitudinal positions, as well as integrating behavioural data (if available), in order to link hydrodynamic fields with catch efficiency and species selectivity.

Acknowledgements

The authors gratefully acknowledge Tiago Veiga-Malta and Valentina Melli for providing the net, rig, and ship plans, together with supplementary information and measurements, which were essential for this work.

References

1. Breddermann, K., Stone, M., and Yochum, N. – Flow analysis of a funnel-style salmon excluder – Proceedings DEMaT 2019, ISBN 978-3-8440-6995-2, p. 29ff
2. Breddermann, K., Lichtenstein, U., Priour, D. – FEMNET - OpenFOAM coupling. A FSI approach to simulate fishing gear – Proceedings DEMaT 2022, ISBN 978-3-946694-06-9, p. 159ff
3. Coombs, S., Bak-Coleman, J., Montgomery, J. – Rheotaxis revisited: a multi-behavioral and multisensory perspective on how fish orient to flow – J. Exp. Biol. 2020 , 223(Pt 23):jeb223008, doi: 10.1242/jeb.223008
4. Liao, J. C. – A review of fish swimming mechanics and behaviour in altered flows – Phil. Trans. R. Soc., 2007, doi.org/10.1098/rstb.2007.2082, B362:1973–1993
5. Løland, G. – Current force on and flow through fish farms – Dr. Eng. Dissertation. Division of Marine Hydrodynamics, Norwegian Institute of Technology, 1991, ISBN 82-7119-269-8
6. OpenFOAM®, Aug . 2022, retrieved from https://www.openfoam.com/
7. OpenFOAM-The OpenFOAM Foundation, Aug. 2022, retrieved from https://openfoam.org/
8. OpenFOAM-extend, Aug. 2022, retrieved from https://sourceforge.net/p/foam-extend/foam-extend-4.1/ci/master/tree/ReleaseNotes
9. ParaView, Aug. 2022, retrieved from https://www.paraview.org/
10. Priour, D. – Calculation of net shapes by the finite element method with triangular elements – Communications in Numerical Methods in Engineering 15(10), 1999, 755-763
11. Priour, D. – Introduction of mesh resistance to opening in a triangular element for calculation of nets by the finite element method – Communications in numerical methods in engineering 17(4), 2001, 229-237
12. Priour, D. – Analysis of nets with hexagonal mesh using triangular elements – International journal for numerical methods in engineering 56(12), 2003, 1721-1733
13. Priour, D. – A Finite element method for netting: Application to fish cages and fishing gear. Springer Science & Business Media, 2013, ISBN: 978-94-007-6843-7